THESIS

This is to certify that the

dissertation entitled

APPLICATIONS OF STOPPED-FLOW MIXING IN HETEROPOLYMOLYBDATE KINETICS STUDIES AND IN REACTION-RATE DETERMINATIONS

presented by

Carl C. Kircher

has been accepted towards fulfillment
of the requirements for

Ph.D. degree in Chemistry

Stanley R. Crouch
Major professor

Date May 18, 1982

APPLICATIONS OF STOPPED-FLOW MIXING IN HETEROPOLYMOLYBDATE KINETICS STUDIES AND IN REACTION-RATE DETERMINATIONS

By

Carl C. Kircher, Jr.

A DISSERTATION

Submitted to
Michigan State University
in partial fulfillment of the requirements
for the degree of

DOCTOR OF PHILOSOPHY

Department of Chemistry

1982

ABSTRACT

APPLICATIONS OF STOPPED-FLOW MIXING IN HETEROPOLYMOLYBDATE KINETICS STUDIES AND IN REACTION-RATE DETERMINATIONS

By

Carl C. Kircher, Jr.

The stopped-flow mixing technique was applied to chemical examples of fast-reaction kinetics studies and reaction rate analytical determinations. The pH-dependent heteropolymolybdate speciation in aqueous solutions was deduced, and the equilibrium constants for each species were found. With experimental data from an automated stopped-flow spectrophotometer, the kinetics of 12-molybdophosphate and 12-molybdosilicate formation, decomposition, and conversion to other heteropolymolybdates were monitored as a function of phosphate, silicate, molybdate, hydrogen ion, and heteropolymolybdate concentrations and the solution ionic strength at 25.0°C. Rate law equations, rate constants, and chemical mechanisms for these reactions in nitric, perchloric, and sulfuric acid media were deduced with the help of computer simulations from various chemical models and mathematical equations. The implications upon phosphate and silicate determinations are discussed.

Reaction-rate determinations for phosphate and silicate in aqueous solutions based on 12-heteropolymolybdate formation were performed. Simultaneous determinations were possible in 0.4-0.5 M acid solutions

because the 12-molybdophosphate reaction reaches equilibrium quickly while the β-12-molybdosilicate formation proceeds at its initial rate. The measured reaction rate varied linearly with phosphate and silicate concentrations over 0.001-1.00 mM and 0.050-1.00 mM ranges, respectively. The analysis time was typically 20 sec. The measured reaction rates were reproducible to within a few percent relative standard deviation. The major sources of error were a synergistic effect of a faster reaction rate for one analyte increasing the reaction rate for the other analyte (less than 8% error in most cases) and the measurement of the β-12-molybdosilicate reaction rate when the sample has a high phosphate concentration and a low silicate concentration.

To My Family

with Much Love

ACKNOWLEDGEMENTS

I wish to thank Dr. Crouch for serving as my research advisor, for providing all the help when research was progressing only slowly and when research publications needed typing and revising, and for sharing many of the lighter, enjoyable aspects of chemistry. I also thank Dr. Dye for being my second reader and Dr. Enke and Dr. Chang for serving on my Guidance Committee as well.

My deepest appreciation goes to Dr. Horne, Dr. Crouch, and Dr. Enke who helped me to receive a National Science Foundation Graduate Fellowship that aided me financially and expedited my research progress. To secretaries Debbie Jahangardi and Debbie Wuethrich I give my gratitude for typing my manuscripts for publication and other official administrative forms. To Jo Kotarski goes my appreciation for doing my seminar slides and drawings for figures and my respect and appreciation for her artistic talent. I also thank graduate secretaries Lori Garn and Dorothy Byrne for being the best liaison people any graduate student could have with university administration.

I also wish to thank the members of Dr. Crouch's research group, past and present: Charlie, Gene, Rob, Nelson, Rytis, Dave, Frank, Cor, King, Jim, Clay, Kim, John, Keith, Pat, Marguerite, Paul, Jim W., and

Mark. Not only will I remember the wide variety of chemistry research you all undertook but also your friendship and fellowship, the good times we shared, and your ideas and experiences that you have brought from all over the nation and the world. Good luck in your careers, and I hope to hear from you often.

My best wishes are extended to the other graduate students, faculty, and staff for the many fun times we had together and for the great parties I'll always remember--hazily at best.

I also acknowledge all my "non-chemistry" friends who enriched my experiences here through Owen Graduate Center, Episcopal Ministry of MSU, Academic Governance, mid-Michigan Mensa, Repertory Concert Band, and the Lansing area party scene.

Finally, I wish to thank my Mom, Dad, and other relatives whose love nurtured my brothers and me through our formative years and encouraged us to try our best in all we undertake and to be the beautiful people that we potentially can be.

Without you, this thesis would not have been possible.

TABLE OF CONTENTS

LIST OF TABLES

Page

LIST OF FIGURES

Chapter I. Overview: The Stopped-Flow Technique in Analytical Chemistry

A. Description of the Technique

Ever since the stopped-flow mixing technique was developed in 1940[1-3], researchers have discovered its enormous potential as a tool for studying many types of chemical reactions. The general description of stopped-flow mixing is simple. Two or more chemical reagents are mechanically sent into motion from their respective reservoirs, mixed so that the chemical reaction among the reactants may begin, and directed to an observation cell where the reaction progress may be monitored. A brief time period is required for reagent mixing and delivery to the observation cell; afterwards, this solution flow is mechanically stopped. The chemistry of the mixed solution can be studied over a predetermined, variable time period within the observation cell by using common, convenient measurement methods such as absorption and fluorescence spectroscopy and conductimetry. With suitable designs for the reagent delivery system, mixer, and observation cell, only small amounts of reagents are required for experiments, and measurements can be made within milliseconds after the mixing of the reagents. In addition, since measurements are made after the solution flow is stopped, the same mixed solution within the observation cell can be studied over a long length of time, minutes if so desired. Thus, the

stopped-flow technique provides the capability of studying a wide variety of chemical processes occurring over time scales ranging from milliseconds to several minutes.

The stopped-flow technique also has certain fundamental limitations. The detection system must have a fast response time in order to measure chemical changes that occur within millisecond time intervals. Also, because of the finite time of mixing required, chemical phenomena occurring within microseconds would not be discernable by stopped-flow methods, so small perturbation techniques (relaxation methods) such as temperature-jump or electrical field variations would be required. However, in assuming the stopped-flow technique is applicable for a given chemical system to be studied, the stopped-flow results would provide information about the entire reaction scheme, from the initial stages to the attainment of equilibrium. Only the chemical reaction steps close to the equilibrium state can be studied with relaxation methods since the methods require only slight fluctuations from equilibrium. Large perturbation methods could enable the study of more chemical reaction steps; however, the species concentrations may not be calculable from a given perturbation or else the chemical system could relax to a different equilibrium state.

In addition to studying the kinetics and elucidating the mechanisms of chemical reactions useful in analytical chemistry, stopped-flow mixing can also be employed in reaction-rate analytical methods. These methods are generally employed in chemical systems where prior studies of kinetics have verified first-order rate conditions with respect to the analyte involved or that pseudo first-order kinetics

apply over a given set of experimental conditions. Consequently, the chemical reaction rate would yield the analytical information because this rate is linearly proportional to the analyte concentration over the course of the reaction. With a valid initial rate approximation, the initial, analytical species concentration is related to the initial reaction rate. Thus, no waiting time is required to reach equilibrium, so the analysis time is much shorter than that of a procedure based on attainment of equilibrium. Since the initial rate reflects only the initial steps of the reaction mechanism, any interferences or decreases in sensitivity caused by unforeseeable side reactions in subsequent mechanistic steps are reduced. If there are several components in the mixture that react similarly as the species of interest does, then, to the extent that these several components react at different initial rates, a multicomponent analysis is possible and the rates corresponding to the interferences may be subtracted from the total rate to give the initial rate corresponding to the analyte's reaction. Furthermore, because relative measurements of transmittance and changes in absorbance with time are involved, constant interferences such as turbidity and background absorbance do not contribute to systematic experimental errors as would happen when equilibrium methods are employed. However, since the final equilibrium state is not reached during the analysis, measurements of the time-varying physical parameter inherently possess a lower signal-to-noise ratio and thus lower sensitivity and precision. Experimental conditions such as pH, ionic strength, and temperature

must be carefully controlled over the measurement time interval so that the measured initial rates are reproducible. Stopped-flow instrumentation may require a complicated design and fairly expensive accessories in order that mixing times are sufficiently small, total reagent volumes are small, cavitation can be eliminated, leakage of solutions does not occur, and the mixer and other components can withstand high solution flow rates and high pressure stresses occurring during the stoppage of flow. Since the chemical reaction rates may show an initial lag time and a subsequent decay as equilibrium is approached, the detection and data acquisition systems must be equipped to perform multipoint analyses and regression.

B. General Principles of Stopped-Flow Mixing

In reviewing the general principles of the stopped-flow technique, the ideal experiment would involve the instantaneous mixing of the chemical reagents and immediate transportation to the observation cell where the solution flow is abruptly stopped and the chemical reaction is monitored. The so-called "dead time", which is characteristic of a particular stopped-flow apparatus, reflects the finite time required between the initial contact between solutions in the mixer and the termination of solution flow in the observation cell. The dead time parameter is important in determining which chemical reactions can be studied. If this dead time is not significantly less than the half-life (the time required to convert half of the reactants into products) of a particular reaction, then the initial reaction rate measured will be significantly slower than the actual initial rate. In order to study

these fast reactions, the reaction time must be evaluated as a function of position within the observation cell.

Another important consideration for stopped-flow involves the promotion of turbulent flow through the mixer and observation cell rather than laminar flow. Turbulent flow gives a more uniform flow velocity profile within a cross section of the flow channel as compared to the parabolic flow velocity profile resulting from laminar flow. This consideration facilitates a better reaction time resolution within the observation cell as well as more homogeneity within the mixed solution. In fact, the reagent mixing is accomplished better under turbulent conditions than with streamlined laminar flow. In addition, the flow velocity is less affected by the driving pressure required to initiate solution flow and by the viscosity of the solutions themselves.

A more detailed presentation of these general principles may be found in an earlier dissertation.[4]

C. The Beckwith Automated Stopped-Flow Analyzer

The stopped-flow spectrophotometer used for most of this research was initially designed by Beckwith.[5] The block diagram of this instrument and the electronic computer interfaces is shown in Figure 1. The basic features of this stopped-flow system include a pneumatic syringe drive system to promote rapid mixing. The vertical flow system minimizes interferences from bubble formation. The valves that direct the solution flow and drain the waste solutions are actuated with air pistons mechanically controlled by solenoids. The stopped-flow operating cycle and valve sequencing may be performed manually with push

Figure 1. Block Diagram of the Beckwith Stopped-Flow Spectrophotometer

A. Solenoid actuated pneumatic drive cylinder
B. Solenoid actuated pneumatic cylinder controlling delivery valve
C. Reagent drive syringes
D. Double 3-way stopcock connecting reagent syringes with reservoirs or flow system
E. Port to reagent reservoirs
F. Mixing chamber
G. Observation cell
H. 3-way waste release valve
I. Spring-loaded stopping syringe
J. Port to drain
K. Solenoid actuated pneumatic cylinder controlling waste release valve

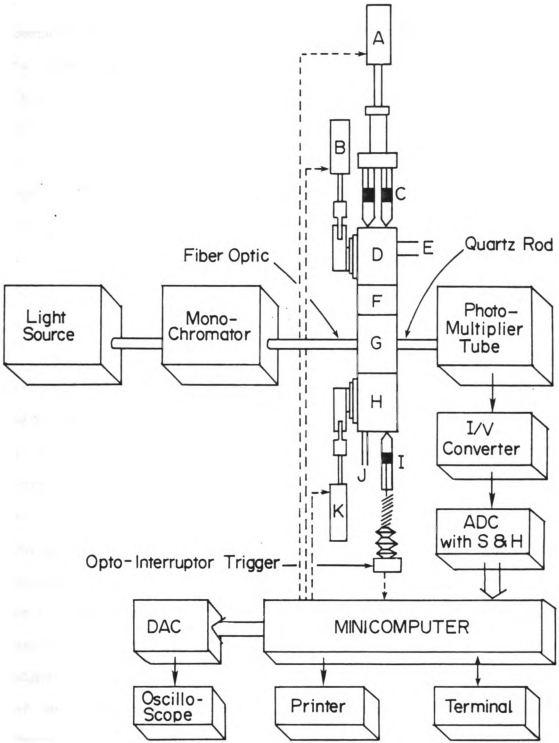
A
B
C
D
E
F
G
H
I
J
K
Fiber Optic
Quartz Rod
Light Source
Mono-Chromator
Photo-Multiplier Tube
I/V Converter
ADC with S & H
Opto-Interruptor Trigger
DAC
MINICOMPUTER
Oscillo-Scope
Printer
Terminal

buttons or automatically with pulses originating from a PDP 8/e minicomputer (Digital Equipment Corporation). The measured light intensity is converted to electrical current with a photomultiplier tube (RCA/IP28A) and subsequently converted to voltage with a Keithley Model 427 current amplifier. This voltage can be recorded on an oscilloscope or digitized automatically with a Datel DAS-16-M12B analog-to-digital converter and stored on a mass storage device (i.e. floppy disk). A trigger signal from a photointerruptor module beneath the stop syringe initiates the data acquisition sequence from the minicomputer. Up to four stopped-flow data pushes may be performed each time the drive syringes are filled.

Although the basic block diagram of the Beckwith instrument has remained the same, several members of Dr. Crouch's research group have made various improvements and modifications. A water circulation system to thermostat the stopped-flow system, a new mixer, and an optoelectronic trigger module (G.E. H13B1) now augment the original stopped-flow system.[4] The observation cell, quartz fiber optic light guide, and quartz rod that interface the stopped-flow to a GCA/McPherson spectrophotometer system have been housed in a stainless steel and black Delrin assembly. The computer programs controlling the stopped-flow operation, data acquisition, and data analysis have been rewritten in higher level languages FORTRAN and SABR[6,7] (Gall and Balciunas). Some of the electrical computer interface components have been replaced to improve the integrity of the monostable pulses and other dialogue between the stopped-flow instrument and minicomputer.[7] The instrument has also been modified to perform conductance measurements within the observation cell.[8]

With the current stopped-flow computer program,[7] the operator may set several options prior to performing stopped-flow pushes. The analog data-taking rate, for example, may vary from one per millisecond to one per second. The number of analog points averaged for each data point may vary from one to 1000. The time delay between the clock start and the stopped-flow trigger is variable; a 7 ms delay time works well for most stopped-flow measurements. Up to 100 data points may be obtained per stopped-flow push. A maximum of four data pushes is possible for each drive syringe filling, and one or two syringe fillings may be performed for each set of solutions in a stopped-flow experiment. The computer program contains automatic routines to rinse the stopped-flow channels with appropriate solutions, measure 100% transmittance with blank solutions, and measure the dark current.[4,6,7] For each stopped-flow experiment, the computer measures the solution transmittance at the specified data-taking rate and calculates the absorbance and its standard deviation at each time point. These data may be plotted as a function of time on an oscilloscope, stored on floppy disk under a specified filename, or listed on a line printer or terminal.[7] Some important considerations for the operator include the volume of solution required to perform the entire stopped-flow experiment for the specified number of syringe fillings. Also, a slower data-taking rate and/or a larger number of analog points averaged per data point result in a larger time interval between data points and a longer time span covered in a stopped-flow run.

Thus, over the last ten years, Dr. Stan Crouch's research group has made considerable improvements in stopped-flow equipment and interfaces

for computer automation, and the equipment currently available (5 ± 1 ms dead time on the Beckwith system[4]) should be adequate for studying many types of chemical reactions. Consequently, this reseach investigates two applications of the stopped-flow technique in Analytical Chemistry. One such application is the kinetics study of two chemical reactions of analytical importance: the complexation of phosphate and silicate with molybdates in acidic solution and the acidic and basic decomposition of these heteropolymolybdate complexes. The other application develops reaction-rate determinations of phosphate and silicate in mixtures based on the rate of formation of their heteropolymolybdate complexes.

D. Some Recent Advances in the Use of Stopped-Flow

The recent literature is filled with new applications of stopped-flow mixing and improvements in existing systems. Most of these advances involve investigations of new and current designs for the essential stopped-flow components and their impact on instrumental performance, new detection methods to monitor chemical reactions within the observation cell, and new chemical reaction systems that can now be studied with stopped-flow techniques.

To extend the analytical utility of the stopped-flow technique, several recent improvements have been reported in the mechanical design and evaluation of stopped-flow components. A complete stopped-flow system was designed and constructed that could withstand hydrostatic pressures up to 3 kbar yet would be able to follow chemical reactions with millisecond half-lives, thus enabling high pressure kinetics studies of chemical reactions in solution.[9] As an accessory to stopped-flow

instruments, a microprocessor-controlled reagent dilution system containing three-way proportioning valves and a homogenizing mixer on-line with the stopped-flow sample delivery loops was developed.[10] For individual stopped-flow components, a chemically inert tangential jet mixer was recently designed.[11] Some considerations regarding the use of stainless steel drive syringes have been discussed.[12] As an example of recent work in investigating stopped-flow instrument performance, the dead time for a stopped-flow that employs fluorescence detection in the observation cell has been reported.[13] The increases in solution temperature during the mixing process were compared for several configurations of the drive syringes, mixer, and observation cell, and subsequent considerations have been presented about controlling these temperature variations.[14] A chemical reaction employing disulfide exchange was presented as another way to evaluate stopped-flow spectrophotometer performance[15] in addition to the iron-thiocyanate reaction.[16]

The stopped-flow technique has been extended to chemical reactions that occur in media other than homogeneous solutions. For example, the gas phase reaction of ozone with organic sulfides was studied with stopped-flow instrumentation coupled to a beam sampling mass spectrometer.[17] Also of note is a recent stopped-flow study of chemical reactions that occur in micelles.[18]

A significant portion of a recent advances encompasses different methods to monitor chemical processes in the observation cell. Calorimetry has been used to study reaction rates by stopped-flow methods. The thermistor used had a 15 ms response time and could detect temperature

changes as small as 1 m°C.[19] By using Fourier methods to reduce the time scale of NMR measurements, a stopped-flow instrument was designed to monitor the kinetics and dynamics of a chemical reaction by line shape analysis of NMR signals.[20] Similarly, a stopped-flow EPR instrument has been used to monitor free radical reaction mechanisms with a time resolution of 4 ms.[21] Furthermore, the use of circular dichroism as a stopped-flow detection method has enabled studies of millisecond conformational changes in biological macromolecules.[22] Thus, recent advances in stopped-flow instrumentation and detection methods have greatly increased the number of chemical reactions than can be studied with stopped-flow techniques and have defined more clearly the limits within which useful information may be obtained.

Chapter II. Equilibrium and Kinetics Studies of Heteropolymolybdates

A. The Molybdenum Blue Reaction

Chemical analyses for phosphate and silicate provide important information about the sample that contains these analytes. Two of the most important applications of phosphate determinations are performed on clinical and agricultural samples. Phosphate levels in biological fluids reveal metabolic information on how chemical energy is stored and utilized in the formation of teeth and bone (calcium phosphate minerals) and in the conversions involving adenosine triphosphate (ATP $\rightarrow$ ADP + P_i). Phosphate levels in soils and fertilizers may determine which crops can grow best in a given growing season. Determination of silicate in soils and rock samples can elucidate the geological history of a given land region or ocean bed, and its detection on mobile machine parts and air filters indicates contamination from dust particles.

The use of Mo(VI) in acidic solutions has been employed extensively in analytical determinations of both phosphate and silicate. Many experimental procedures for these assays are based on the reaction of phosphate or silicate with acidified Mo(VI) to form the yellow 12-molybdophosphate anion (12-MPA) or the 12-molybdosilicate anion (12-MSA), respectively. The formations of these heteropolymolybdates are

most often monitored spectrophotometrically.[23,24] Many other procedures use the so called "molybdenum blue" reaction in which the 12-MPA and 12-MSA complexes are reduced to intensely blue-colored species.[25] In addition to equilibrium methods, the applicability of reaction-rate methods based upon the rate of formation of 12-MPA,[26] 12-MSA,[6] and reduced 12-MPA blue[27] has been demonstrated. As required in developing each experimental procedure, the phosphate or silicate concentration ranges in which the stable, colored complexes formed will obey Beer's Law and under which stoichiometric amounts of the complexes will be formed were evaluated for the equilibrium methods. For reaction-rate methods, those concentration ranges in which Beer's Law is followed and under which pseudo first-order kinetics with respect to phosphate or silicate prevail were evaluated.

Despite the sensitivity and applicability of the heteropolymolybdate system in analytical chemistry, many details of the chemical reactions involved have not yet been resolved beyond all doubt. Table I reflects what is known with certainty about these reactions. The specific Mo(VI) species which combine with phosphate or silicate were unknown prior to this thesis; however, 12-MPA and 12-MSA were known to form in amounts proportional to the total phosphate and silicate concentrations present in solution if the Mo(VI) present is in large, constant excess.[27.28] The uncertainties in the stoichiometric coefficients Y_1, Y_2, Z_1, and Z_2 reflect the uncertain nature of the complexing Mo(VI) species. With different pH and total Mo(VI) conditions, different isomers of 12-MPA and 12-MSA may form, each isomer having different spectrophotometric properties.[29,30] In addition, the compositions of the reduced molybdenum blue species vary with different

Table I

Chemical Equations for Phospho- and Silicomolybdenum Blue Reactions

PHOSPHATE DETERMINATIONS

$$H_3PO_4 + Y_1\ Mo(VI) \xrightarrow{pH\ 0.5} PMo_{12}O_{40}^{3-} + Z_1H^+$$

$$PMo(VI)_{12}O_{40}^{3-} \xrightarrow{Sn^{2+}} PMo(V)_4Mo(VI)_8O_{40}^{3-}$$

yellow 12-MPA — Phosphomolybdenum Blue

SILICATE DETERMINATIONS

$$Si(OH)_4 + Y_2\ Mo(VI) \xrightarrow{pH\ 1\text{-}5} (\alpha/\beta)SiMo_{12}O_{40}^{4-} + Z_2H^+$$

$$SiMo(VI)_{12}O_{40}^{4-} \xrightarrow{Sn^{2+}} SiMo(V)_4Mo(VI)_8O_{40}^{4-}$$

$$SiMo(VI)_{12}O_{40}^{4-} \xrightarrow[Acid]{Ascorbic} SiMo(V)_3Mo(VI)_9O_{40}^{4-}$$

yellow 12-MSA — Silicomolybdenum Blue

experimental conditions. The reduction of 12-MPA and 12-MSA has been shown to proceed, at least initially, in two-electron steps.[31,32] Many reagents can reduce 12-MPA and 12-MSA since these heteropoly compounds are good oxidizing agents.[33] With the addition of two and four electrons, the molybdenum blue complexes would have Mo(VI) : Mo(V) ratios of 5:1 (i.e. $PMo(V)_2Mo(VI)_{10}O_{40}^{5-}$) and 2:1 ($PMo(V)_4Mo(VI)_8O_{40}^{7-}$), respectively; the existence of such species and others have been reported.[34-36] The composition of the blue complex and its absorption spectrum depend in part upon which reducing agent is used and how long the reduction takes place. The blue color is most intense when ascorbic acid is the reducing agent.[37] Some reducing agents such as ascorbic acid, thiourea, and HI exhibit autocatalysis because the reaction products increase the reaction rate for unreacted species. By contrast, Sn(II), Fe(II), and hydroquinone are non-autocatalytic reducing agents. According to Kriss and coworkers[37] autocatalytic reducing agents form multiple oxidation products whereas non-autocatalytic reagents produce only one oxidation product. Strong reducing agents such as Zn-HCl decompose 12-MPA and 12-MSA.[33] Reduction of the two different 12-MSA isomers with Sn(II) results in different reduction products.[33] The use of metallic reducing agents such as Sn(II), Ti(III), and Cr(II) can further complicate the molybdenum blue composition since one or two of the Mo atoms may be substituted with these other transition metal atoms.[38] The reversibility of certain redox reactions, though reported by some workers,[39] is still in question.

B. Literature Background on Mo(VI) and Heteropolymolybdate Chemistry

The speciation of Mo(VI) compounds as a function of pH is quite complicated. In aqueous solution, Mo(VI) forms either multiple bonds with oxygen as Mo = O or single bonds in the bridging systems Mo–O–Mo and Mo$\langle^{O}_{O}\rangle$Mo. At pH 7, the colorless, tetrahedral molybdate anion (MoO_4^{2-}) is the predominant Mo(VI) species. As the acid concentration increases, molybdenum becomes octahedrally coordinated and polymerizes rapidly to give various polyacid anions.[40] Predominant molybdenum species in the pH range of 1-6 include Mo(VI) monomers ($HMoO_4^-$, H_2MoO_4), heptamers ($Mo_7O_{24}^{6-}$, $HMo_7O_{24}^{5-}$, $H_2Mo_7O_{24}^{4-}$), and octamers ($Mo_8O_{26}^{4-}$); their distribution as a function of pH has been plotted.[41] Other clusters have been identified as having 2,3,4,6,10,12,16, and 24 Mo(VI) atoms.[41] Mo(VI) precipitates as MoO_3 at an isoelectric point that occurs at pH 0.9. Under more acidic conditions the precipitate redissolves as $Mo(OH)_6$ (commonly written as MoO_3) and accepts a proton to become the cationic monomer $Mo(OH)_5(H_2O)^+$ (or $HMoO_3^+$). These monomers dimerize to form the cationic species $Mo_2O(OH)_9(H_2O)^+$ (or $HMo_2O_6^+$), $Mo_2O(OH)_8(H_2O)_2^{2+}$ (or $H_2Mo_2O_6^{2+}$), and $Mo_2O(OH)_7(H_2O)_3^{3+}$ (or $H_3Mo_2O_6^{3+}$).[42] These two monomers and three dimers are the predominant Mo(VI) species in strong acid solution (pH < 0.9).[42] A summary of the Mo(VI) speciation as a function of pH is given in Table II.

Strickland first reported that two isomeric products are possible in 12-MSA formation.[29] Other researchers[43] have argued that pH and total Mo(VI) concentration determine which of the α and β isomers form, rather than Strickland's acid-to-molybdenum ratio. The isomer α-12-MSA

Table II

pH-Dependent Speciation of Molybdate Complexes in Aqueous Solution

Mo(VI)

pH > 7 tetrahedral MoO_4^{2-}

pH 6-7 octahedral (unsymmetrical)

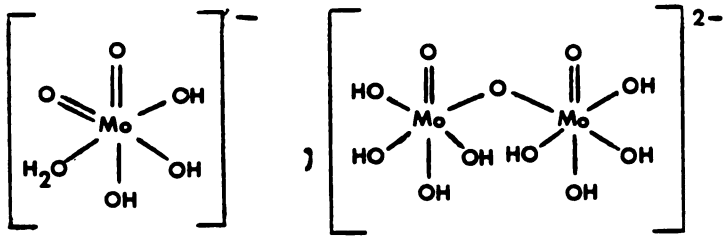

pH < 6 polymeric Mo-Complexes

$Mo_7O_{24}^{6-}$ when $\frac{[ACID]_{tot}}{[Mo(VI)]} \geq 1.14$

$Mo_8O_{26}^{4-}$ when $\frac{[ACID]_{tot}}{[Mo(VI)]} \geq 1.5$

pH = 0.9 isoelectric point; MoO_3 ppt.

pH < 0.9 monomeric & dimeric Mo-cations

$HMoO_3^+$, $H_2MoO_3^{2+}$, $H_2Mo_2O_6^{2+}$, $H_3Mo_2O_6^{3+}$

was observed to form between pH 1.8 and 4.8, and the β-12-MSA isomer between pH 1.0 and 3.8.[43] Thus, studies of the kinetics of 12-MSA formation and decomposition would require measurements of both measurements $\frac{d[\alpha\text{-12-MSA}]}{dt}$ and $\frac{d[\beta\text{-12-MSA}]}{dt}$. The analytical reagent concentrations should be chosen to give pH conditions under which only one isomer forms, especially since the absorption spectra of the α and β isomers differ.[30] In addition, the kinetics of the conversion of β-12-MSA to α-12-MSA must be sufficiently slow that $\frac{d[\beta\text{-12-MSA}]}{dt}$ may be measured for both growth and decay before this conversion takes place. Less is known about possible α and β isomers of 12-MPA. Halasz and Pungor reported the absorption spectra for α- and β-12-MPA against a Mo(VI) reference solution and that the α-form would convert almost instantaneously to the β-isomer under strongly acidic conditions.[30] Thus, the kinetic studies concerning 12-MPA would involve only measurements of $\frac{d[\beta\text{-12-MPA}]}{dt}$. Other phosphomolybdates have been observed; Souchay illustrated the chemical relationships between species (see Figure 2).[44] A similar equilibrium scheme has not been reported for molybdosilicates.

C. Literature Background on Past, Pertinent Kinetics Studies

Because so many Mo(VI) species abound in aqueous solutions with various degrees of polymerization and protonation, the kinetics of interconversion among the various species must be considered along with the heteropolymolybdate formation kinetics. If the Mo(VI) interconversions were found to proceed at rates comparable to 12-MPA and 12-MSA formations, steady state approximations would be invalid, and rate expressions for a consecutive reaction model would be required (i.e.

Figure 2

Equilibria Among the Molybdophosphates[44]

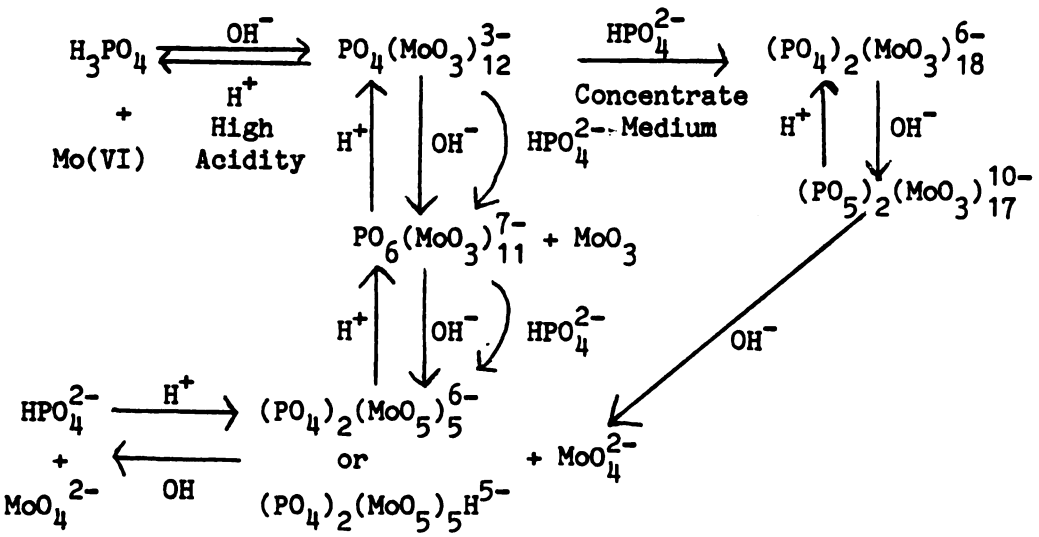

$A \longrightarrow B \longrightarrow C$) and would appear more complex in form. The kinetics studies of molybdate protonation and polymerization reported in the literature were generally performed with relaxation methods, while the depolymerization kinetics were studied with fast mixing techniques. With ultrasonic absorption measurements of relaxation times, the protonations of $Mo_7O_{24}^{6-}$ and MoO_4^{2-} were observed to follow second-order kinetics with rate constants of $(4.8 \pm 1.2) \times 10^9\ M^{-1}sec^{-1}$ for $H^+ + MoO_4^{2-} \longrightarrow HMoO_4^-$ and $(6.9 \pm 0.7) \times 10^{10}\ M^{-1}sec^{-1}$ for $Mo_7O_{24}^{6-} + H^+ \longrightarrow HMo_7O_{24}^{5-}$.[45] The latter second-order rate constant is similar in magnitude to the value for the protonation of inorganic acids, suggesting that the kinetics are diffusion controlled. The first protonation is slower because the tetrahedral MoO_4^{2-} converts to octahedral coordination before the proton is accepted.[46] A temperature-jump relaxation study was conducted on the polymerization equilibria at 25°C and 1.0 M ionic strength. Values of the rate constants were found to be $k_1 = (9.5 \pm 1.9) \times 10^{32}\ M^{-14}sec^{-1}$, $k_{-1} = (7.5 \pm 3.8)\ sec^{-1}$, $k_2 = (5.0 \pm 4.5) \times 10^{23}\ M^{-5}sec^{-1}$, and $k_{-2} = (4.9 \pm 1.0) \times 10^3\ sec^{-1}$.[47] These results indicated rapid Mo(VI) polymerization. The base hydrolysis kinetics of $Mo_7O_{24}^{6-} + 8\ B + 4H_2O \longrightarrow 7\ MoO_4^{2-} + 8\ HB^+$ depolymerization were studied at 25°C and 3.0 M ionic strength; the observed rate equation had the following form:[48]

$$-\frac{d[Mo_7O_{24}^{6-}]}{dt} = (k_w[H_2O] + k_B[B])\ [Mo_7O_{24}^{6-}]$$

The overall reaction kinetics were second-order with strong bases such as OH^-, ϕO^-, and $NH_2CH_2CO_2^-$ and first-order with weaker bases. The dimerization kinetics of $2\ HMoO_3^+ \longrightarrow H_2Mo_2O_6^{2+}$ were studied at 25°C

and 3.0 M ionic strength with temperature-jump relaxation techniques.[49] A forward rate constant of (1.71 ± 0.10) x 10^5 $M^{-1}sec^{-1}$ and a reverse rate constant of (3.20 ± 0.02) x 10^3 sec^{-1} were observed.

The kinetics of heteropolymolybdate formation and decomposition have been investigated by several researchers. Stopped-flow experiments at 25°C and 3.0 M ionic strength were used to study the OH^- hydrolysis of the $H_nMo_5P_2O_{23}^{n-6}$ and $H_nMo_7O_{24}^{n-6}$ species.[50] The second-order reaction rate constants observed were 16.7 ± 0.9 $M^{-1}sec^{-1}$ and 13000 ± 1300 $M^{-1}sec^{-1}$, respectively. Stopped-flow kinetics studies of 12-MPA formation in nitric acid solution were first performed by Javier and coworkers.[51] Since then, Beckwith has repeated these experiments in perchloric and sulfuric acids,[5] and Beckwith, Scheeline and Crouch[52] published a rate law and chemical mechanism for 12-MPA formation. Notz[4] and Gall[6] did subsequent rate measurements under the assumptions that some (2.5) analytical acid equivalents are consumed in the formation of the protonated Mo(VI) cations and that ionic strength must be held constant (at 2.0 M). The consequences of Beckwith not controlling the ionic strength affected only the magnitudes of the rate constants but not the reaction mechanism.[6] Because 12-MPA formation proceeds more slowly than the dimerizations and protonations of Mo(VI), steady state is established rapidly among all the prominent Mo(VI) complexes prior to their coordination with phosphate. Gall also performed some preliminary studies on β-12-MSA formation kinetics.[6] Despite all these past efforts, the rate equations were expressed in terms of total analytical Mo(VI) concentration without regard to Mo(VI) speciation. The first heteropolymolybdate formation rate equation expressed in terms of

individual Mo(VI) species concentrations was published recently.[41] In this paper, the α- and β-12-MSA formation kinetics were studied in HCl media at 1.0 M ionic strength; the initial concentrations of prominent Mo(VI) complexes were calculated by using Aveston's equilibrium constant data[53] and the HALTAFALL computer program.[54]

The repeat of 12-MSA and 12-MPA formation kinetics studies which consider individual Mo(VI) species is important for two reasons. First, this research considers and appreciates the consequences of the relative change in Mo(VI) speciation as the pH varies. Second, experimental rate equations in terms of individual species concentrations provide a better understanding of the actual chemistry of Mo(VI) polymerizations around phosphate or silicate and thus established a firmer foundation for the analytical methods used.

Chapter III. Reaction Models

A. Computer Programs to Calculate pH-Dependent Mo(VI) Speciation

In order to determine empirically the kinetic rate laws in terms of individual Mo(VI) complexes, equilibrium constant data must be used to calculate individual complex concentrations from given analytical acid and total Mo(VI) concentrations. In strong acid solutions ($pH < 0.9$), the equilibrium constant data reported by Cruywagen, et. al. from U.V. spectrophotometric measurements[42] were used. The acid and Mo(VI) mass balance equations were formulated under the assumption that only the five strong acid, monomeric and dimeric Mo(VI) cations[42] are present in significant concentrations. These equations are shown in Table III. Two FORTRAN II programs were written for the PDP-8/e minicomputer to solve the two simultaneous equations and calculate the concentrations of individual Mo(VI) complexes. The program MOLYB.FT was written for HNO_3 and $HClO_4$ solutions while MOSO4.FT was used for H_2SO_4 media. The programs first assume an initial estimate of $[H^+] = CH - 3CM$, corresponding to three protons required to convert MoO_4^{2-} to $HMoO_3^+$. Successively, the $[H^+]$ is used to calculate $[HMoO_3^+]$, then the $[HMoO_3^+]$ is used to calculate a new $[H^+]$, and so forth until the old and new values of $[HMoO_3^+]$ agree within a given tolerance. Usually, convergence of

Table III

Molybdenum (VI) Equilibria in Strong Acid Solutions

6 Unknowns: $[H^+]$, $[HMoO_3^+]$, $[MoO_3]$, $[HMo_2O_6^+]$, $[H_2Mo_2O_6^{2+}]$, $[H_3Mo_2O_6^{3+}]$

6 Equations:

Cruywagen's equilibrium constant data at 25°C and I = 3.0 M[42]

$$HMoO_3^+ \overset{K_1}{\rightleftharpoons} MoO_3 + H^+ \qquad K_1 = \frac{[HMoO_3^+]}{[H^+][MoO_3]} = 11.36$$

$$2\ HMoO_3^+ \overset{K_d}{\rightleftharpoons} H_2Mo_2O_6^{2+} \qquad K_d = \frac{[H_2Mo_2O_6^{2+}]}{[HMoO_3^+]^2} = 97 \pm 15$$

$$H^+ + HMo_2O_6^+ \overset{K_2}{\rightleftharpoons} H_2Mo_2O_6^{2+} \qquad K_2 = \frac{[H_2Mo_2O_6^{2+}]}{[H^+][HMo_2O_6^+]} = 4.7 \pm 2.0$$

$$H_2Mo_2O_6^{2+} + H^+ \overset{K_3}{\rightleftharpoons} H_3Mo_2O_6^{3+} \qquad K_3 = \frac{[H_3Mo_2O_6^{3+}]}{[H^+][H_2Mo_2O_6^{2+}]} = 0.24 \pm 0.07$$

Mass Balance equations

$$C_M = [MoO_3] + [HMoO_3^+] + 2[HMo_2O_6^+] + 2[H_2Mo_2O_6^{2+}] + 2[H_3Mo_2O_6^{3+}]$$

$$C_H = [H^+] + 2[MoO_3] + 3[HMoO_3^+] + 5[HMo_2O_6^+] + 6[H_2Mo_2O_6^{2+}] + 7[H_3Mo_2O_6^{3+}]$$

Results:

$$C_M = [HMoO_3^+]\left(1 + \frac{1}{K_1[H^+]}\right) + 2[HMoO_3^+]^2\left(\frac{K_d}{K_2[H^+]} + K_d + K_dK_3[H^+]\right)$$

$$C_H = [H^+] + [HMoO_3^+]\left(\frac{2}{K_1[H^+]} + 3\right) + K_d[HMoO_3^+]\left(\frac{5}{K_2[H^+]} + 6 + 7K_3[H^+]\right)$$

Thus, two quadratic equations with two unknowns must be solved simultaneously. The positive roots from the quadratic formulas are used.

Table III (cont'd)

Same situations as for the HNO_3 and $HClO_4$ solutions except for one more unknown, $[HSO_4^-]$, and one more equilibrium, $HSO_4^- \overset{K_a}{\rightleftharpoons} H^+ + SO_4^{2-}$

Since $K_1 = \dfrac{[H^+][SO_4^{2-}]}{[HSO_4^-]}$, $[HSO_4^-] = \dfrac{C_A[H^+]}{K_a + [H^+]}$.

Acid mass balance equation:

$$2\,C_A = [H^+] + [HSO_4^-] + 2[MoO_3] + 3[HMoO_3^+] + 5[HMo_2O_6^+] + 6[H_2Mo_2O_6^{2+}] + 7[H_3Mo_2O_6^{3+}]$$

Result:

$$2C_H[H^+](K_a + [H^+]) = [H^+]^3 + K_a[H^+]^2 + [HMoO_3^+]\left(\frac{2K_a + 2[H^+]}{K_1} + 3K_a[H^+] + 3[H^+]^2\right) + K_d[HMoO_3^+]^2\left(\frac{5K_a + 5[H^+]}{K_2} + 6[H^+](K_a + [H^+]) + 7K_3[H^+]^2(K_a + [H^+])\right) + C_H[H^+]$$

Thus, a quadratic equation and a cubic equation must be solved simultaneously. The cubic equation may be solved analytically be setting

$$A = 1 + 7K_3K_d[HMoO_3^+]^2$$

$$B = K_a - C_A + 3[HMoO_3^+] + K_d[HMoO_3^+]^2(6 + 7K_3K_a)$$

$$C = \frac{2[HMoO_3^+]}{K_1} - 2C_AK_a + 3K_a[HMoO_3^+] + K_d[HMoO_3^+]^2\left(\frac{5}{K_2} + 6K_a\right)$$

$$D = \frac{2K_a[HMoO_3^+]}{K_1} + \frac{5K_dK_a[HMoO_3^+]^2}{K_2}$$

and solving

Table III (cont'd)

$$P = \frac{B}{A},\ Q = \frac{C}{A},\ R = \frac{D}{A},\ a = \frac{3Q - P^2}{3},\ \&\ b = \frac{2P^3 - 9PQ + 27R}{27}.$$

Because the discriminant $\frac{b^2}{4} + \frac{a^3}{27} < 0$ for our chemical system, the cubic equation has three real roots. The solution which has physical meaning is $X = \cos^{-1}(\frac{-b}{2}\sqrt{\frac{27}{-a}})$ and $[H^+] = 2\sqrt{\frac{-a}{3}} \cos \frac{X}{3}$

consecutive approximations is achieved after three or four iterations. Both programs chain to MOOUT.FT, which displays calculated concentrations on the computer terminal. Based on the value of CA, which represents the HSO_4^- acid dissociation constant, MOOUT chains back to either MOLYB or MOSO4. A specified total Mo(VI) concentration (CM) of zero returns computer control to the OS/8 operating mode. Listings of MOLYB.FT, MOSO4.FT, and MOOUT.FT are found in the Appendix.

For the dilute acid solutions, the equilibrium constant equations and data from Aveston, et. al.[53] and mass balance equations are given in Table IV. The two resulting simultaneous equations can not be solved analytically, so a successive approximations algorithm must be used. The general-purpose HALTAFALL program mentioned earlier uses a successive approximations routine and the secant method to calculate equilibrium concentrations of complexes A_nB_m from their overall (not stepwise) formation constants from n A and m B.[54] This program, written in ALGOL-60 and run on a high-speed CDC Cyber 760 computer system, calculates the analytical acid concentration and Mo(VI) apecies concentrations:

(1) when C_{Mo} = 0.05 M and pH varies from 1.2 to 6.8,

(2) when pH = 1.2 (where β-12-MSA forms exclusively) and C_{Mo} varies from 0.01-0.20 M,

and (3) when pH = 3.6 (where α-12-MSA forms exclusively) and C_{Mo} varies from 0.01-0.20 M.

The ALGOL (Algorithmic Language, a precursor of PASCAL) programming language works well for numerical computations and simple data structures; the formal syntactic definitions express recursive procedures conveniently and give the operator the benefits of locally defined symbols.

Table IV

Molybdenum (VI) Equilibria in Dilute Acid Solution

Unknowns: $[H^+]$, $[MoO_4^{2-}]$, $[HMoO_4^-]$, $[H_2MoO_4]$, $[Mo_7O_{24}^{6-}]$, $[HMo_7O_{24}^{5-}]$, $[H_2Mo_7O_{24}^{4-}]$, $[Mo_8O_{26}^{4-}]$

Equations: Avestion's equilibrium constant data at 25°C and I = 1.0 M[53]

General form $p\ H^+ + q\ MoO_4^{2-} \rightleftharpoons H_p(MoO_4)_q^{p-2q}$

$$K_{eq} = \frac{[H_p(MoO_4)_q^{p-2q}]}{[H^+]^p[MoO_4^{2-}]^q}$$

p	q	log K_{eq}	p	q	log K_{eq}
1	1	3.53 (± 0.07)	9	7	57.46 (± 0.07)
2	1	7.26	10	7	60.84
8	7	52.80	12	8	71.56

Mass Balance equations

$$C_M = [MoO_4^{2-}] + [HMoO_4^-] + [H_2MoO_4] + 7[Mo_7O_{24}^{6-}] + 7[HMo_7O_{24}^{5-}] + 7[H_2Mo_7O_{24}^{4-}] + 8[Mo_8O_{26}^{4-}]$$

$$C_H = [H^+] + [HMoO_4^-] + 2[H_2MoO_4] + 8[Mo_7O_{24}^{6-}] + 9[HMo_7O_{24}^{5-}] + 10[H_2Mo_7O_{24}^{4-}] + 12[Mo_8O_{26}^{4-}]$$

For the two simultaneous equations, one is an 8th degree polynomial in $[MoO_4^{2-}]$ and the other is 12th degree in $[H^+]$.

In the execution of the program, the concentrations converged to within the given tolerance after about eight to twelve iterations through the successive approximations routine. In running the HALTAFALL program, an undefined array value for TOL(IA) was encountered when IA = 3 at the third line after label "SLINGOR:". The substitution of

'IF' IA > NA 'THEN' 'BEGIN' IA: = IA-1; 'GOTO' SLINGOR 'END';

for the second line after label "NYA1:" corrected this problem because the program then compared the defined value in TOL(2) rather than the undefined TOL(3). In addition, when the calculations in subroutine TOTBER required a value for TOLY(1), the statement "IA: = IA-1" had to be inserted between "KARL[IA]: = 1" and "'END'" in the fourth line of "SLINGOR:" so that a value for TOLY(1) could be specified.

Thus, from using HALTAFALL for the dilute acid solutions and MOLYB.FT and MOSO4.FT for the strong acid solutions, the initial reactant concentrations were calculated. Rate equations were experimentally determined from stopped-flow measurements of the maximum reaction rate as a function of these initial concentrations. Some graphs of the distribution of Mo(VI) species with C_M, C_H, C_A, and pH are plotted in Figures 3-6.

B. Modeling for 12-Molybdophosphate and 12-Molybdosilicate Formation

After the initial reaction rates were measured with various analytical acid, Mo(VI), and phosphate concentrations, these data were fit by a variety of rate laws with KINFIT[55], which is a general purpose curve-fitting program executed on the CDC Cyber 760 computer. With input of a rate law equation, concentration data and their variances, rate data and

Figure 3. Distribution of Molybdate Complexes in Dilute Acid Solution With variable C_M and constant pH (I = 1.0)

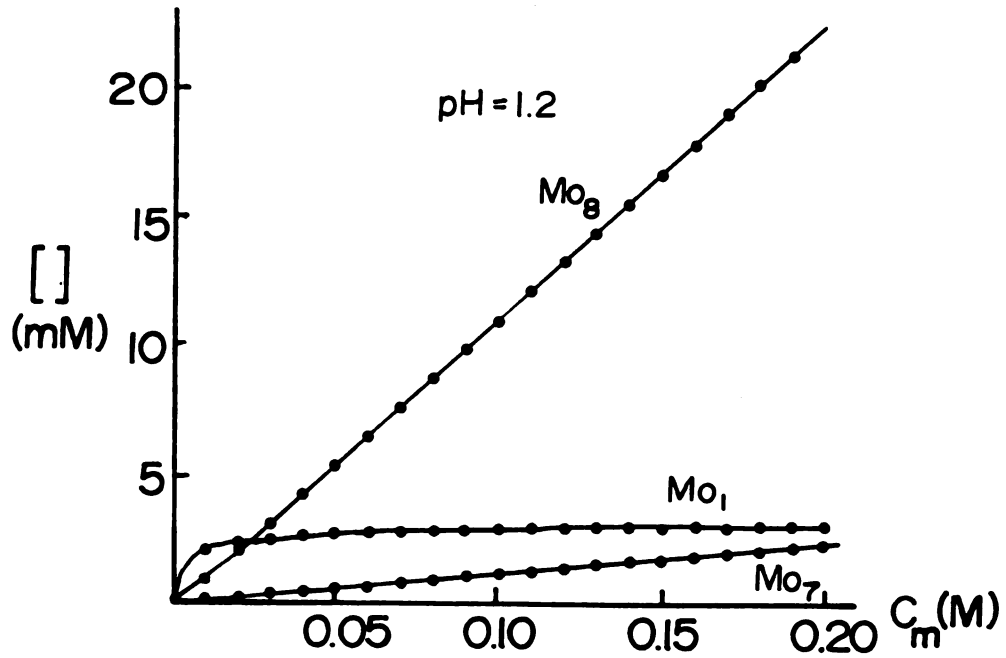
pH = 1.2
Mo8
Mo1
Mo7
[ ]
(mM)
20
15
10
5
0.05
0.10
0.15
0.20
Cm(M)

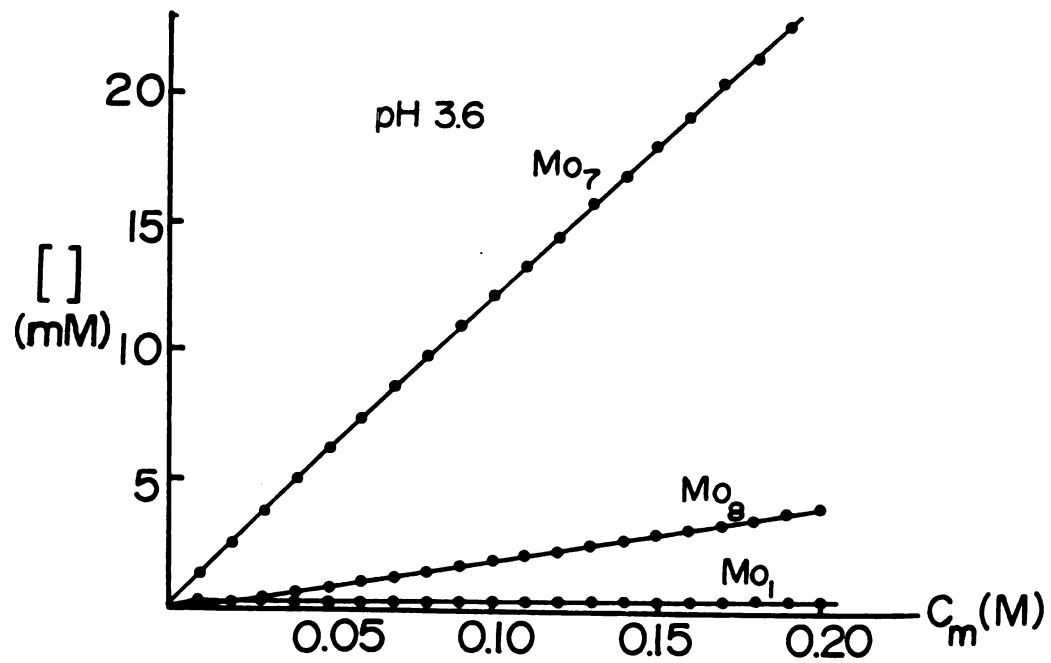
pH 3.6
Mo7
Mo8
Mo1
[ ]
(mM)
20
15
10
5
0.05
0.10
0.15
0.20
Cm(M)

Figure 4. Distributions of Molybdate Complexes in Strong Acid Solutions (HNO_3 , $HClO_4$) with Variable Total Molybdate Concentration

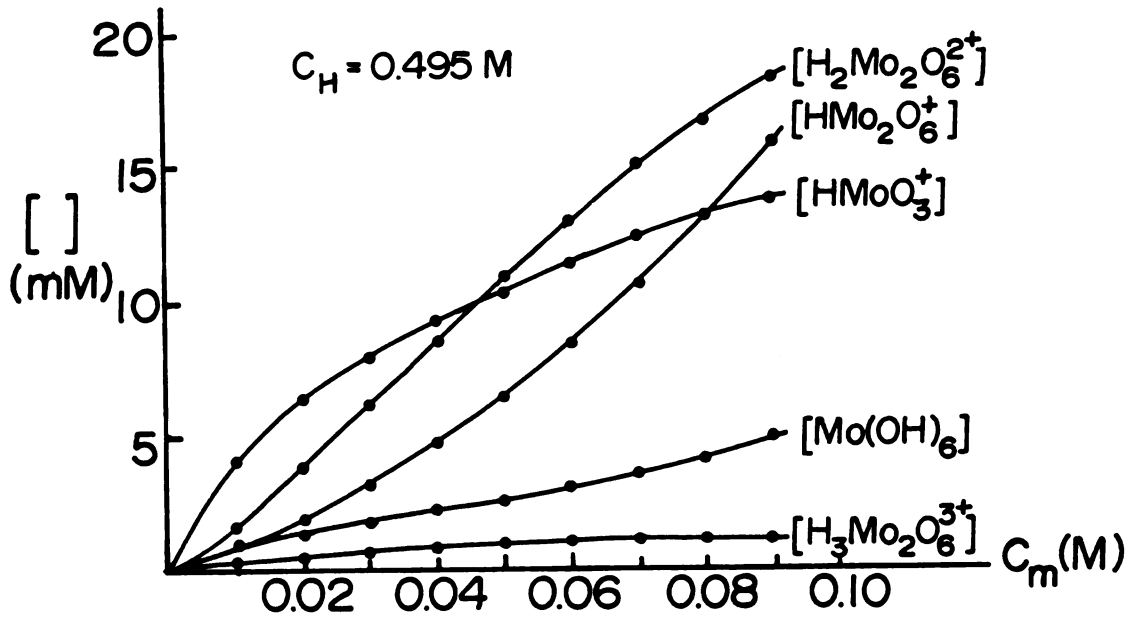
20
15
10
5
[ ]
(mM)
C_H = 0.495 M
$[H_2Mo_2O_6^{2+}]$
$[HMo_2O_6^{+}]$
$[HMoO_3^{+}]$
$[Mo(OH)_6]$
$[H_3Mo_2O_6^{3+}]$
C_m(M)
0.02
0.04
0.06
0.08
0.10

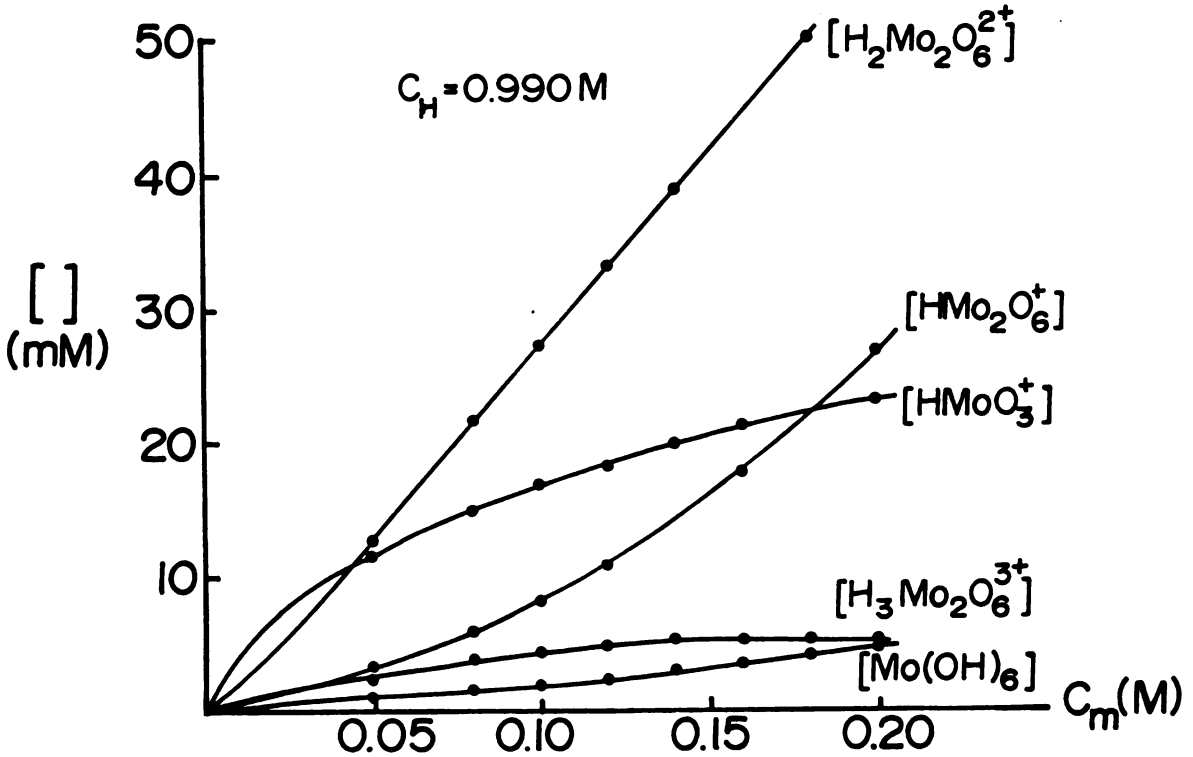
50
40
30
20
10
[ ]
(mM)
C_H = 0.990 M
$[H_2Mo_2O_6^{2+}]$
$[HMo_2O_6^{+}]$
$[HMoO_3^{+}]$
$[H_3Mo_2O_6^{3+}]$
$[Mo(OH)_6]$
C_m(M)
0.05
0.10
0.15
0.20

Figure 5. Distributions of Molybdate Complexes in Strong Acid Solutions (pH < 0.9, H_2SO_4) with Variable Total Molybdate Concentration

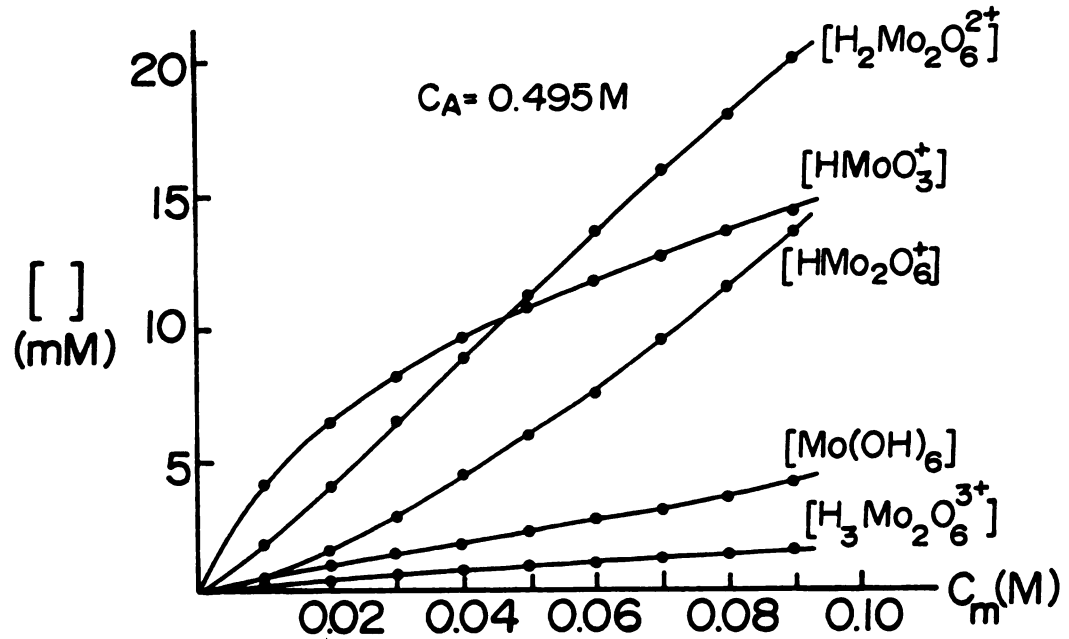
20
15
10
5
[ ]
(mM)
C_A= 0.495 M
$[H_2Mo_2O_6^{2+}]$
$[HMoO_3^+]$
$[HMo_2O_6^+]$
$[Mo(OH)_6]$
$[H_3Mo_2O_6^{3+}]$
0.02
0.04
0.06
0.08
0.10
C_m(M)

lu-

Con-

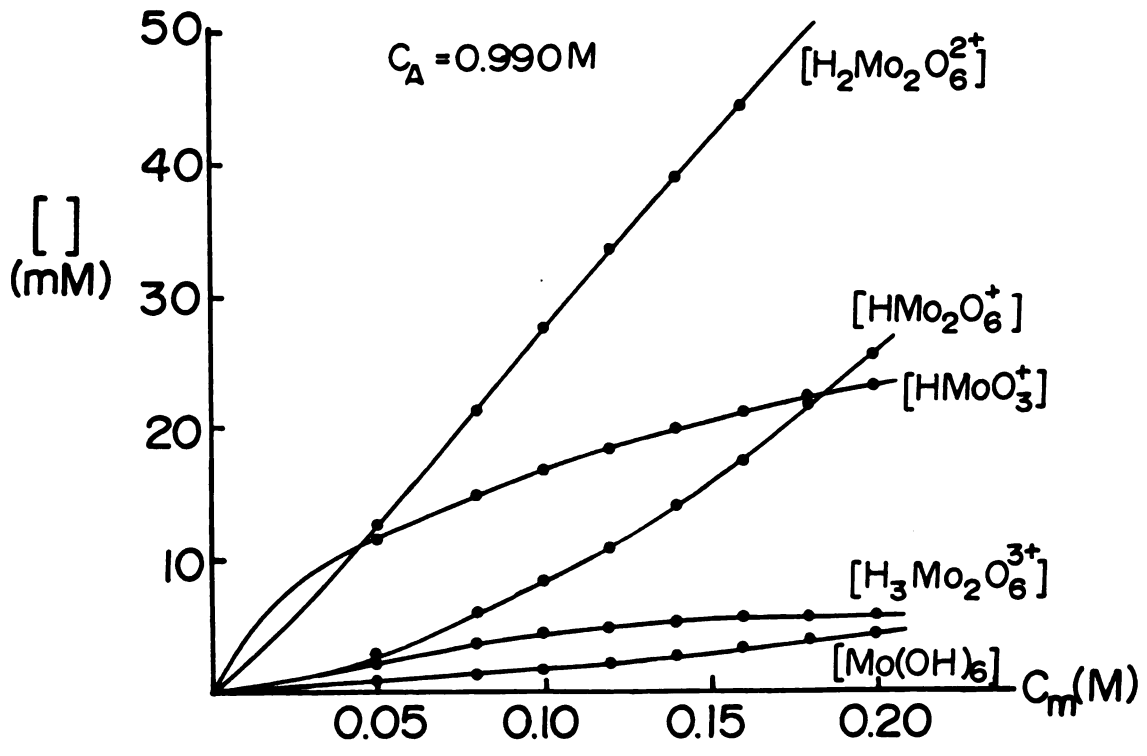
50
40
30
20
10
[ ]
(mM)
C_A = 0.990 M
$[H_2Mo_2O_6^{2+}]$
$[HMo_2O_6^+]$
$[HMoO_3^+]$
$[H_3Mo_2O_6^{3+}]$
$[Mo(OH)_6]$
0.05
0.10
0.15
0.20
C_m(M)

Figure 6. Distributions of Molybdate Complexes in Strong Acid Solutions (pH < 0.9) with Variable Acid Concentration

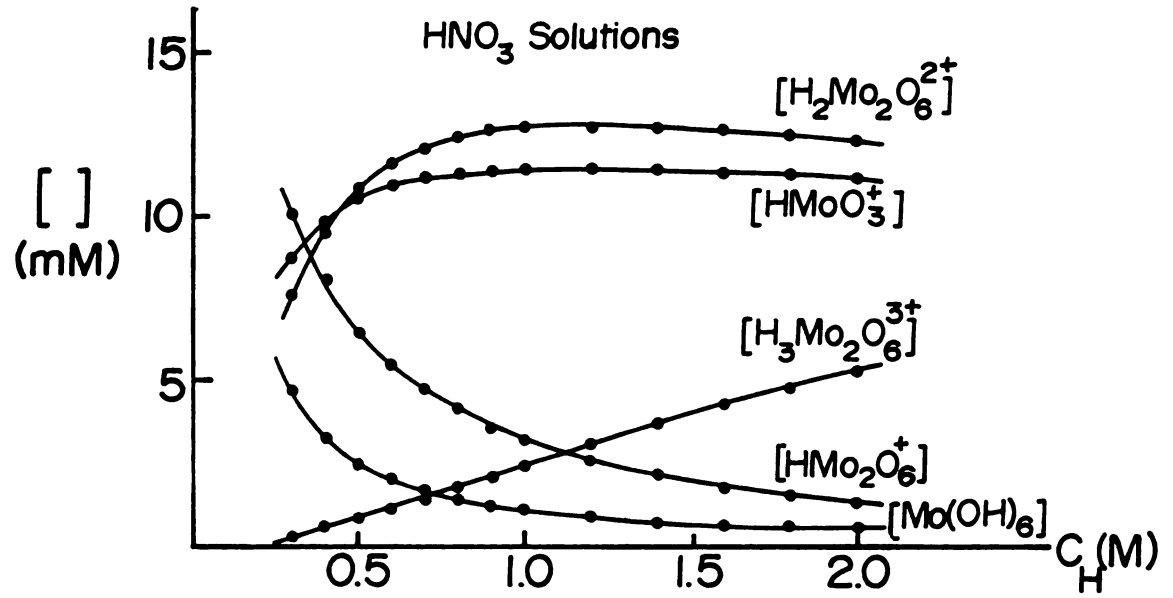
HNO3 Solutions
[ ]
(mM)
15
10
5
[H2Mo2O6 2+]
[HMoO3+]
[H3Mo2O6 3+]
[HMo2O6+]
[Mo(OH)6]
0.5
1.0
1.5
2.0
CH(M)

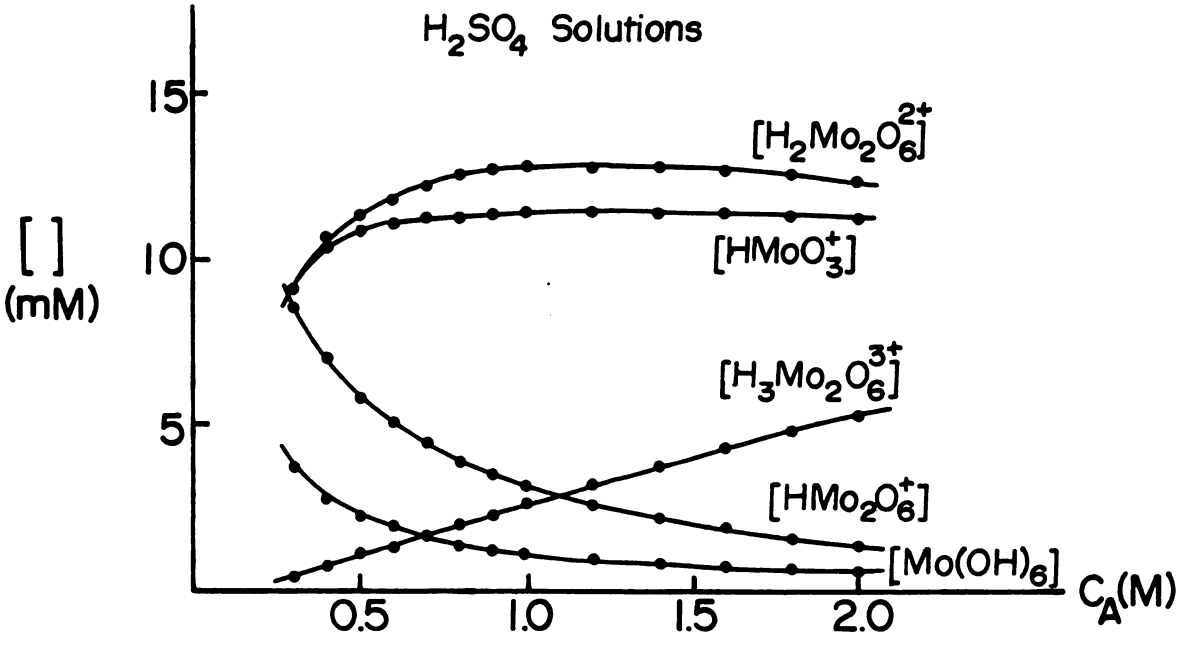
H2SO4 Solutions
[ ]
(mM)
15
10
5
[H2Mo2O6 2+]
[HMoO3+]
[H3Mo2O6 3+]
[HMo2O6+]
[Mo(OH)6]
0.5
1.0
1.5
2.0
CA(M)

their variances, and initial estimates of the rate law constants, KINFIT uses a Runga-Kutta procedure to adjust the rate law constants to give the best fit of the given rate equation within the variances of the rate and concentration data. Initial estimates for the adjustable rate law constants should be as close to the actual values as possible, or else the Runga-Kutta procedure might converge to a false residual minimum. The criteria for the best fit rate equations include a low sum of the residuals squared from KINFIT, low average relative standard deviations of the adjusted rate law constants, a low number of experimental data points not within 10% of the values calculated from the rate equation, and a random distribution of residuals as a function of the measured rates.

To reduce the number of possible rate equations to be fit with KINFIT, the rate equations from past research and from chemical modeling were considered. Javier, et. al. discovered that in the low acid limit ($0.14\ M < C_H < 0.20\ M$) 12-MPA formation follows second-order kinetics independent of the $[H^+]$, but that the kinetics shows a complicated dependence upon $[H^+]$ in more strongly acidic solutions.[51] The various rate equations for 12-MPA formation, along with their rate constants, are tabulated in Table V. Because the $[H^+]$ range that can be varied spans less than two orders of magnitude, there is not a $[H^+]$ range where only one of the denominator terms in $[H^+]$ predominates significantly over the others. It is thus not surprising that several different rate equations have been reported. The chemical modeling was based upon the stepwise coordination of a Mo(VI) species about phosphate. Table VI shows one such consecutive step mechanism with $HMo_2O_6^+$ as the ligand; a

Table V

Proposed Rate Equation for 12-MPA Formation

Javier, et. al.[51]

$$RATE = \frac{k_1[H_3PO_4][Mo(VI)]}{1 + \frac{k_{-1}[H^+]^4}{k_2[Mo(VI)]}}$$

Kinetics carried out in HNO_3 solutions only.

Notz[4]

$$RATE \propto \frac{1}{K_1[H^+]^9 + K_2[H^+]}$$

Constants K_1 and K_2 are dependent upon $[H_3PO_4]$ and $[Mo(VI)]$.

Beckwith[5]

$$RATE = \frac{K_1[Mo(VI)][H_3PO_4]}{\frac{K_2[H^+]^3}{[Mo(VI)]^5} + \frac{k_3[H^+]^4}{[Mo(VI)]^4} + K_4[H^+]^2 + 1}$$

for HNO_3, $HClO_4$ Sol'ns

$$RATE = \frac{K_1[Mo(VI)][H_3PO_4]}{1 + K_2[H^+]^2 + \frac{K_3[H^+]^4}{[Mo(VI)]^2} + \frac{K_4[H^+]^6}{[Mo(VI)]^4}}$$

for H_2SO_4 Sol'ns

Although Mo(VI) was specified as $HMo_2O_6^+$, no conclusive evidence has been given as to the specific Mo(VI) complexes involved.

Scheeline[52]

$$RATE = \frac{K_1[Mo(VI)][H_3PO_4]}{\frac{K_2[H^+]^7}{[Mo(VI)]^4} + \frac{K_3[H^+]^4}{[Mo(VI)]^3} + K_4[H^+]^2 + 1}$$

Gall[7] (Same RATE as Beckwith reported for HNO_3)

In this study, ionic strength was controlled, measurements were made under automated computer control, and $[H^+] = C_H - 3C_M$, rather than C_H, were used for $[H^+]$ dependence.

Table VI

A Mechanism for 12-MPA Formation from $HMo_2O_6^+$ and the Step to Form $H_{3-m-n}PMo_{12}^{(m+n)-}$ Presumed to be Rate-Determining

1	$H_3PO_4 + HMo_2^+ \underset{}{\overset{k_1}{\rightleftharpoons}} H_{3-m}PMo_2^{m-} + (m+1)H^+$	$m = 0,1,2,3$
2	$H_{3-m}PMo_2^+ \underset{k_{-2}}{\overset{k_2}{\rightleftharpoons}} H_{3-m-n}PMo_2^{(m+n)-} + n\ H^+$	$n = 0,1,2,3$
3	$H_{3-m-n}PMo_2^{(m+n)-} + P_1HMo_2^+ \underset{k_{-3}}{\overset{k_3}{\rightleftharpoons}} H_{3-m-n}PMo_{2P_1+2}^{(m+n)-} + P_1H^+$	$P_1 = 0,1,2,3,4,5$
4	$H_{3-m-n}PMo_{2P_1+2}^{(m+n)-} + P_2HMo_2^+ \underset{k_{-4}}{\overset{k_4}{\rightleftharpoons}} H_{3-m-n}PMo_{2P_1+2P_2+2}^{(m+n)-} = P_2H^+$	$P_2 = 0,1,2,3,4,5$
5	$H_{3-m-n}PMo_{2P_1+2P_2} + P_3HMo_2^+ \underset{k_{-5}}{\overset{k_5}{\rightleftharpoons}} H_{3-m-n}PMo_{2P_1+2P_2+2P_3+2}^{(m+n)-} + P_3H^+$	$P_3 = 0,1,2,3,4,5$
6	$H_{3-m-n}PMo_{2P_1+2P_2+2P_3+2} + P_4HMo_2^+ \underset{k_{-6}}{\overset{k_6}{\rightleftharpoons}} H_{3-m-n}PMo_{12-2P_5}^{(m+n)-} + P_4H^+$	$P_4 = 0,1,2,3,4,5$

Table VI (cont'd)

7 $H_{3-m-n}PMo_{12-2P_5}^{(m+n)-} + P_5HMo_2^+ \xrightarrow{k_7} H_{3-m-n}PMo_{12}^{(m+n)-} + P_5H^+$ $\quad P_5 = 0,1,2,3,4,5$

8 $H_{3-m-n}PMo_{12}^{(m+n)-} \underset{}{\overset{\text{rapid}}{\rightleftharpoons}} PMo_{12}^{3-} + (3-m-n)\ H^+$ $\quad P_1+P_2+P_3+P_4+P_5 = 5$

$$\text{RATE} = \frac{K_1[HMo_2^+]^6[H_3PO_4]}{K_2[H^+]^{6+m+n-P_5} + K_3[HMo_2^+]^{P_5}[H^+]^{P_3+P_2+P_1+m+n+1} + K_4[HMo_2^+]^{P_5+P_4}[H^+]^{P_2+P_1+m+n+1}}$$

(omit this term if $P_4=P_3=P_2=P_1=0$) (omit if $P_3=P_2=P_1=0$)

$$+ K_5[HMo_2^+]^{P_5+P_4+P_3}[H^+]^{P_1+m+n+1} + K_6[HMo_2^+]^{5-P_1}[H^+]^{m+n+1} + K_7[HMo_2^+]^5[H^+]^{m+1} + [HMo_2^+]}$$

(omit if $P_2=P_1=0$) (omit if $P_1=0$) (omit if $n=0$)

where

$$K_1 = k_1 \quad K_7 = \frac{k_{-1}}{k_2} \quad K_2 = \frac{k_{-1}k_{-2}k_{-3}k_{-4}k_{-5}k_{-6}}{k_2k_3k_4k_5k_6k_7} \quad K_3 = \frac{k_{-1}k_{-2}k_{-3}k_{-4}k_{-5}}{k_2k_3k_4k_5k_6}$$

$$K_4 = \frac{k_{-1}k_{-2}k_{-3}k_{-4}}{k_2k_3k_4k_5} \quad K_5 = \frac{k_{-1}k_{-2}k_{-3}}{k_2k_3k_4} \quad K_6 = \frac{k_{-1}k_{-2}}{k_2k_3}$$

similar model and rate equation can be diagramed and derived for the other Mo(VI) complexes. The model considers the possibility that one or more of the proton dissociations may not be rapid compared with the Mo(VI) complexation steps (thus, nonnegative integers m and n were defined such that $m + n \leq 3$) and that one or more of the Mo(VI) polymerization steps may not proceed rapidly (thus, nonnegative integers P_1, P_2, P_3, P_4, and P_5 were defined such that $P_1 + P_2 + P_3 + P_4 + P_5 = 5$). This model assumes that the last step to form $H_{3-m-n}PMo_{12}^{(m+n)-}$ is rate-determining; other models with different forms of the rate law may be derived if any other step is presumed to be rate-determining. The rate law and mechanism reported by Javier and coworkers[51] presumed the second step (to form $H_{3-m-n}PMo_4^{(m+n)-}$) to be rate-determining, with the subsequent steps taking place more rapidly. Beckwith's mechanism[52] fits the model presented in Table VI, with m=1, n=2, $P_1=P_2=P_3=0$, $P_4=4$, and $P_5=1$. The mechanisms for H_2SO_4 solutions involve the $H_{3-m-n}PMo_{10}^{(m+n)-}$ formation (the P_4 step) as the rate-determining step with m=1, n=2, $P_3=2$, and $P_4=2$ for Beckwith's rate law and with m=1, n=2, $P_3=3$, and $P_4=1$ for Scheeline's rate law. All of these mechanisms assume that phosphate combines with a Mo(VI) species in the first step, as shown by Javier, *et al.*[51], and that the final product 12-MPA is completely deprotonated in the acidic solution, as reported by Murata and Kiba.[56]

Based upon preliminary measurements, Gall found that 12-MSA forms in a similar mechanism as in Table VI.[6] However, the preliminary measurements from this research (see Section B, Chapter V) indicate that 12-MSA is not formed appreciably in strongly acidic solutions where

Mo(VI) complexes are positively charged; this observation has been reported and utilized in analytical techniques in which phosphate and silicate are determined simultaneously.[57] Similarly, 12-MPA was not observed to form in more dilutely acidic solutions, although phosphate can react with Mo(VI) anions to form a colorless heteropoly intermediate.[58] Thus, the chemical system under which 12-MPA formation kinetics will be studied is noticeably different than the system to be used for the 12-MSA kinetics study.

In dilutely acidic solution, the kinetics of α- and β-12-MSA formation in terms of individual Mo(VI) anions and polyanions was studied spectrophotometrically.[41] The β-12-MSA formation followed pseudo first-order kinetics with respect to silicon; the overall rate was given by measurements $\frac{d[\beta\text{-12-MSA}]}{dt} = \frac{K_1[Mo_1][Mo_8][Si]}{K_2 + [Mo_8]}$ with K_1 = 8.74 x 10^7 l g-ion^{-1}min^{-1} and K_2 = 6.17 g-ion l^{-1} at 25.0°C., 1.0 M ionic strength, and pH 1.2 (acidified with HCl). Mo_1 refers to monomeric Mo(VI) species, and Mo_8 refers to octameric species. Since the protonation of the various complexes proceeds rapidly, specific species of MoO_4^{2-}, $HMoO_4^-$, and H_2MoO_4 were not considered in the rate equation. The Mo_8 species in the equation was postulated because the pH where the pseudo first-order rate constant is maximum (pH 1.8) corresponds to the pH region where $Mo_8O_{26}^{4-}$ is the predominant Mo(VI) species. α-12-MSA formation followed more complicated kinetics, requiring an exponential model with two exponential terms. The reaction schemes consistent with the model and observed chemical phenomena are shown in Table VII. X and Y refer to reactants or intermediates that convert chemically to α-12-MSA. The postulation of these schemes requires a third silicon species

Table VII

Possible Reaction Schemes for α-12-MSA Formation

Competitive-Consecutive Reactions	Consecutive Reactions with Reversible Step	Parallel Reactions
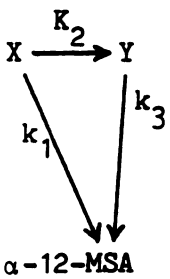	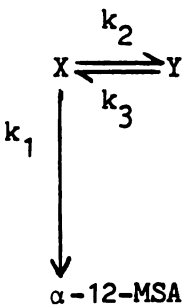	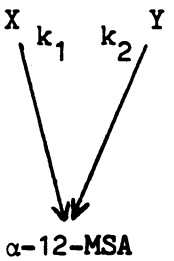

along with the silicon reactant (X) and α-12-MSA (Z). At present, it is unknown whether the third species is another condensed or depolymerized silicate or another molybdosilicate; the possibility of β-12-MSA as the third species has been ruled out, however.[41]

Chapter IV. Equilibrium Studies

A. Equilibrium Studies of 12-Molybdophosphate Formation

1. Spectrophotometric Instrumentation

In hopes of eliminating some possible mechanisms and rate laws from further consideration, the chemical equilibria among 12-MPA, H_3PO_4, and Mo(VI) were re-examined. Theoretically, the sum of all the steps in a valid chemical mechanism should yield an overall reaction equation consistent with the stoichiometry of the process considered. The equilibrium studies were carried out on a spectrophotometer consisting of several individual modules (GCA/McPherson EU 700 Series). The individual components are listed below.

Heath Tungsten light source	EU-701-50
GCA/McPherson monochromator with programmable filter attachment	EU-700-56
Heath sample cell module	EU-701-11
Heath photomultiplier module	EU-701-30
Heath photometric readout module	EU-703-31
Constant temperature bath	

The slew-driven monochromator contained its own programmable filter attachment which was kept on an automatic adjustment mode throughout the equilibrium experiments. The slit width was 1000 μm,

which corresponded to a spectral bandpass of 2.0 nm. The accuracy of the monochromator was checked by a spectrophotometric scan of a holmium oxide filter. The monochromator exhibited a positive error of +1.7 nm with an average deviation of $\pm$0.1 nm about this positive error. The sample cell module was modified to house a brass, thermostated cuvette block constructed by Ingle[59] and a water-driven magnetic stirrer (G.F. Smith Co.). Because of the large monochromator light throughput with the wide slit width, a photomultiplier tube voltage of around -400v was sufficient to read solution transmittances on the 10^{-6} amp scale of the readout module. A potentiometer on the readout module was used to adjust the 0% T (shutter closed), and the 100% T was adjusted by varying the photomultiplier voltage to give full-scale meter deflection for the distilled-deionized (DDI) water blank. Except for spectrophotometric scans conducted from 350 nm to 450 nm with a Cary 17 instrument, all the spectrophotometric experiments for the equilibrium studies were measured with the modular Heath system at 400, 410, or 430 nm. Beckman quartz cuvettes were used, even though ordinary glass cuvettes would have sufficed for the wavelengths used.

2. Reagents Used and Standardizations

The reagents and solutions used in the 12-MPA and 12-MSA studies were prepared as follows. Stock solutions approximately 5 M in HNO_3, H_2SO_4, and $HClO_4$ were prepared by dilution with DDI water of the corresponding concentrated acid solutions available commercially, from Fisher Scientific Co. (HNO_3 and H_2SO_4) and Mallinckrodt, Inc. (70% $HClO_4$). The acid stock solutions were standardized by titrations with NaOH solution which had been previously standardized with KHP.

Contamination from H_3PO_4 and silicate in these concentrated acids was determined to be negligible from blank measurements. The 0.5 M stock Mo(VI) solution was prepared, without further purification, from the $Na_2MoO_4 \cdot 2H_2O$ reagent (Baker Chemical Co.). A stock 10^{-2} M phosphate solution was similarly prepared from reagent grade KH_2PO_4 (Mallinckrodt, Inc.). A 10^{-2} M silicate stock solution was prepared from $Na_2SiO_3 \cdot 9H_2O$ (Allied Chemical and Dye Corp.) and standardized by titrations with a diluted HNO_3 solution immediately after preparation in order to avoid interference form airborne CO_2. The titration with acid was carried to the bromphenol red endpoint as in a carbonate-HCl titration. A 5 M $NaClO_4$ (G. Frederick Smith Chemical Co.) reagent was determined to be free of silicate contamination. The solutions were stored in polyethylene bottles to avoid additional silicate contamination from the glassware. The second H_2SO_4 acid dissociation constant pK_2, required for computer calculations with the MOSO4.FT program, was measured at ionic strengths 1.0 M and 3.0 M by titrations of 0.1 M $NaHSO_4$ with 1 M NaOH. The pH was measured with a glass electrode as various increments of NaOH titrant were added. The electrodes and pH meter were calibrated with 0.05 m tetraoxalate buffer (pH = 1.679 at 25°C).[60] The value of pK_2, calculated from pH data nearly halfway to the equivalence point, was found to be 1.51 ± 0.04 at I = 1.0 M, and 1.12 ± 0.04 at I = 3.0 M.

3. Stoichiometric Studies

The studies of equilibria among 12-MPA, H_3PO_4, and Mo(VI) were conducted with two different experimental designs. One such design was a continuous variations study carried out at constant ionic strength

and temperature, but at different $[H^+]$ for the different acidic media. The stoichiometric studies were implemented with the experimental design used by Crouch, et. al.[31] These experiments were repeated here with ionic strength control and more nearly monochromatic incident radiation. In the previous research[31] the ionic strength was not controlled, and a filter photometer was used.

The basis for the experimental procedure begins with the logarithmic expression for the 12-MPA equilibrium constant.

$$\log K_f = \log[12\text{-MPA}] + Z \log[H^+] - x \log[H_3PO_4] - Y \log[Mo(VI)]$$

$$\text{from } X\ H_3PO_4 + Y\ Mo(VI) \rightleftharpoons (12\text{-MPA})^{3-} + Z\ H^+ \qquad (1)$$

With the assumptions that only 12-MPA absorbs light of a particular wavelength and that 12-MPA obeys Beer's Law, $\Delta A_\lambda = \varepsilon_\lambda b [12\text{-MPA}]$, at that wavelength, a rearrangement of terms in the above equation gives $\log \Delta A_\lambda = \log K_f \varepsilon b + X \log[H_3PO_4] + Y \log[Mo(VI)] - Z \log[H^+]$. The use of ΔA to denote an increase in absorbance corrects for a negligibly changing background absorbance at wavelength λ. If 12-MPA were the only molybdophosphate present, the use of mass balance equations in phosphate (total concentration C_P), molybdate (C_M), and hydrogen ions ($[H^+]$) would transform the equation to

$$\log \Delta A_\lambda = \log K_f \varepsilon_\lambda b + X \log(C_P - X[12\text{-MPA}]) + Y \log(C_M - Y[12\text{-MPA}])$$

$$-Z \log([H^+] + Z[12\text{-MPA}])$$

The use of $[H^+]$ instead of C_H considers that a portion of the acid protons were consumed in protonating the Mo(VI) complexes from MoO_4^{2-}.

If experimental conditions were established such that a small but measurable absorbance increase is measured and that 12-MPA has a high absorptivity ε_λ, then the second terms in the log expressions may be ignored. Thus, by varying C_P while holding C_M and $[H^+]$ constant and measuring ΔA_λ at each C_P, followed by subsequent linear regression of log ΔA_λ versus log C_P, one obtains the coefficient X as the slope of the regression. Similarly, the linear regressions of log ΔA_λ with log C_M or log$[H^+]$ should give values for stoichiometric coefficients Y and Z, respectively.

Cary 17 spectrophotometric scans from 350-450 nm were made on a 0.05 M Mo(VI) and 1.386 M H_2SO_4 solution and a 0.025 M Mo(VI), 0.693 M H_2SO_4, and 0.0025 M phosphate solution. The latter solution exhibited considerably more absorption in the 400-440 nm wavelength range relative to the absorption by the first solution, presumably due to the polymerization of twelve Mo(VI) atoms in 12-MPA.[56]

Thus, the increase in absorbance at 430 nm was measured as C_P, C_M, and $[H^+]$ were successively varied in HNO_3 and H_2SO_4 media at different ionic strengths. The temperature bath and brass cuvette block maintained the solution temperature within the cuvette at 25.0 $\pm$ 0.1°C. The actual concentrations and ionic strengths are tabulated in Table VIII. The slopes of the linear regressions are tabulated by ionic strength in Table IX. Plots of the stoichiometric coefficients as a function of ionic strength are graphed in Figures 7, 8, and 9. The ionic strengths for the solutions used by previous researchers[31] were calculated, and the values for X, Y, and Z in HNO_3 and H_2SO_4 solutions coincide, within experimental error, with those values predicted from the graphs (Figures 7-9) at those ionic strengths.

Table VIII

Concentration Data Used in 12-MPA Stoichiometry Studies

Concentration Data for HNO_3 Solutions ($25^{\circ}C$)

Varied	C_M	C_P	C_H	I
KH_2PO_4	0.050 M	0.1-0.4 mM	0.495 M	0.75, 3.0 M
Na_2MoO_4	4.95-14.6 mM	2.50 mM	0.495 M	0.75, 1.75, 3.0 M
HNO_3	0.025 M	2.50 mM	0.495-1.014 M	1.2,1.5,2.0,2.5,3.0 M

Concentration Data for H_2SO_4 Solutions ($25.0^{\circ}C$)

KH_2PO_4	0.090 M	0.1-0.9 mM	0.792 M	0.75,2.0,3.0 M
Na_2MoO_4	4.95-14.6 mM	2.50 mM	0.495 M	0.5,1.12,1.75,3.0 M
H_2SO_4	0.0125 M	2.50 mM	0.69-1.09 M	1.0,1.5,2.5,3.0 M

Table IX

Stoichiometric Coefficient X, Y, Z for 12-MPA Formation as a Function of Ionic Strength

Linear Regression	Ionic Strength(M)	Slope
	HNO_3 Solutions	
log ΔA vs. log C_P	0.75	X = 0.99 $\pm$ 0.05
log ΔA vs. log C_P	3.0	X = 0.96 $\pm$ 0.05
log ΔA vs. log C_M	0.75	Y = 6.25 $\pm$ 0.40
log ΔA vs. log C_M	1.75	Y = 4.53 $\pm$ 0.20
log ΔA vs. log C_M	3.0	Y = 2.66 $\pm$ 0.15
log ΔA vs. log $[H^+]$	1.20	Z = 3.34 $\pm$ 0.35
log ΔA vs. log $[H^+]$	1.5	Z = 2.40 $\pm$ 0.25
log ΔA vs. log $[H^+]$	2.0	Z = 1.29 $\pm$ 0.20
log ΔA vs. log $[H^+]$	2.5	Z = 1.03 $\pm$ 0.10
log ΔA vs. log $[H^+]$	3.0	Z = 0.81 $\pm$ 0.10
	H_2SO_4 Solutions	
log ΔA vs. log C_P	0.75	X = 0.95 $\pm$ 0.05
log ΔA vs. log C_P	2.0	X = 0.95 $\pm$ 0.04
log ΔA vs. log C_P	3.0	X = 0.94 $\pm$ 0.05
log ΔA vs. log C_M	0.5	Y = 4.59 $\pm$ 0.55
log ΔA vs. log C_M	1.12	Y = 2.36 $\pm$ 0.20
log ΔA vs. log C_M	1.75	Y = 1.77 $\pm$ 0.15
log ΔA vs. log C_M	3.0	Y = 0.89 $\pm$ 0.10
log ΔA vs. log $[H^+]$	1.0	Z = 5.43 $\pm$ 0.45
log ΔA vs. log $[H^+]$	1.5	Z = 4.22 $\pm$ 0.30
log ΔA vs. log $[H^+]$	2.5	Z = 3.12 $\pm$ 0.20
log ΔA vs. log $[H^+]$	3.0	Z = 3.02 $\pm$ 0.10

Figure 7. Variation of the Phosphoric Acid Coefficient (X) with Ionic Strength

C_M = 0.050 M (HNO_3); 0.090 M (H_2SO_4) C_H = 0.495 M; C_P = (1.0-9.1) x 10^{-4} M C_A = 0.792 M

Error bars are within the circles drawn.

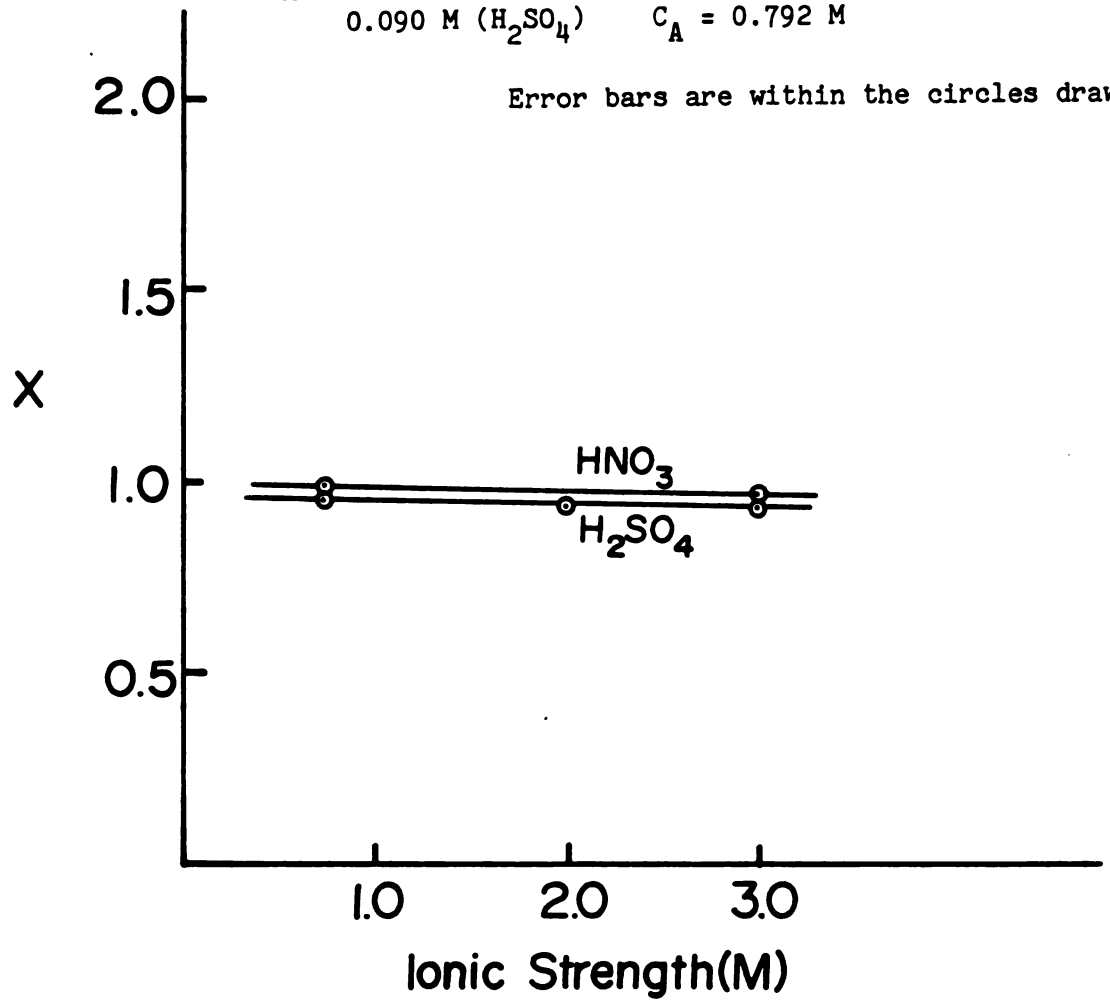

Figure 8. Variation of the Molybdate Coefficient (Y) with Ionic Strength

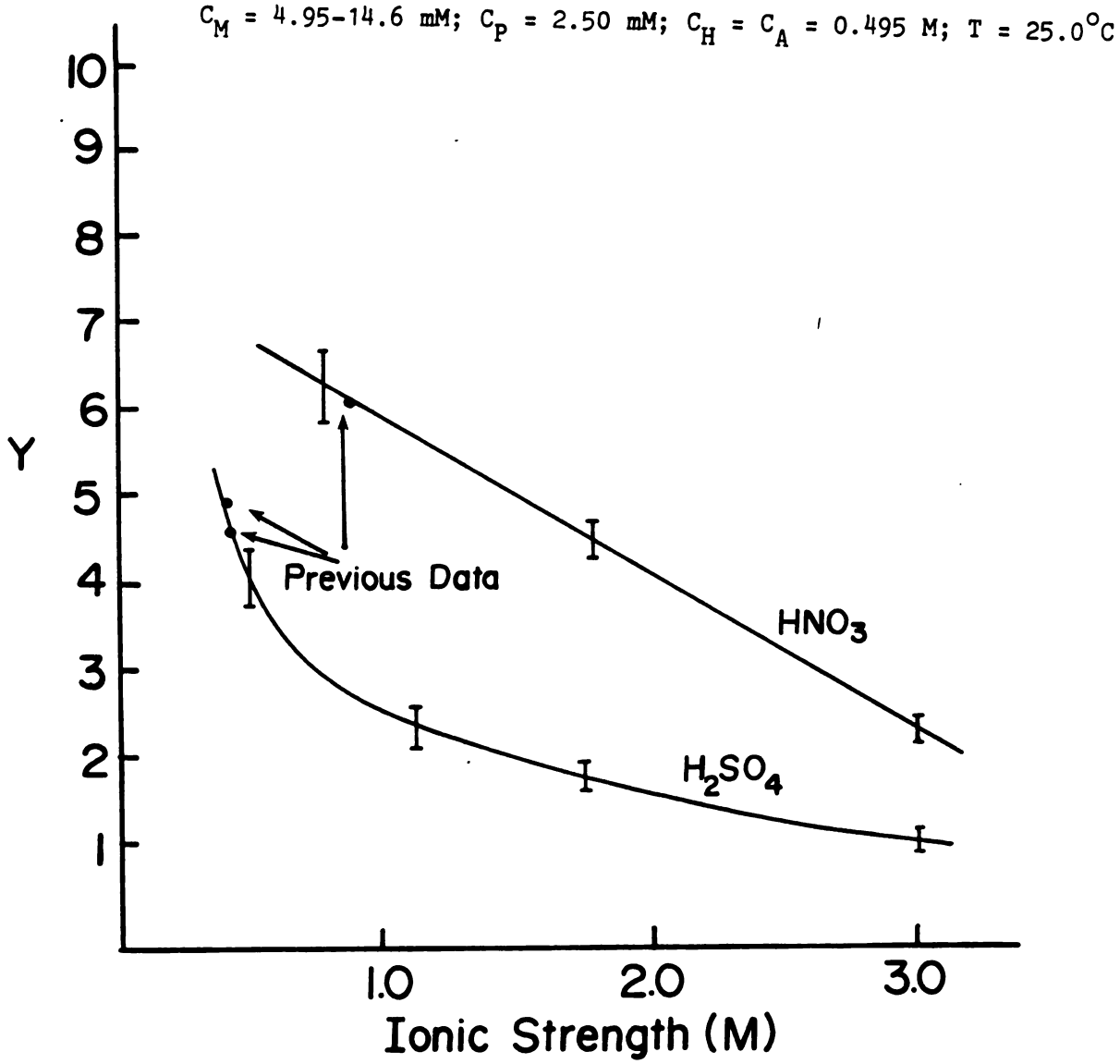

Figure 9. Variation of the Hydrogen Ion Coefficient (Z) with Ionic Strength

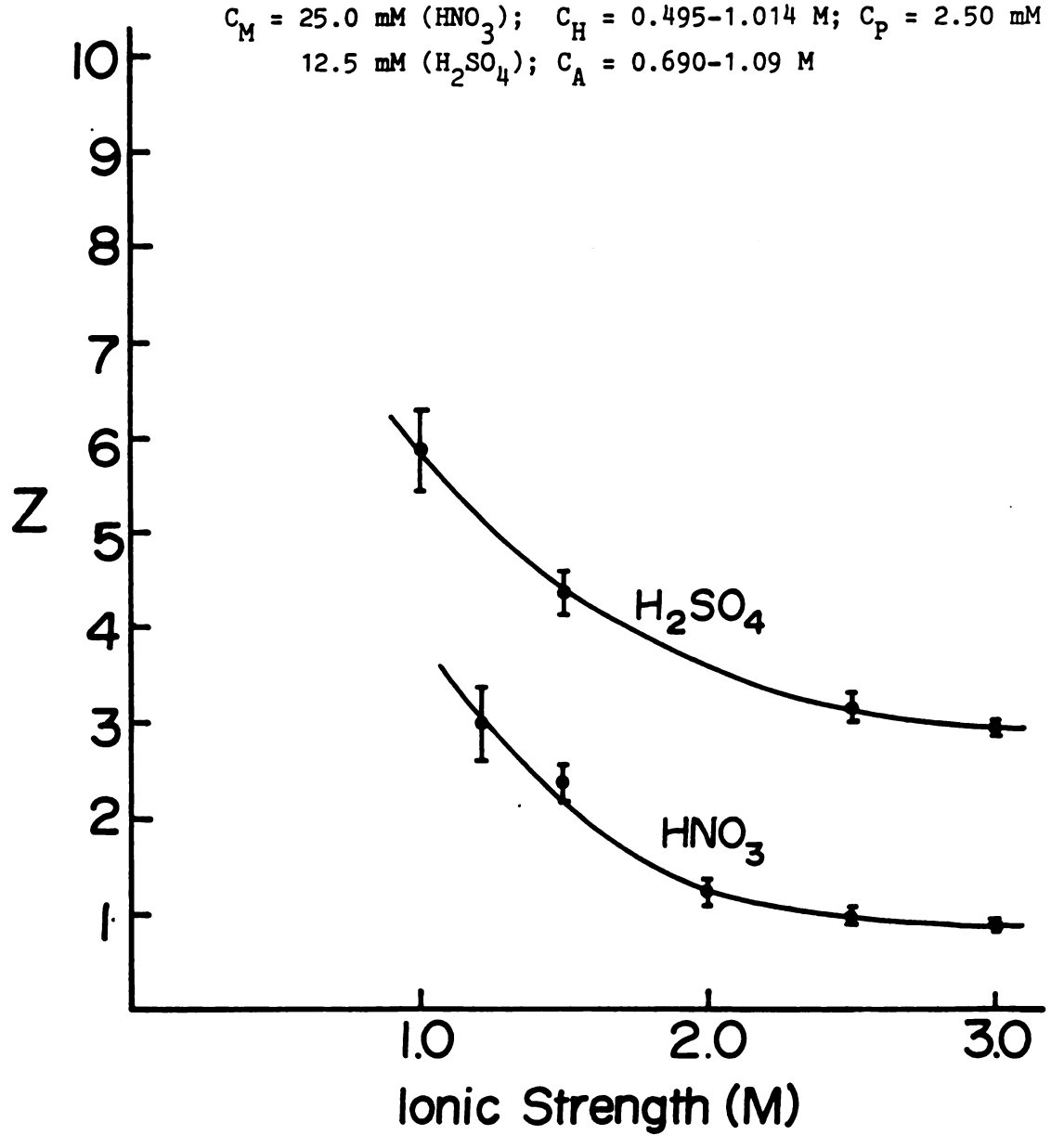

The values for X seem to be independent of ionic strength. This result is expected since most of the phosphate exists as neutral H_3PO_4 in the strong acid solutions and the neutral species would not be as subject to ionic strength effects or variations in the activity coefficient as charged species would. Furthermore, the value X = 1.0 is consistent with the known crystallographic structure and empirical formula of the 12-MPA complex.[61] The values for Y and Z vary significantly with ionic strength, in contrast. The Y values observed are all less than twelve; even extrapolation of the graphs in Figure 8 to zero ionic strength produces Y-intercepts less than twelve. The proposed chemical model of 12-MPA formation from H_3PO_4 and Mo(VI) monomers and dimers cannot explain the large variation of Y and Z coefficients with ionic strength. In addition, much difficulty exists in determining the activity coefficients of triply-charged 12-MPA and other charged species in aqueous solution as the ionic strength is varied from 0.5 M to 3.0 M.

4. Some Unsuccessful Studies with Methyl Violet Indicator and Strong Acid Potentiometry

Two other experimental procedures were tried in order to obtain a value for the H^+ coefficient Z. Both procedures attempted to measure the increase in $[H^+]$ after a specified amount of phosphate is added to an acidified molybdate solution. The spectrophotometric method was supposed to measure the absorbance change of a pH indicator as hydrogen ions are released during 12-MPA formation. The electrochemical method measured the increase in pH glass electrode potential as additional H^+ ions are released into solution.

The pH dye indicator methyl violet was selected for its availability and its color transition pH (0.1-3.0) being within the $[H^+]$ range in the strong acid solutions. Cary 17 spectrophotometric scans of acidic (pH 0.0) and basic (pH 7.0) solutions with equal methyl violet concentrations revealed 580 nm as a suitable working wavelength where the methyl violet deprotonated form absorbs substantially better than the corresponding yellow, protonated form (see Figure 10). The structure of methyl violet and its acidic sites is shown below.

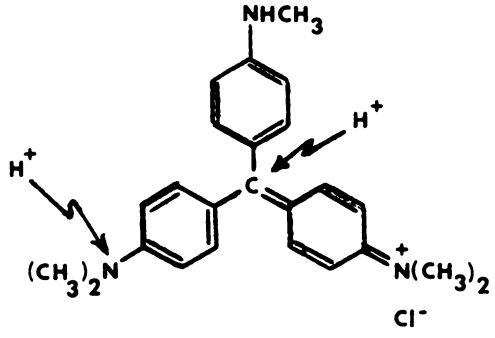

Methyl violet--violet, deprotonated form

The experiment was not conducted further for two reasons. First, since the colorimetric dye species are all cationic, the transition pH range between the yellow and violet colors theoretically should shift to greater pH values as ionic strength increases, if the Debye-Huckel Equation is valid. Methyl violet solutions were prepared in a series of HNO_3 solutions of different pH values and at two different ionic strengths. Absorbance measurements of these solutions and the subsequent plot shown in Figure 11 support the theoretical predictions. As a result, the 580 nm absorbance change is not large enough in the pH 0.3

Figure 10. Visible Absorption Spectra of the Protonated and Deprotonated Methyl Violet Indicator Species

(vs. DDI-H_2O Blank)

Ionic Strength Controlled with $NaClO_4$, T = 25.0°C

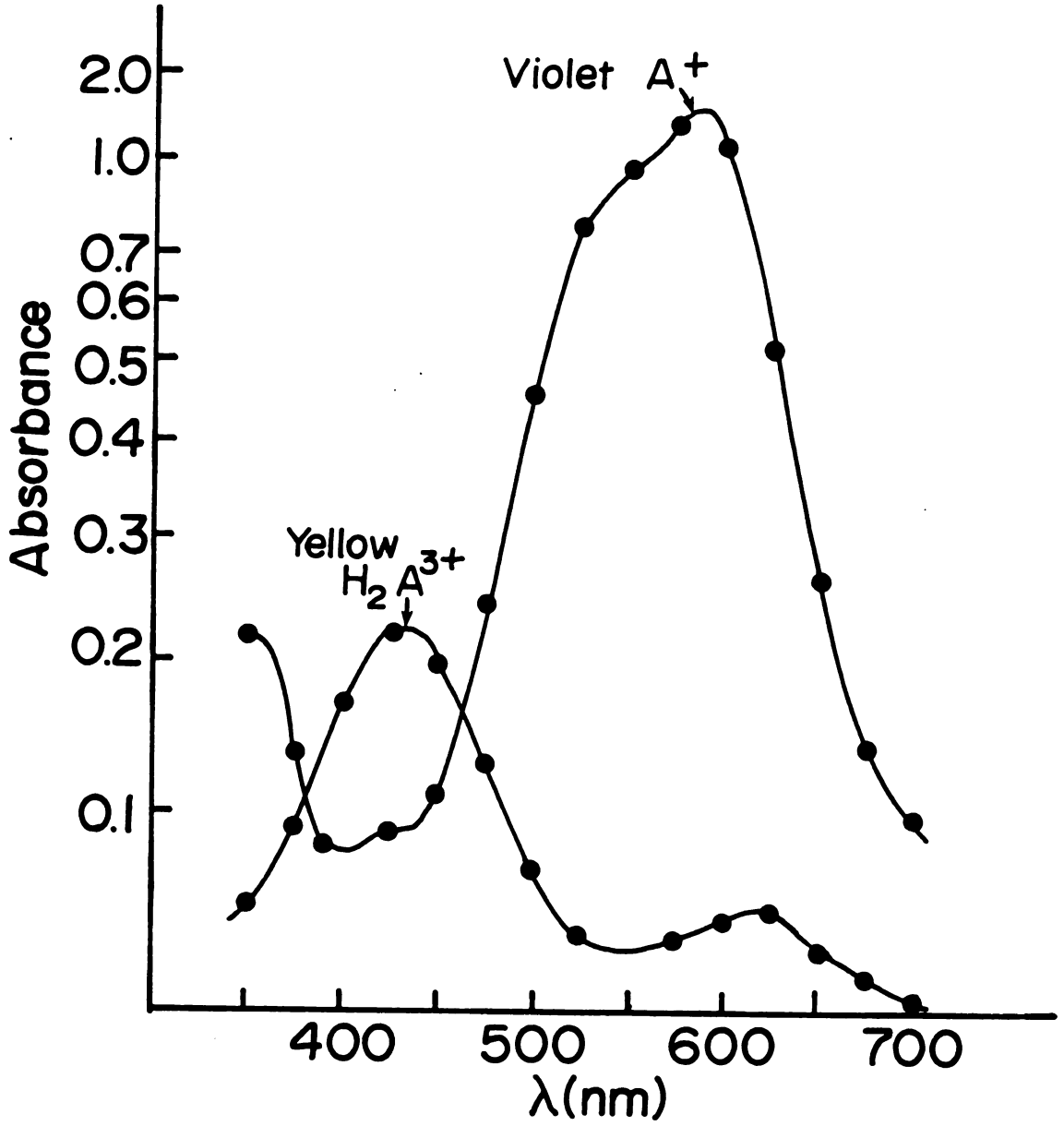

Figure 11. Variation of the Methyl Violet Color Transition pH with Solution Ionic Strength

A^{o}_{580} = Absorbance of Same Methyl Violet Solution at pH 4.0, λ = 480 nm

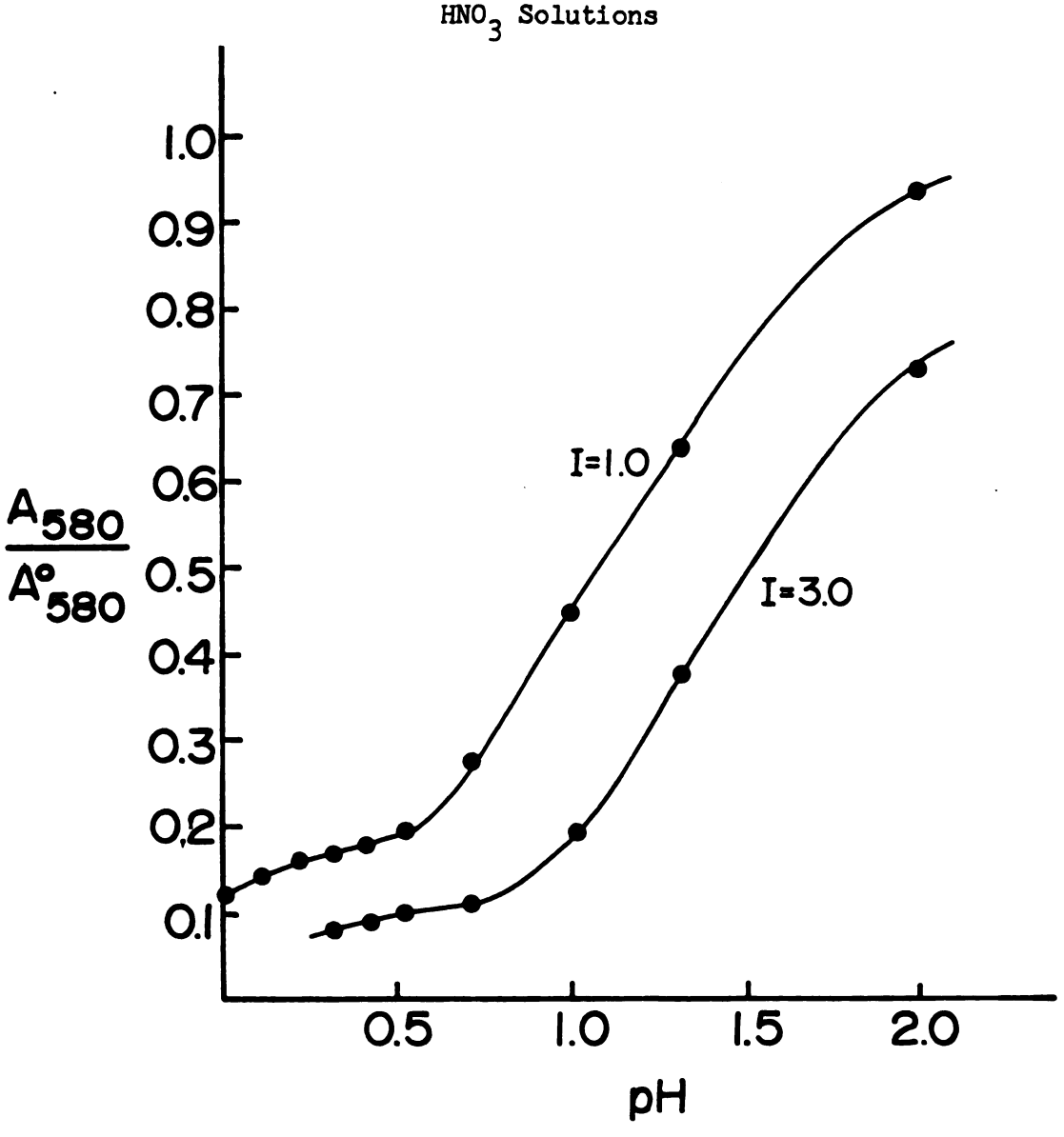

0.3 to 0.7 range to detect millimolar increases in $[H^+]$ at high ionic strengths. Second, and more important, methyl violet was observed to reduce 12-MPA to the molybdenum blue species. Thus, methyl violet indicator was unsuitable to monitor the release of H^+ as 12-MPA forms.

After having been conditioned for a day in 1 M acid solution, the Orion pH glass electrode gave reproducible, stable potential measurements in strong acid solution. Calibration curves of electrode potential versus $[H^+]$ were prepared for both HNO_3 and H_2SO_4 solutions (see Figure 12). However, the $[H^+]$ increase when phosphate was added to an acidified molybdate solution was detectable only for HNO_3 solutions with initial $[H^+]$ values between 0.20 M and 0.55 M. For four such solutions the $[H^+]$ increase was measured, and the 12-MPA concentration was estimated from C_P data under the assumption that essentially all phosphate is complexed to form 12-MPA when Mo(VI) is in a 100:1 excess.[31] Because of the instrumental limitations of measuring small changes in $[H^+]$ when the initial $[H^+]$ is large, a substantial propagated standard deviation in Z resulted. The Z value, as calculated from $Z = \frac{\Delta[H^+]}{[12\text{-MPA}]}$, was 16.6 ± 4.8.

5. Continuous Variations Experiments

The Job method of continuous variations[62] was also used to determine the Z coefficient and to calculate the 12-MPA formation constant K_{12}. A series of solutions was prepared in which the combined analytical concentrations ($C_P + C_M$) and the ionic strength were held constant at 0.01 M and 3.0 M, respectively. The mole fraction of phosphate ($X_P = \frac{C_P}{C_P + C_M}$) was varied within each series. The computer programs MOLYB.FT and MOSO4.FT were used to calculate the analytical

Figure 12. pH Glass Electrode Calibration Curve for Perchloric Acid Solutions at 25°C

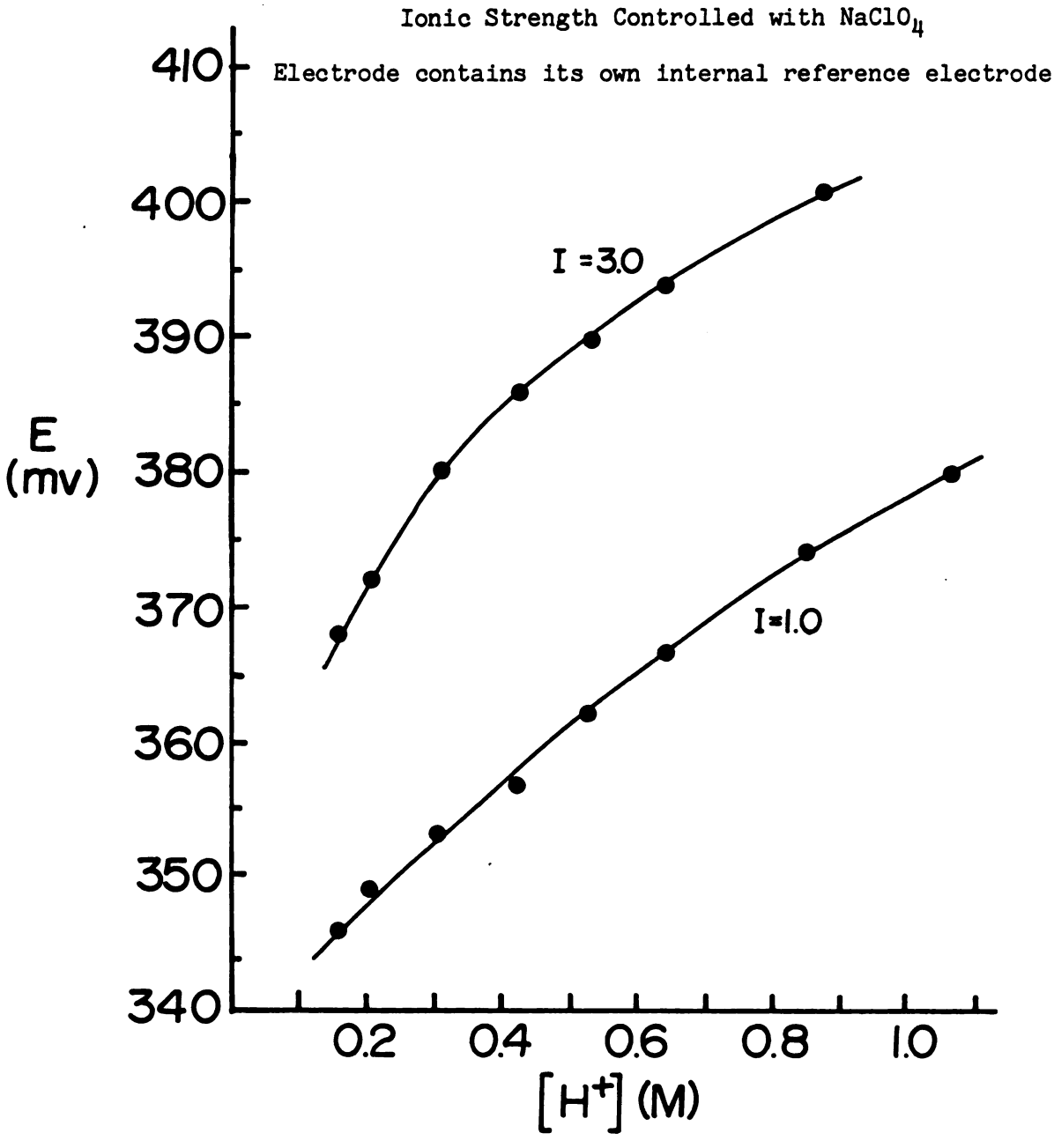

HNO_3, $HClO_4$, and H_2SO_4 concentrations necessary to maintain the initial solution $[H^+]$ at 0.2, 0.3, 0.4, and 0.5 M for each acid (thus, there were twelve series of solutions prepared). The background absorbance at 430 nm was measured for the $X_P = 0.0$ solution (0.01 M Mo(VI)), and the increase in 430 nm absorbance was measured for each solution in the twelve series. In addition, as a slight experimental modification, the increases in absorbance at 430 nm were measured for an acidified molybdate solution in which successive amounts of a phosphate solution with the same $[H^+]$, acid type, and ionic strength were added. The brass thermostated cuvette block and temperature bath maintained the cuvette solution temperature at $25.0 \pm 0.1^{\circ}C$. When solutions were added to the cuvette, a micro stir bar (Nalgene) and water-driven magnetic stirrer facilitated rapid mixing and ensured solution homogeneity. The quantities Z and K_{12} may be calculated from these experimental absorbance data if the following assumptions are valid.

(1) With a large excess of Mo(VI) (i.e. $X_P \leq 0.010$), essentially all the phosphate is complexed as 12-MPA. Thus, the proportionality εb between ΔA_{430} and [12-MPA] is established.

(2) The complexation stoichiometry between phosphate and molybdate in 12-MPA is 1:12.

(3) H_3PO_4 + 12 Mo(VI) $\rightleftharpoons$ 12-MPA is the only molybdophosphate equilibrium present in solution. Free, uncomplexed $[H_3PO_4]$ and [Mo(VI)] may then be calculated from mass balance equations C_P-[12-MPA] and C_M-12[12-MPA], respectively.

(4) The release of H^+ during 12-MPA formation does not alter the solution $[H^+]$ significantly.

(5) The relative concentrations of $HMoO_3^+$, $H_2Mo_2O_6^{2+}$, and the other prominent Mo(VI) species do not vary in the pH range 0.3 to 0.7; otherwise, the coefficient Z will vary with pH (see the mathematical modeling, Table X).

A conditional 12-MPA equilibrium constant K'_{12} can be calculated for each $[H^+]$ according to:

$$K'_{12} = \frac{[12\text{-MPA}]}{[H_3PO_4][Mo(VI)]^{12}},$$

and these K'_{12} values are related to K_{12}, the overall equilibrium constant in I = 3.0 M solutions, by

$$\log K'_{12} = \log K_{12} - Z \log [H^+].$$

Thus, a plot of $\log K'_{12}$ versus $\log[H^+]$ should give a linear graph with slope -Z and Y-intercept $\log K_{12}$.

To check the validity of some assumptions used, the experiments were repeated for series of solutions with $[H^+]$ = 0.20 M (HNO_3) in which the combined $C_P + C_M$ concentrations were varied from 0.008 M to 0.05 M. In addition, the spectrophotometric measurements were repeated at 410 nm for the $[H^+]$ = 0.20 M (HNO_3) solution series with $C_P + C_M$ = 0.010 M. No experimental data were obtained for 0.4 M and 0.5 M $[H^+]$ in H_2SO_4; the absorbance increases were too small to be detected with the instrumentation available.

Several experimental observations invalidate most of the assumptions used. The presence of an inflection point at $X_P < 0.10$ in the plot of ΔA_{430} versus X_P (which has the same shape as the 12-MPA curve in Figure 16) contradicts a result predicted from assumption (3). One-equilibrium chemical systems studied with Job's method would be

Table X

Equilibria Between 12-MPA and Prominent Mo(VI) Complexes in Strong Acid Solution

(a) $H_3PO_4 + 12MoO_3 \rightleftharpoons (12\text{-MPA})^{3-} + 3\ H^+$

(b) $H_3PO_4 + 12\ HMoO_3^+ \rightleftharpoons (12\text{-MPA})^{3-} + 15\ H^+$

(c) $H_3PO_4 + 6\ HMo_2O_6^+ \rightleftharpoons (12\text{-MPA})^{3-} + 9\ H^+$

(d) $H_3PO_4 + 6\ H_2Mo_2O_6^{2+} \rightleftharpoons (12\text{-MPA})^{3-} + 15\ H^+$

(e) $H_3PO_4 + 6\ H_3Mo_2O_6^{3+} \rightleftharpoons (12\text{-MPA})^{3-} + 21\ H^+$

$H_3PO_4 + Y\ Mo(VI) \rightleftharpoons (12\text{-MPA})^{3-} + Z\ H^+$

Because of the steady state re-equilibration among all Mo(VI) complexes, the Y and Z coefficients observed will be a weighted average of those coefficients depicted above, weighted with respect to the relative contribution of each Mo(VI) species concentration to the total C_M. These relative contributions vary with $[H^+]$ (see Figure 6).

Equilibria Between the Dimeric 9-MPA and 12-MPA in Strong Acid Solution

(a) $(12\text{-MPA})^{3-} + H_3PO_4 + 6\ MoO_3 \rightleftharpoons (9\text{-MPA})^{6-} + 3\ H^+$

(b) $(12\text{-MPA})^{3-} + H_3PO_4 + 6\ HMoO_3^+ \rightleftharpoons (9\text{-MPA})^{6-} + 9\ H^+$

(c) $(12\text{-MPA})^{3-} + H_3PO_4 + 3\ HMo_2O_6^+ \rightleftharpoons (9\text{-MPA})^{6-} + 6\ H^+$

(d) $(12\text{-MPA})^{3-} + H_3PO_4 + 3\ H_2Mo_2O_6^{2+} \rightleftharpoons (9\text{-MPA})^{6-} + 9\ H^+$

(e) $(12\text{-MPA})^{3-} + H_3PO_4 + 3\ H_3Mo_2O_6^{3+} \rightleftharpoons (9\text{-MPA})^{6-} + 12\ H^+$

expected to have only upward or downward concavity in the mole fraction plot; the appearance of both concavities indicates that two or more molybdophosphate equilibria are present. In addition, the X_P where ΔA_{430} has its maximum value is less than the $\frac{1}{12 + 1} = 0.0769$ value expected for a 1:12 stoichiometry in 12-MPA. The position of the maximum ΔA_{430} varies with $C_P + C_M$ (see Table XI). Within experimental error, the $[H^+]$ does not affect the X_P where ΔA_{430} has a maximum, though. However, if assumption (1) held and $C_P = [12\text{-MPA}]$ for $X_P \leq 0.01$, then an increase in $[H^+]$ would decrease the 12-MPA absorptivity. Because the increase in absorbance at 430 nm results only from increase in 12-MPA , according to Beer's Law, the experimental data shown that [12-MPA] is proportional to C_P when $X_P \leq 0.010$ but that the relative amounts of [12-MPA] for a given C_P decrease with increased $[H^+]$. No method or experimental observation to check assumption (4) was conceived. The graphs plotted in Figure 6 show a significant variation in the relative distribution of Mo(VI) species with $[H^+]$ ranging from 0.2 to 0.5 M; thus, assumption (5) is not valid.

The implication of two or more molybdophosphate equilibria is that independent measurements for each of the heteropoly species are required or else conjectures and approximations must be introduced. Three aqueous solutions with identical $C_P + C_M$, $[H^+]$, and ionic strength, but different X_P were prepared. Rapid cyclic voltammetric scans with a stationary Pt electrode between -0.5 v and +0.5 v (vs. SCE) produced one or two distinct, reversible waves and what appears to be several unresolved waves due to reductions and oxidations of the 12-MPA, other molybdophosphates, and the Mo(VI) species present in the solutions.

Table XI

Variation of $(X_P)_{max\ \Delta A}$ with $(C_P + C_M)$

$[H^+]$ = 0.200 M (in HNO_3) I = 3.0, T = 25.0°C

$C_P + C_M$ (M)	$(X_P)_{max\ \Delta A}$
0.008	0.049 ± 0.004
0.010	0.050 ± 0.005
0.020	0.055 ± 0.004
0.050	0.063 ± 0.004

Cary 17 spectrophotometric scans between 350 and 450 nm of these solutions, shown in Figure 13, reveal similar absorption spectra for the X_P = 0.00 and 0.50 solutions. The X_P = 0.05 solution, which is expected to contain more 12-MPA, shows considerably more absorption for 410-440 nm radiation. Thus, because of large, overlapping Mo(VI) background absorption and interfering 12-MPA absorption, independent measurements of other molybdophosphates would be nearly impossible spectrophotometrically. To substantiate this conclusion further, the experimental data of ΔA versus X_P with $C_P + C_M$ = 0.010 M and $[H^+]$ = 0.20 M (HNO_3) shows proportionality between the absorbance increases at 410 nm and those increases at 430 nm. Deviation from proportionality at the larger X_P values probably arises through the systematic error of larger Mo(VI) absorbance changes relative to 12-MPA absorbance changes encountered when $X_P > 0.20$.

Another implication for two or more molybdophosphates present is that $[H_3PO_4] \neq C_P - [\text{12-MPA}]$ and $[\text{Mo(VI)}] \neq C_M - 12[\text{12-MPA}]$. In the stoichiometry studies the concentrations of the other molybdophosphates may be significant, even though the [12-MPA] may be negligible, compared to C_P and C_M. Thus, in the Y-coefficient determinations, the log $[H_3PO_4]$ term may not be constant over the range of C_M studied (4.95-14.7 mM), and log [Mo(VI)] may not be proportional to log C_M.

In yet another implication, the results for Z from the glass electrode measurements are invalid. Those calculations for Z assume that all phosphates exists as [12-MPA] and that no additional protons are released when other molybdophosphates are formed.

Figure 13. UV-VIS Absorption Spectra of Three Phosphomolybdenum Solutions

With $(C_P + C_M)$ = 0.010 M, $[H^+]$ = 0.2 M (HNO_3), I = 3.0, T = 25.0°C

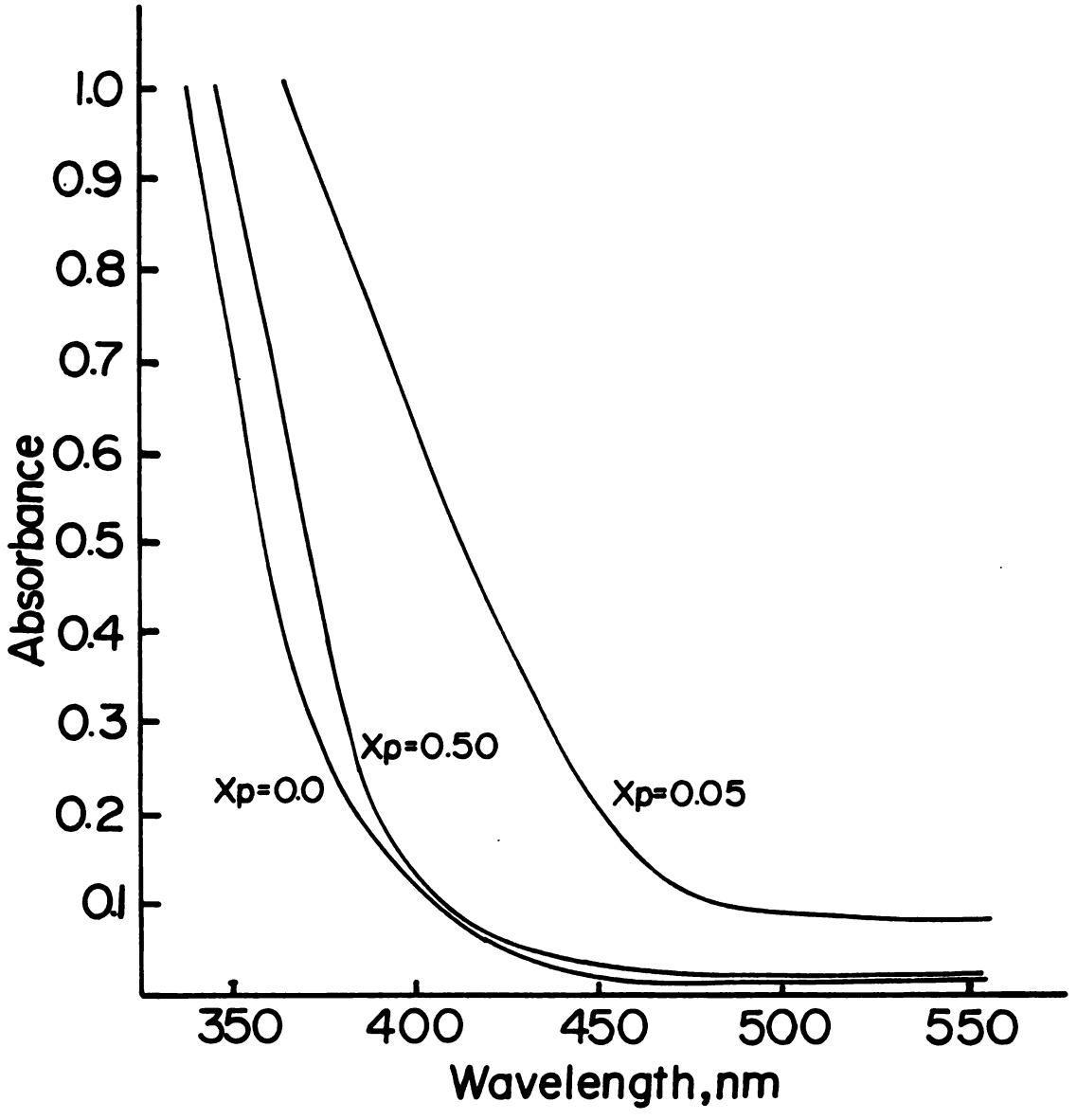

6. Computer Simulation: Molybdophosphate Equilibrium Constants

Because of the concentrations of other heteropoly compounds present in solution are difficult to measure, the H^+ coefficient and 12-MPA equilibrium constant had to be obtained by approximation. The HALTAFALL program was used to provide computer simulation of the continuous variations data. Under the assumption that only 12-MPA is responsible for the increase in 430 nm light absorption, the stoichiometries and overall formation constants for two or more molybdophosphates were adjusted until the computer-calculated [12-MPA] values match the experimental ΔA_{430} values proportionally for each solution. The best fit of the experimental data for a given series of solutions satisfied the following criteria:

(1) Computer-calculated [12-MPA] values (C_1 in HALTAFALL) have their maximum value at C_P and C_M conditions matching the experimental conditions that give the maximum ΔA_{430} value measured.

(2) A ratio of [12-MPA] values from the fifth data point to the second data point ($\frac{C_1(5)}{C_1(2)}$) matches the ratio of absorbance increases at 430 nm for the fifth to the second experimental points ($\frac{\Delta A(5)}{\Delta A(9)}$). This criterion considers the different proportionalities between [12-MPA] and C_P for the different $[H^+]$ in solution.

(3) A ratio of [12-MPA] values from the fifth data point to the ninth data point ($\frac{C_1(5)}{C_1(9)}$) matches the ratio of absorbance increases at 430 nm for the fifth and ninth experimental points ($\frac{\Delta A(5)}{\Delta A(9)}$). This criterion attempts to approximate the overall, general shape of the ΔA_{430} vs. X_P graph, especially in the region $0.05 \leq X_P \leq 0.20$.

(4) The K'_{12} conditional equilibrium constants vary with pH in such a manner as to give reasonable Z values through linear regression. This criterion was formulated because several choices of molybdophosphate equilibrium constants could satisfy the first three criteria for a given experimental data set, but subsequent linear regression could give either poor linear fit or a H^+ coefficient that is physically impossible (see Table X).

The HALTAFALL computer simulation data was run in the titration mode to duplicate exactly the experimental conditions in which 50 µl successive volumes of an acidified phosphate solution were added to 2.50 ml initial volume of acidified molybdate. In all cases except for the 0.5 M $H^+(HNO_3)$ solutions, the maximum ΔA_{430} was observed after the fifth addition of phosphate (X_P = 0.048), thus rationalizing the choice of the fifth data point in criteria (2) and (3). The correct choice of equilibrium constants could be verified through precise computer fitting of the continuous variations data and other experimental (i.e. stoichiometric) data where the same conditional equilibrium constants should apply.

A two molybdophosphate chemical model with 12-MPA and 9-MPA was assumed, and various estimates of their conditional, overall formation constants, K'_{12} and K'_9, respectively, were supplied as HALTAFALL input in the attempts to approximate the experimental observations. The species 9-MPA was chosen because of its reported formation when phosphate is present in excess over molybdate.[33] The species 9-MPA actually exists as a dimeric complex with a 2:18 phosphate to molybdate stoichiometry.

Several interesting features are observed in the computer-simulated data for $C_P + C_M = 0.01$ M. First, unless the K'_{12} value is sufficiently large, the X_P value at which C_1 ([12-MPA]) is a maximum is less than the value 0.0769 expected for a one-to-twelve complex, even if [9-MPA] is negligibly small. For example, if $K'_{12} = 10^{30}$, the value of X_P at maximum C_1 ($(X_P)_{\max C_1}$) is always 0.067 or less, and if $K'_{12} = 10^{20}$, this limiting X_P value is 0.038. Second, the proper $(X_P)_{\max C_1}$ is obtained whenever the $\frac{\log K'_9}{\log K'_{12}}$ ratio is 1.62 ± 0.02. However, this condition no longer holds true when K'_{12} is so small that $(X_P)_{\max C_1}$ never reaches the value 0.048. Third, whenever $K'_{12} > 10^{27}$, essentially all the phosphate exists as [12-MPA] when $X_P \leq 0.020$. A paradox develops because if the K'_{12} values are too high, then one has difficulty explaining the apparent change in 12-MPA absorptivity with $[H^+]$ changes since [12-MPA] is constant for corresponding data points (i.e. the same X_P conditions). Alternatively, if K'_{12} values are too low, difficulties arise in reconciling the larger experimental $(X_P)_{\max C_1}$ values which are constant with $[H^+]$ variations, within experimental error. Finally, and most importantly, another paradox arises from attempts to choose K'_{12} and K'_9 values that satisfy criteria (1), (2), and (3) simultaneously. Even if criterion (1) has been satisfied, choosing K'_{12} and K'_9 to satisfy (2) always results in a $\frac{C_1(5)}{C_1(9)}$ ratio which is too small, and choosing K'_{12} and K'_9 to satisfy (3) always results in a $\frac{C_1(5)}{C_1(2)}$ ratio which is too large. These observations are illustrated in Figure 14. The chemical model must be modified to include at least one additonal molybdophosphate in equilibrium with H_3PO_4 and Mo(VI).

Figure 14. Comparisons Between Experimental Data and Computer Simulation with a 12-Molybdophosphate and Dimeric 9-Molybdophosphate Chemical Model

——— computer simulated results; εb adjusted to match the experimental ΔA_{430} data.

..... experimental ΔA_{430} data at I = 3.0 M, T = 25.0°C, $C_P + C_M$ = 0.010 M, $[H^+]$ = 0.30 M (HNO_3)

(A) K_9' and K_{12}' are chosen to fit $\frac{C_1(5)}{C_1(2)} = \frac{\Delta A(5)}{\Delta A(2)}$. As a result, $\frac{C_1(5)}{C_1(9)} < \frac{\Delta A(5)}{\Delta A(9)}$.

(B) K_9' and K_{12}' are chosen to fit $\frac{C_1(5)}{C_1(9)} = \frac{\Delta A(5)}{\Delta A(9)}$. As a result, $\frac{C_1(5)}{C_1(2)} > \frac{\Delta A(5)}{\Delta A(2)}$.

(C) K_9' and K_{12}' are chosen to fit $\frac{C_1(5)}{C_1(2)} = \frac{\Delta A(5)}{\Delta A(2)}$ and $\frac{C_1(5)}{C_1(9)} = \frac{\Delta A(5)}{\Delta A(9)}$. As a result, $(X_P)_{\max C_1} \neq (X_P)_{\max \Delta A}$.

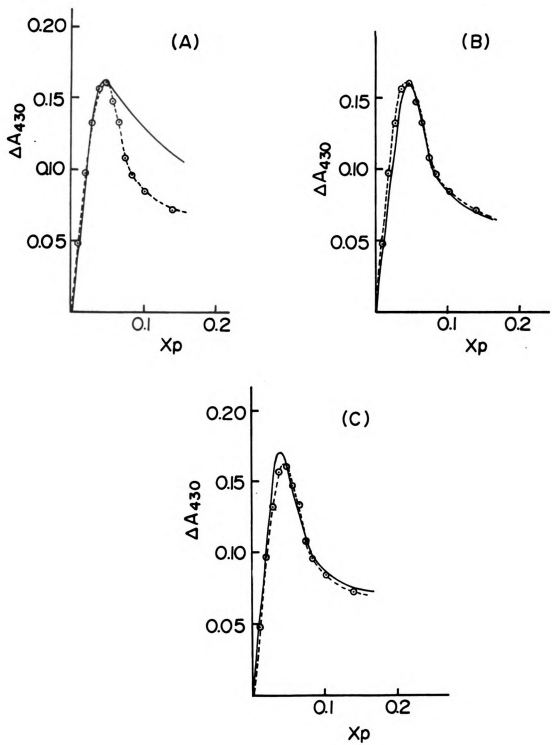
(A)
(B)
(C)
0.20
0.15
0.10
0.05
ΔA430
0.1
0.2
Xp

A chemical model with 12-MPA, dimeric 9-MPA, and monomeric 11-MPA was postulated. The 11-MPA species was selected because of its stoichiometric position between 9-MPA and 12-MPA and because 11-MPA is reported as the first product in the basic hydrolysis of 12-MPA (see Figure 2).[44] From the attempted computer simulations with this model, the relative magnitudes of the conditional, overall 12-MPA and 11-MPA formation constants, K'_{12} and K'_{11}, respectively, primarily determined the value of $\frac{C_1(5)}{C_1(2)}$. Only fairly large K'_9 values affected the $\frac{C_1(5)}{C_1(2)}$ ratio. Therefore, the general procedure of fitting each set of experimental data involved choosing K'_{12} and K'_{11} such that the $\frac{C_1(5)}{C_1(2)}$ ratio matched the experimental $\frac{\Delta A(5)}{\Delta A(2)}$ ratio and then adjusting the K'_9 value until $\frac{C_1(5)}{C_1(9)}$ matched the experimental $\frac{\Delta A(5)}{\Delta A(9)}$. While a continuum of K'_{12}, K'_{11}, and K'_9 values satisfies these two conditions, only certain values of these constants produced maximum C_1 concentration and the C_P and C_M conditions that match the experimental conditions. Yet, most sets of K'_{12}, K'_{11}, and K'_9 had to be eliminated because linear regressions of their logarithms with $\log[H^+]$ gave physically improbable Z values or poor linearity. For instance, the set $\log K'_{12} = 30.3$, $\log K'_{11} = 28.6$, and $\log K'_9 = 49.1$ which fit the experimental data for 0.200 M $[H^+]$ in H_2SO_4 had to be discarded because the closest precise computer fit for the data at $[H^+] = 0.300$ M in H_2SO_4 would have given a Z value of nearly twenty-four from the $\log K'_{12}$ versus $\log [H^+]$ linear regression. Not even if all the C_M existed as $H_3Mo_2O_6^{3+}$ would so many H^+ be released into solution for each 12-MPA complex produced (see Table X).

Nevertheless, some values for K'_{12}, K'_{11}, and K'_9 satisfy all four criteria listed earlier; these molybdophosphate equilibrium constants

are tabulated in Table XII. As a check on these values, the ratio between the experimental ΔA_{430} and the computer-simulated [12-MPA] was calculated for each data point. These proportionalities are tabulated for two sets of experimental data in Table XIII. The relative standard deviation of these proportionality constants are approximately 10% within each experimental data set as well as among all the data sets. As a grand average, 12-MPA's molar absorptivity at 430 nm is 1061 $\pm$ 78 l $mole^{-1}cm^{-1}$. The variances within each data set appear to be randomly distributed.

Another chemical model with monomeric 12-MPA and 10-MPA and dimeric 9-MPA was tried in an attempt to simulate the experimental data better. However, the K_9' value could not be adjusted so that $\frac{C_1(5)}{C_1(9)}$ matched $\frac{\Delta A(5)}{\Delta A(9)}$ under given experimental conditions.

7. Modeling and Discussion

The molybdophosphate chemical model with 12-MPA, 11-MPA, and dimeric 9-MPA provides the best fit of the experimental measurements. Other molybdophosphates may be present, but their equilibrium concentrations are not expected to be significantly large. The 12-MPA, 11-MPA, and 9-MPA conditional equilibrium constants were observed to fit the continuous variations data as well as the data in which phosphate was successively added to molybdate. The computer calculated the concentrations of each molybdophosphate species for the various mole fractions; some of these results are graphed as Job plots in Figures 15, 16, and 17. The X_P values where [12-MPA] and [11-MPA] are maximum increase with increased $C_P + C_M$ and decreased $[H^+]$ while the X_P values

Table XII

The Equilibrium Constants That Best Fit the Experimental Data Through Computer Simulation (I = 3.0, T = 25.0°C)

K'_{12}	K'_9	K'_{11}	$[H^+]$	$C_1(5)/C_1(2)$	$C_1(5)/C_1(9)$	$(X_P)_{max}\ C_1$
			HNO_3 Solutions			
1.0×10^{36}	2.7×10^{58}	4.0×10^{33}	0.200 M	1.774 (1.771)	2.558 (2.551)	0.050
5.0×10^{33}	1.5×10^{54}	3.5×10^{31}	0.300 M	1.643 (1.643)	1.677 (1.674)	0.048
1.0×10^{32}	1.2×10^{52}	1.0×10^{30}	0.400 M	1.543 (1.534)	1.824 (1.771)	0.046
5.0×10^{30}	4.0×10^{50}	1.2×10^{29}	0.500 M	1.400 (1.376)	1.658 (1.685)	0.042
			$HClO_4$ Solutions			
1.0×10^{36}	4.0×10^{58}	6.0×10^{33}	0.200 M	1.686 (1.673)	2.809 (2.797)	0.048
5.0×10^{33}	1.5×10^{54}	3.0×10^{31}	0.300 M	1.686 (1.657)	1.654 (1.648)	0.048
1.0×10^{32}	6.0×10^{51}	1.2×10^{30}	0.400 M	1.521 (1.528)	1.563 (1.583)	0.046
5.0×10^{30}	1.2×10^{50}	1.2×10^{29}	0.500 M	1.422 (1.423)	1.391 (1.385)	0.042
			H_2SO_4 Solutions			
1.2×10^{29}	2.7×10^{47}	2.1×10^{27}	0.200 M	1.571 (1.563)	1.858 (1.852)	0.050
1.5×10^{27}	7.0×10^{43}	5.0×10^{25}	0.300 M	1.457 (1.436)	1.333 (1.329)	0.048

(corresponding experimental ΔA ratios are given in parentheses)

Table XII (cont'd)

Possible

Models:

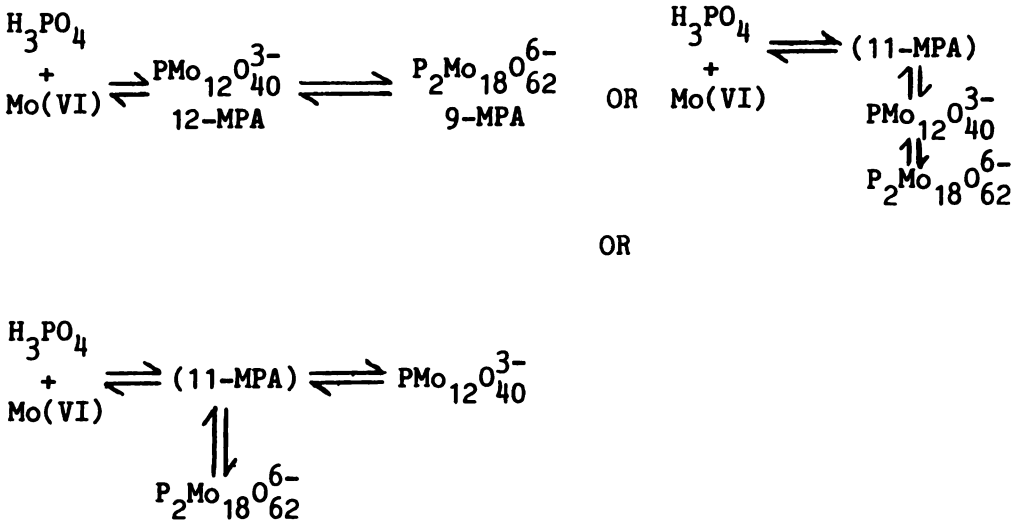

Table XIII

Comparison Between Experimental Data and Computer Simulated 12-MPA Concentrations (C_1)

$I = 3.0$, $T = 25^{\circ}C$

$[H^+] = 0.500$ M (HNO_3)

$C_P + C_M = 0.01$ M

$\log K'_{12} = 30.7$, $\log K'_9 = 50.6$, $\log K'_{11} = 29.1$

X_P	C_1(mM)	ΔA_{430}	$\varepsilon b(M^{-1})$
0.0100	0.026	0.0294	1131
0.0198	0.045	0.0556	1236
0.0294	0.058	0.0731	1260
0.0388	0.063	0.0765	1213
0.0481	0.061	0.0754	1235
0.0572	0.052	0.0604	1162
0.0748	0.038	0.0454	1194
0.0883	0.035	0.0427	1220

$[H^+] = 0.200$ M (H_2SO_4)

$C_P + C_M = 0.02$ M

$\log K'_{12} = 29.1$, $\log K'_9 = 47.6$, $\log K'_{11} = 27.3$

X_P	C_1(mM)	ΔA_{430}	$\varepsilon b(M^{-1})$
0.0100	0.097	0.0868	1118
0.0198	0.175	0.160	1094
0.0294	0.232	0.209	1110
0.0388	0.267	0.241	1108
0.0481	0.275	0.250	1100
0.0572	0.250	0.243	1029
0.0660	0.200	0.214	935
0.0748	0.167	0.172	971
0.0883	0.148	0.135	1096
0.0917	0.136	0.113	1204

Figure 15. Continuous Variations Plot for Molybdophosphate

$C_P + C_M = 0.01M$, $[H^+] = 0.50$ M

$K'_{12\text{-MPA}} = 5.0 \times 10^{30}$, $K'_{9\text{-MPA}} = 4.0 \times 10^{50}$, $K'_{11\text{-MPA}} = 1.2 \times 10^{29}$, I = 3.0, T = 25.0°C

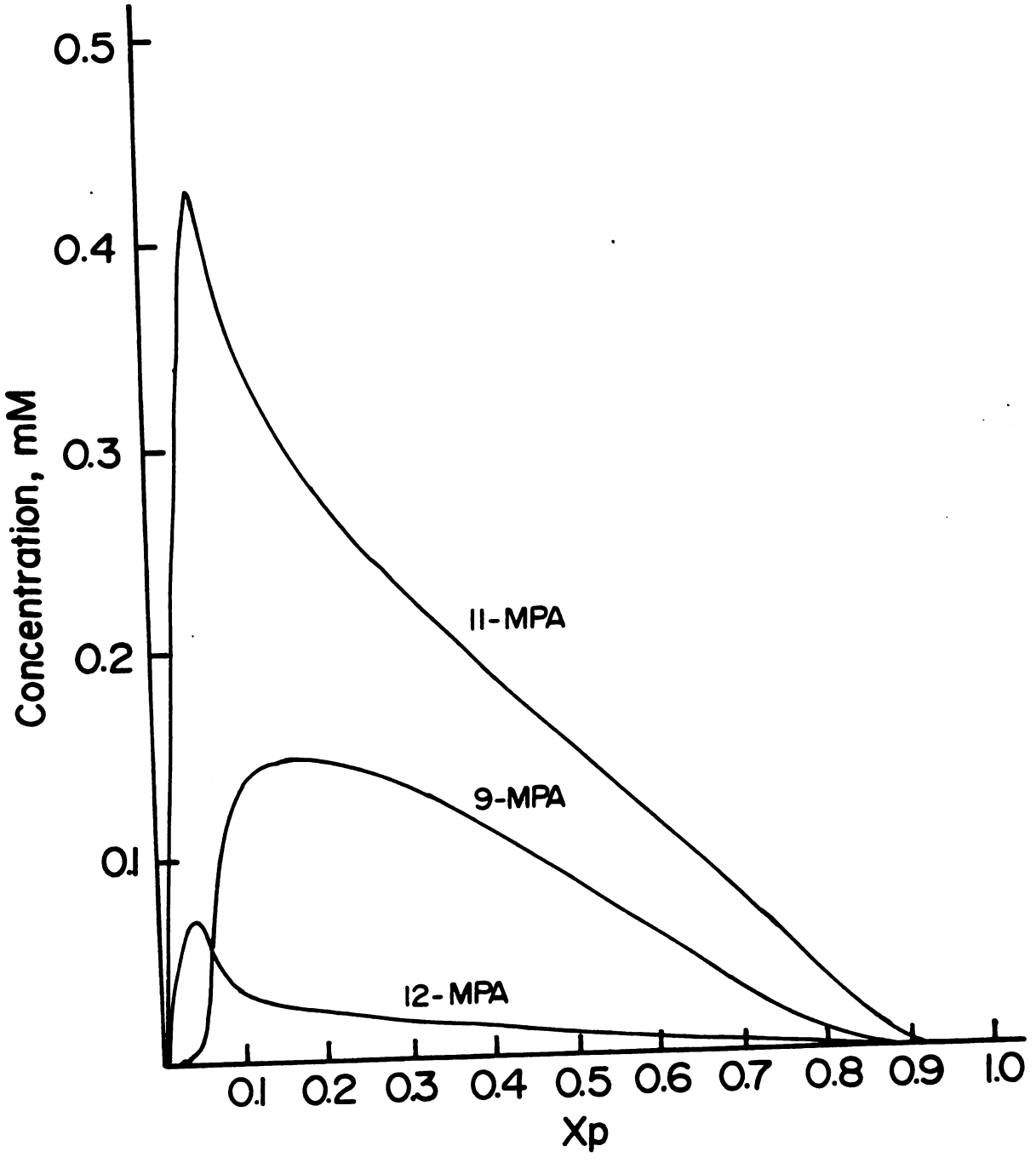

Figure 16. Continuous Variations Plot for Molybdophosphates,

$C_P + C_M = 0.01$ M, $[H^+] = 0.20$ M

$K'_{12\text{-MPA}} = 1.0 \times 10^{36}$, $K'_{9\text{-MPA}} = 2.7 \times 10^{58}$, $K'_{11\text{-MPA}} = 4.0 \times 10^{33}$, I = 3.0, T = 25.0°C

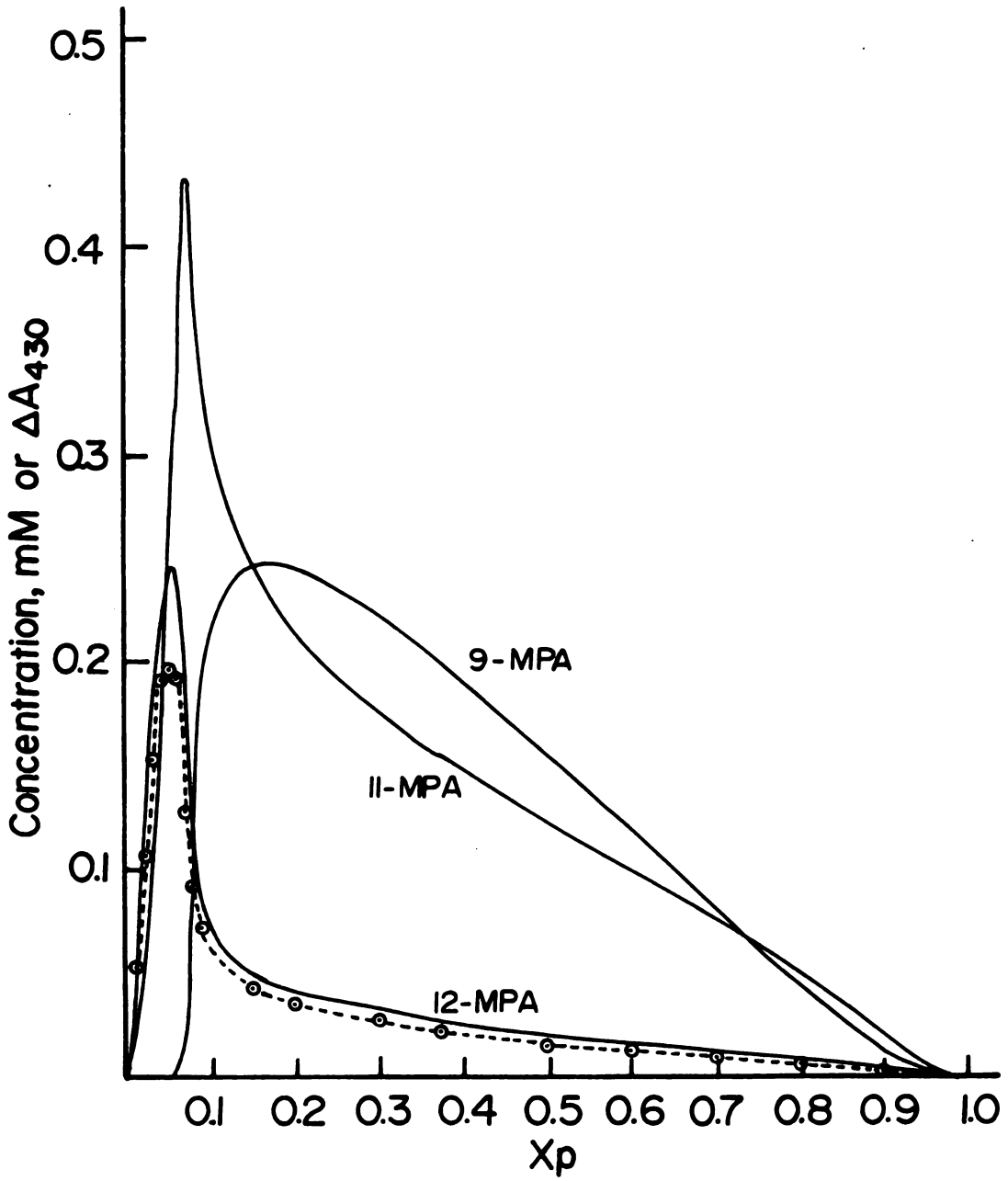

Figure 17. Continuous Variations Plot for Molybdophosphates,

$C_P + C_M = 0.05$ M, $[H^+] = 0.20$ M

$K'_{12\text{-MPA}} = 1.0 \times 10^{36}$, $K'_{9\text{-MPA}} = 2.7 \times 10^{58}$, $K'_{11\text{-MPA}} = 4.0 \times 10^{33}$, $I = 3.0$, $T = 25.0^{\circ}C$

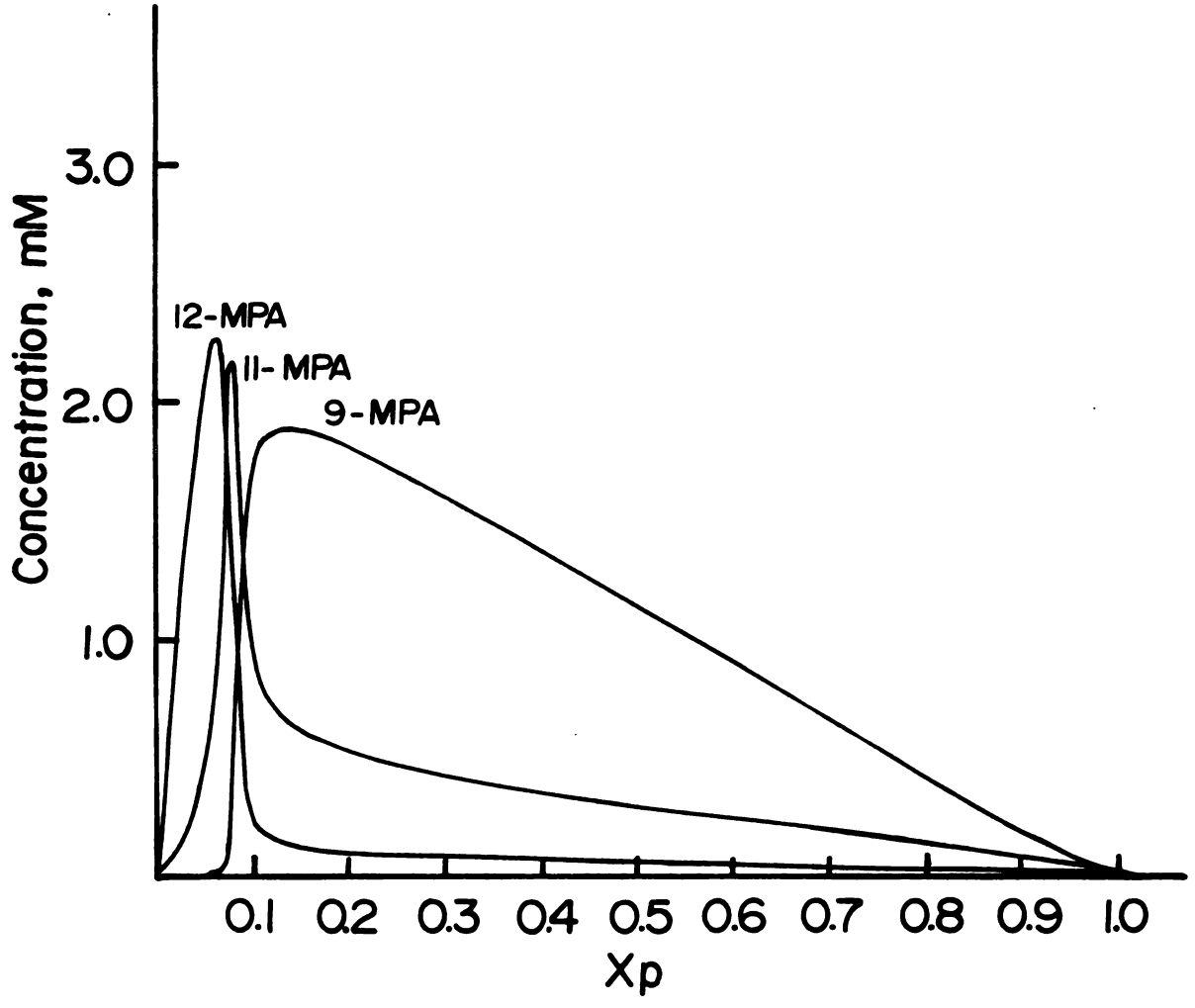

where [9-MPA] is maximum decrease under the same C_p + C_M and [H^+] variations. Linear regressions of the logarithms of these conditional equilibrium constants with log [H^+] were performed, and the resulting Z and log K_f values are tabulated in Table XIV. In fitting the experimental data, a slight variation in log K'_{12}, log K'_{11}, or log K'_9 by 0.1 or 0.2 logarithmic units caused a significant change in the $\frac{C_1(5)}{C_1(2)}$ and $\frac{C_1(5)}{C_1(9)}$ ratios.

Experimentally, there were three main sources of error. One source, in the [H^+] value, resulted from the propagation of errors in Cruywagen's equilibrium constants[42] used to calculate [H^+](possibly 10% RSD). Another source of error occurred in the ΔA_{430} measurements, which resulted from errors in measuring spectrophotometric transmittance ($\pm$ 0.1% T) and from a possible systematic error in assuming that the background Mo(VI) absorbance at 430 nm changed negligibly as H_3PO_4 was added. The other error source occurred in determining the X_p where ΔA_{430} is maximum. Even though the extrapolation error between data points was reduced with more data points and a smaller X_p interval between the two data points encompassing $(X_p)_{max\Delta A}$, the error in [H^+] resulted in an $(X_p)_{max\,\Delta A}$ variance of $\pm$ 0.003. If the conditional equilibrium constants could be calculated directly from the experimental data, propagation of the above experimental errors would impart a $\pm$ 0.5 variance to log K'_{12}. Because of a large relative error propagated in [Mo(VI)] = C_M-12 [12-MPA] and of propagating the [Mo(VI)] error to the twelfth power, the equilibrium constants may be determined only to within one order of magnitude or power of ten. Thus, the errors in the choices of constants used for the computer simulation were smaller than the propagated experimental errors.

Table XIV

Linear Regression Results From log K' vs. log $[H^+]$ for Different Acidic Media at I = 3.0 and T = 25.0°C

$$\log K' = \log K - Z \log [H^+]$$

	12-MPA			9-MPA			11-MPA		
ACID	$\log K_{12}$	Z	r_{xy}	$\log K_9$	Z	r_{xy}	$\log K_{11}$	Z	r_{xy}
HNO_3	26.70	13.3	0.999	44.38	19.7	0.988	25.56	11.5	0.998
$HClO_4$	26.70	13.3	0.999	43.26	21.6	0.991	25.44	11.8	0.997
H_2SO_4	21.53	10.8	-----	33.21	20.4	-----	20.88	9.2	-----

The equilibrium constants reported were in terms of the total concentration of all Mo(VI) species rather than the concentration of any particular species. Because the stoichiometric and the continuous variations experiments both involved equilibrium methods, no information was available on which Mo(VI) species actually coordinate(s) with the phosphate anion. Instead, stopped-flow studies of 12-MPA kinetics must be performed to provide this information.

Linear regression of $\log[\text{12-MPA}] - X \log[H_3PO_4]$ versus $\log[\text{Mo(VI)}]$ (see Eqn. (1) on P. 48) was performed on the computer simulation results to determine the stoichiometric coefficient Y. From the regression slope the Mo(VI) coefficient was 12.0 (r_{xy} = 0.999+) for both HNO_3 and H_2SO_4 media. Thus, the proposed chemical model appeared to fit the experimental data from the stoichiometry studies, though the assumptions used to calculate Y from $\log \Delta A_{430}$ versus $\log C_M$ regressions were not valid (i.e. $[H_3PO_4]$ not constant; more than one molybdophosphate present).

The Z coefficient associated with 11-MPA formation is less than the Z value associated with 12-MPA formation. If the 11-MPA were present in solution as a result of basic 12-MPA hydrolysis, then three or four additional equivalents of H^+ would have been released to the solution according to the reaction

$$\underset{\text{(12-MPA)}}{PMo_{12}O_{40}^{3-}} + 2\ H_2O \xrightarrow{OH^-} \underset{\text{(11-MPA)}}{PMo_{11}O_{39}^{7-}} + \underset{\text{(Mo(VI))}}{HMoO_3^+} + 3\ H^+ \quad .^{44}$$

Instead, the postulated third molybdophosphate seems to be a colorless intermediate between uncomplexed H_3PO_4 and Mo(VI) and the yellow 12-MPA complex. According to this model, the complexation of H_3PO_4 with Mo(VI)

produces the third molybdophosphate prior to complexation with more Mo(VI) to form 12-MPA. The constitution of this third molybdophosphate is uncertain, but the relative magnitudes of its Z, log K'_{11}, and standard error of the estimate values are consistent with a 1:11 phosphate to molybdate stoichiometry.

The equilibrium constants K_{12}, K_{11}, and K_9 are a few orders of magnitude lower in H_2SO_4 than in the corresponding HNO_3 and $HClO_4$ solutions. These lower values result from probable sulfate complexation[63] with Mo(VI) species or else incorporation of sulfate into the heteropoly cage.[64] Either case would lead to a lower 12-MPA concentration for a given C_M. The equilibrium reactions for 12-MPA and 9-MPA with and without Mo(VI)-sulfate complexation are modeled in Table XV. Here, sulfate complexation with Mo(VI) is assumed. From the results for the Z coefficient in HNO_3 and $HClO_4$, the m values are calculated to be 0.858 (12-MPA equilibrium), 0.761 (9-MPA in HNO_3), and 0.867 (9-MPA in $HClO_4$). These m values reflect the occurrence of $HMoO_3^+$, $H_2Mo_2O_6^{2+}$, and $HMo_2O_6^+$ as the three most predominant Mo(VI) species in strong acid solution. The n value reflects smaller, observed Z coefficients in H_2SO_4 solutions; the sulfate displaced from Mo(VI) species accepts a proton equivalent to become HSO_4^-, the prominent sulfate-containing species in strong acid solution. However, since the decreased free [Mo(VI)] alters the relative distribution of Mo(VI) species in solution, the m values calculated above may not be used in the calculation of n. With an assumed value m = 0.858, n = 0.208 for the 12-MPA model, and n = 0.067 for the 9-MPA model.

Table XV

An Overall Model for 12-MPA and 9-MPA Formations From H_3PO_4 and Mo(VI)

Without sulfate complexation

$$H_3PO_4 + 12\ HmMo(VI)^{m+} \rightleftharpoons \underset{(12\text{-MPA})}{PMo_{12}O_{40}^{3-}} + (3 + 12m)\ H^+$$

m = 0 for Mo(VI) = MoO_3 ($Mo(OH)_6$), m = 0.5 for ½ $HMo_2O_6^+$

m = 1.0 for Mo(VI) = $HMoO_3^+$ + ½ $H_2Mo_2O_6^{2+}$, m = 1.5 for ½ $H_3Mo_2O_6^{3+}$

$$2\ H_3PO_4 + 18\ HmMo(VI)^{m+} \rightleftharpoons (9\text{-MPA})^{6-} + (6 + 18m)\ H^+$$

With sulfate complexation

$$H_3PO_4 + 12\ HmMo(VI)(SO_4)_n^{(m-2n)+} \rightleftharpoons (12\text{-MPA})^{3-} + (3 + 12m - 12n)H^+ + 12n\ HSO_4^-$$

$$2\ H_3PO_4 + 18\ HmMo(VI)(SO_4)_n^{(m-2n)+} \rightleftharpoons (9\text{-MPA})^{6-} + (6 + 18m - 18n)\ H^+ + 18n\ HSO_4^-$$

Certain analytical implications were observed from the experimental data of the relationship between [12-MPA] (or ΔA_{430}) and C_P. In most cases the [12-MPA] was proportional to C_P for $X_P \leq 0.01$, but the proportionality varied with the different acid media used (HNO_3, H_2SO_4, and $HClO_4$) and the solution $[H^+]$. The ratio $\frac{[12\text{-MPA}]}{C_P}$ ranged in values from 0.25 in the 0.5 M $[H^+]$ $HClO_4$ medium to 0.80 in the 0.2 M $[H^+]$ HNO_3 medium. This information emphasizes the need for reproducible C_H(or C_A) and C_M concentrations between the samples and the phosphate standards. Nevertheless, a 100-to-1 excess of molybdate over the phosphate present in the samples guarantees a proportionality between [12-MPA] and C_P. These considerations are important for reaction-rate methods based upon the initial reduced molybdenum blue formation rate as well as analytical procedures based on the equilibrium 12-MPA concentration.

B. Equilibrium Studies of 12-MSA Formation

1. Equilibrium Constants of β-12-MSA at pH 1.2

To measure the equilibrium constants for 12-MSA formation, continuous variations studies were carried out at constant pH in three acidic media (HNO_3, $HClO_4$, and H_2SO_4). The total molar silicate and molybdate concentration ($C_S + C_M$) was varied between 0.01 M and 0.05 M but was held constant within each series of solutions as the mole fraction of silicate ($X_S = \frac{C_S}{C_S + C_M}$) was varied. These experiments were carried out at pH 1.2 where only the β isomer of 12-MSA forms and at pH 3.6 where α-12-MSA forms exclusively at 1.0 M ionic strength.[41] The required amounts of acid necessary to bring the solution pH to the specified values were calculated with the HALTAFALL computer program

described in Section A, Chapter III. Also, once the conditional formation constant was determined from one set of data, HALTAFALL was used to predict β-12-MSA concentrations for other data sets.

Absorbance measurements were made with the modular GCA/McPherson UV-visible spectrophotometer with the modified sample cell module. The temperature of the cuvette block (see Section A and ref. 59), cuvette, and solution was maintained at 25.0 ± 0.1°C by circulating water from a constant temperature bath through the cuvette block. Absorbance measurements were made at 410 nm and 430 nm (monochromator spectral bandpass of 4 nm) where 12-MSA absorbs strongly and the Mo(VI) background absorption is small.

A plot of one set of continuous variations data for the formation of β-12-MSA is shown in Figure 18. The absorbance change at 430 nm (ΔA_{430}) is a maximum at a silicate mole fraction X_S of 0.077, which corresponds to a 12:1 complexation ratio of molybdate to silicate. Continuous variations studies were also carried out with different total concentrations of silicate and molybdate, $C_S + C_M$, and with absorbances measured at 410 nm. All continuous variations plots have a similar shape to that shown in Figure 18. Within experimental error all plots have a maximum absorbance change at a 12:1 mole ratio of molybdate to silicate. Because of the identical results at two different wavelengths and several different total C_S and C_M values, it is concluded that β-12-MSA is the only molybdosilicate species that forms at pH 1.2.

The formation constant was calculated in the following manner. From the linear increase in ΔA_{430} with C_S at low mole fractions of silicate (see Figure 18), it was concluded that essentially all the

Figure 18. Continuous Variations Plot for β-12-Molybdosilicate,

$C_S + C_M = 0.01$ M, pH = 1.2

Ionic Strength 1.0 M, T = 25°C

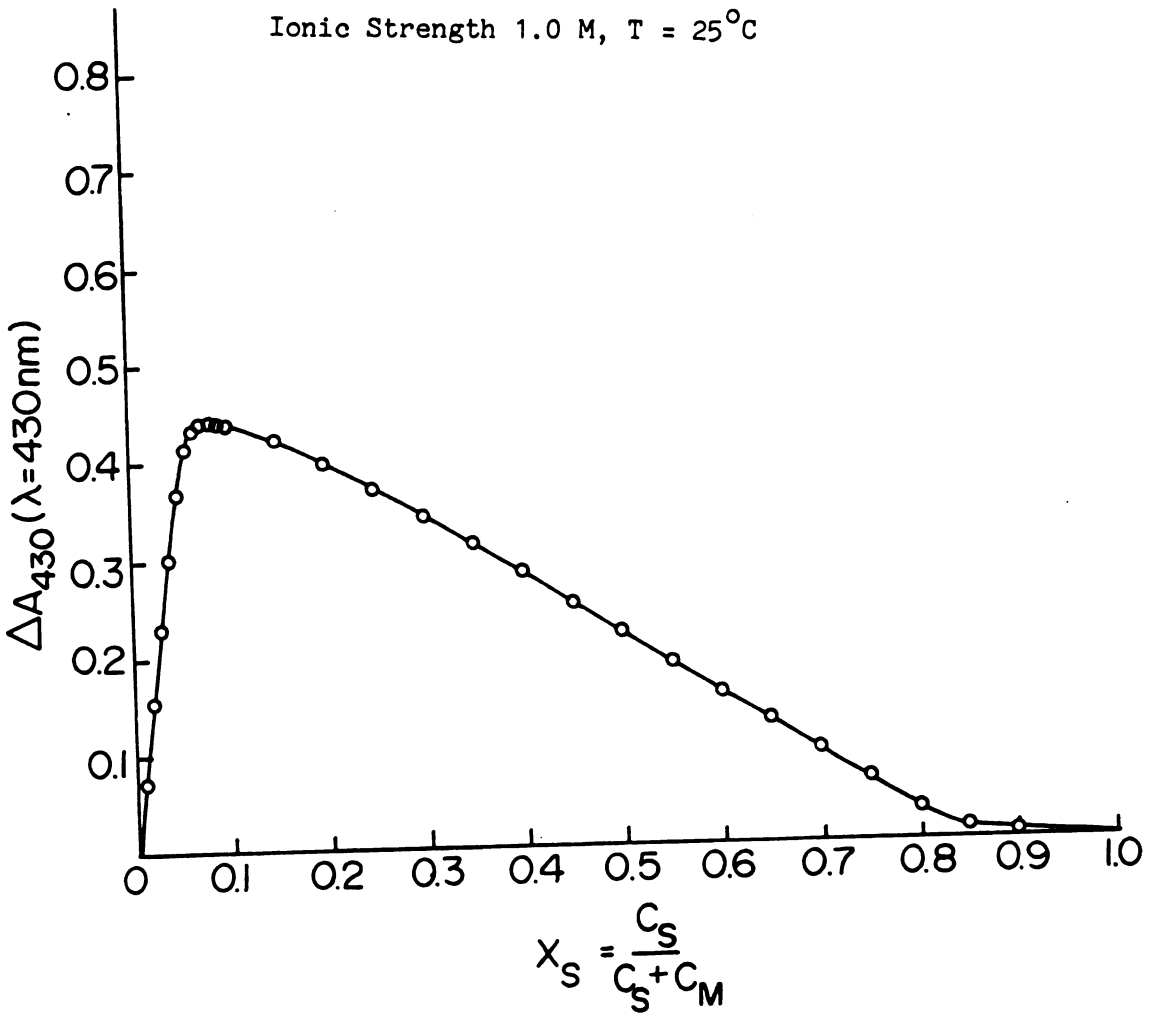

silicate present was converted to β-12-MSA for $X_S \leq 0.02$. The slope of the ΔA versus C_S plot under these conditions yielded the molar absorptivity ε of β-12-MSA (r_{xy} values typically were 0.9998). Equilibrium β-12-MSA concentrations were then calculated from ΔA values measured near the maximum in the continuous variations plot ($0.07 < X_S < 0.10$). The conditional formation constant K_f' was then calculated from

$$K_f' = \frac{[\beta\text{-12-MSA}]}{[Si(OH)_4][Mo(VI)]^{12}} = \frac{[\beta\text{-12-MSA}]}{(C_S - [\beta\text{-12-MSA}])(C_M - 12[\beta\text{-12-MSA}]^{12}}$$

Results for the log K_f' values in HNO_3, $HClO_4$, and H_2SO_4 were 32.2, 31.9, and 31.6, respectively. These values are conditional constants at pH 1.2 and 1.0 M ionic strength. From the variances in the ΔA measurements and the value of ε obtained, a propagation of error analysis showed that the experimental error in log K_f' values is about $\pm$ 0.5.

To test how well the calculated K_f' values describe the entire continuous variations curves, β-12-MSA concentrations were calculated at each X_S value and compared to the measured values of ΔA. A proportional relationship (constant εb value) over the entire range of X_S values would indicate excellent agreement. For one data set in HNO_3 at 430 nm, the average and standard deviation of the εb value were 740 $\pm$ 37 M^{-1}(RSD = 5%). Similar correspondence was obtained for all three acidic media and for the different total $C_S + C_M$ values. The grand average for the β-12-MSA molar absorptivity was 803 $M^{-1}cm^{-1}$ at 430 nm, 25°C., and 1.0 M ionic strength. Thus, a single equilibrium with the given conditional formation constants adequately describes the formation of β-12-MSA.

2. Discussion and Comparison with the 12-MPA Equilibria

The pH dependence of the K_f' values was observed by obtaining continuous variations data at pH 1.6 and pH 2.0. However, significant amounts of the α isomer were found at pH values higher than 1.8 as noted by an apparent decrease in the molar absorptivity of β-12-MSA with increasing pH. The determination for the formation constant of the α isomer at pH 3.6 was attempted. However, the lower molar absorptivity of the α isomer in comparison to that of the β isomer led to uncertainties in the K_f' values that spanned several orders of magnitude. Within experimental error, the β-12-MSA formation constants are the same at pH 1.2 and pH 1.6 for a given acid solution.

Some interesting similarities and differences exist between these results and those for the corresponding molybdophosphate system. The conditional formation constants of β-12-MSA at pH 1.2 in all the acidic media are of the same order of magnitude as those for 12-MPA at pH 0.6 in HNO_3 and $HClO_4$ (one should note that the ionic strength was 3.0 M in the 12-MPA study). In addition, the molar absorptivity for β-12-MSA at 430 nm is within 25% of the molar absorptivity for 12-MPA at the same wavelength (again, ionic strengths were different in the two studies). On the other hand, the optimum pH for forming 12-MSA is higher than that for forming 12-MPA. The β-12-MSA formation constant is nearly independent of the type of acid used to adjust the pH, whereas the formation constant of 12-MPA is much lower in H_2SO_4 than in $HClO_4$ and HNO_3. Apparently, the degree of sulfate complexation with Mo(VI) or with the heteropoly anion is much less in the 12-MSA case because of the smaller total sulfate concentration.

The β-12-MSA species appears to be the only molybdosilicate species formed at pH 1.2. As a consequence, stoichiometric amounts of β-12-MSA can be formed from silicate and molybdate when the mole fraction of silicate is less than 0.02. Because the molybdophosphate system is influenced by equilibria among three species, only 20-80% of the available phosphate is converted to 12-MPA at mole fractions of phosphate less than 0.02.

Chapter V. Kinetic Studies

A. Kinetics of 12-MPA Formation

1. Some Preliminary Stopped-Flow Studies

To verify the reproducibility of the 12-MPA rate data of Beckwith[5] and Gall[6], some preliminary stopped-flow measurements of 12-MPA and 12-MSA were performed at 400 nm on solutions with various analytical concentrations of acid, Mo(VI), and phosphate. The ionic strength was not controlled in these preliminary experiments, but the temperature was maintained at 25.0 $\pm$ 0.1°C. The stopped-flow components were allowed to equilibrate with the 25°C temperature bath for five minutes before rate measurements were made. The stopped-flow system was operated in the manual mode, and photographs were taken of the time-dependent spectrophotometric readout on an oscilloscope. The rates measured here agreed with Notz's previous data within experimental error[4] but were twice those measured by Gall[6] for 0.1 mM phosphate solutions. This discrepancy resulted from my not controlling the solution ionic strength (see Section D for studies of ionic strength effects). As long as the 0% T and 100% T voltage levels were accurately known, the rate data obtained here showed good day-to-day reproducibility. The ten minute equilibration of acidified molybdate solutions in

the 25°C temperature bath reduced the standard deviation in the transmittance data and initial reaction rates, as earlier observations had indicated.[31] In addition, rates obtained when acidified phosphate solutions were mixed with molybdate agreed with rates obtained when neutral, aqueous phosphate solutions were mixed with molybdate solutions having twice the acidity (same C_H for the mixed solutions) within experimental error. Hence, the heat of mixing between neutral and acidic solutions did not seem to alter the initial reaction rates significantly.

In another preliminary study, the reaction time for 12-MPA formation was extended to 10 s (100 analog points per run on the Beckwith stopped-flow system) in order to observe a greater range of kinetics as equilibrium is attained. The absorbance at 430 nm was plotted versus time for each kinetics run; afterwards, the data were fit to a simple exponential equation of the form $Y = \theta_1 + \theta_2 \exp \theta_3 t$ or to a double exponential equation of the form $Y = \theta_1 + \theta_2 \exp \theta_3 t + \theta_4 \exp \theta_5 t$. The absorbance value at equilibrium A_∞ was obtained from an asymptotic extrapolation of the data points between 6 s and 10 s. Then $\ln(A_\infty - A_t)$ was plotted against time. A linear plot over the entire time range would indicate that the simple exponential equation fits the experimental kinetics data. Experimental plots, however, (see Figure 19 for an example) showed negative concavity in the first few seconds of the chemical reaction and linearity for all times thereafter. This observation suggested that a double exponential equation would better describe the formation of 12-MPA and that the parameters θ_2 and θ_4 would be opposite in sign ($\theta_2\theta_4 < 0$). All the experimental kinetics runs fit this equation well, as evidenced by the low value of the sum of squares of the residuals and by the satisfaction of the necessary constraint

Figure 19. Semilogarithmic Plots of 12-Molybdophosphate Kinetics Data to Fit Exponential Equations

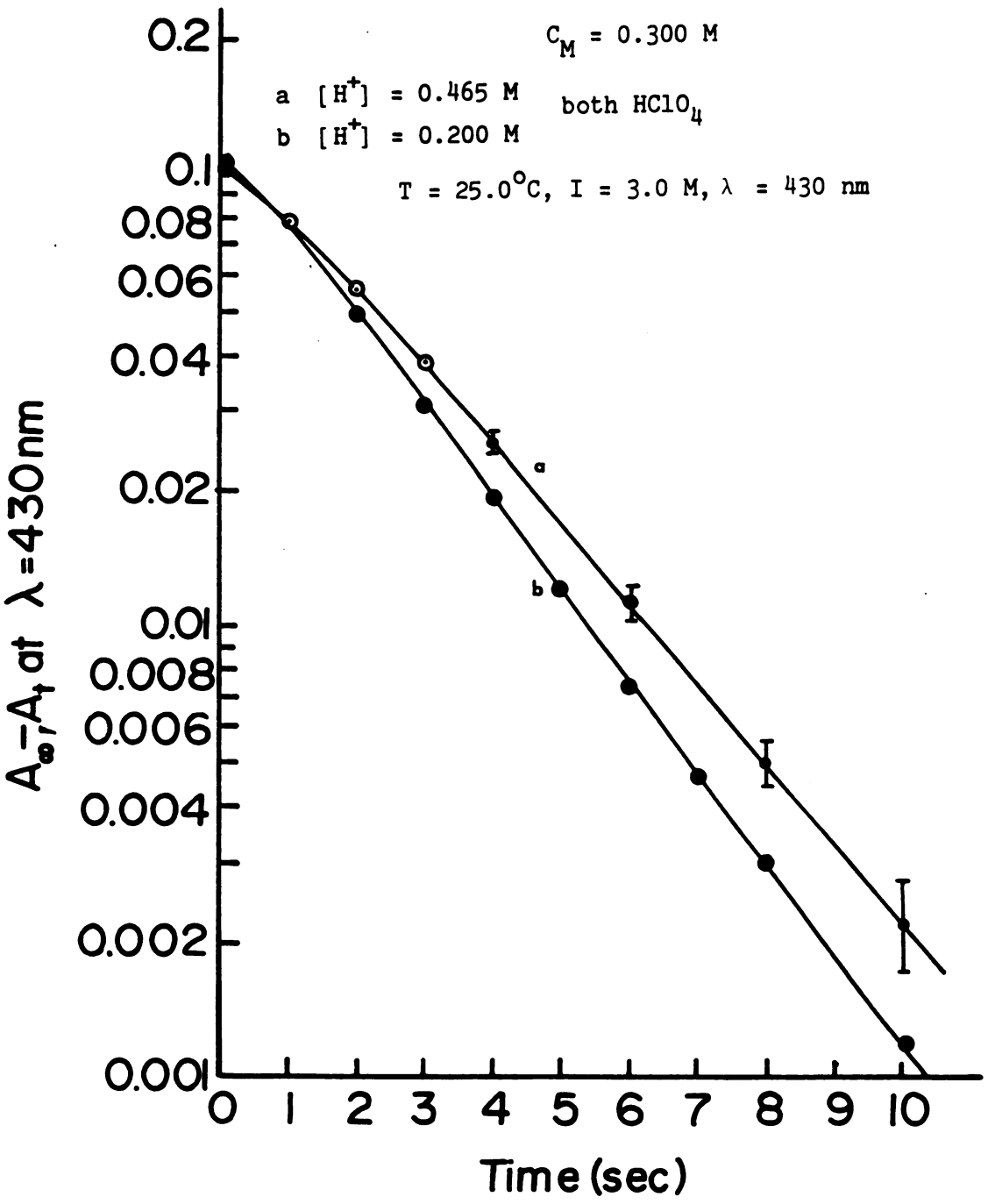

that $\Theta_1 = \Theta_2 + \Theta_4$ when the background absorbance at 430 nm was negligible. Though constant within a given kinetics run, the Θ parameters varied in the different experimental runs as the molybdate and H^+ concentrations in solution were varied. Some chemical reaction schemes consistent with this mathematical function are shown in Table XVI.

2. Experimental Section

The stopped-flow observation cell path length and the solution volumes delivered from the drive syringes were determined with potassium dichromate solutions in 1 M H_2SO_4. A dichromate solution was mixed with water in which the dichromate was introduced first from the sample syringe and then from the reagent syringe. The variance in absorbance was within 1%; both drive syringes thus delivered the same volume of solutions to the mixer. When compared with the absorbance measured in a 1.00 cm quartz cuvette on the Cary 17 Spectrophotometer, the stopped-flow cell path length was found to be 1.87 $\pm$ 0.02 cm.

The solutions used in the kinetics studies were prepared with the consideration that both the sample and the reagent solutions are diluted 1:1 during stopped-flow mixing. The reagent solution contained specified amounts of the stock acid solutions, molybdate, and $NaClO_4$ as calculated with the FORTRAN program MOLYB. If the acid, molybdate, and perchlorate concentrations required for a given pH or isopolymolybdate concentration at 3.0 M ionic strength were C_H, C_M, and $[NaClO_4]$, respectively, then the reagent solution of composition $2C_H$, $2C_M$, and $2[NaClO_4]-3$ gave the desired concentrations when mixed with the phosphate sample solution. A Latin square experimental design was employed, with the final acid concentrations varying from 0.150-1.00 M and C_M

Table XVI

Reaction Schemes Consistent with the Double Experimental Equation

$$Y = \theta_1 + \theta_2 \exp \theta_3 t + \theta_4 \exp \theta_5 t$$

with $\theta_2\ \theta_4 < 0$

(1) Consecutive Reactions with a reversible step: $A \xrightarrow{k_1} B \underset{k_3}{\overset{k_2}{\rightleftharpoons}} C$

$$A = A_o \exp(-k_1 t)$$

$$B = \frac{K_3(A_o+B_o+C_o)}{k_2 + k_3} + \frac{(k_1-k_3)A_o}{k_1+k_3-k_1} \exp(-k_1 t) + \frac{k_2B_o + k_3C_o}{k_2 + k_3} - \frac{A_o k_1 k_2}{(k_2+k_3)(k_2+k_3-k_1)} \exp(-k_2-k_3)t$$

$$C = \frac{k_2(A_o+B_o+C_o)}{k_2 + k_3} - \frac{k_2A_o}{k_2+k_3-k_1} \exp(-k_1 t) - \left[\frac{k_2B_o+k_3C_o}{k_2 + k_3} - \frac{k_1k_2A_o}{(k_2 + k_3)(k_2 + k_3-k_1)}\right] \exp(-k_2-k_3)t$$

(2) Consecutive Reactions with two reversible steps: $A \underset{k_4}{\overset{k_1}{\rightleftharpoons}} B \underset{k_3}{\overset{k_2}{\rightleftharpoons}} C$

At $t = 0$, $B_o = C_o = 0$

Table XVI (cont'd)

$$A = \frac{k_3 k_4 A_o}{\lambda_1 \lambda_2} + \frac{k_1(\lambda_1 - k_2 - k_3)A_o}{\lambda_1(\lambda_1 - \lambda_2)} \exp(-\lambda_1 t) + \frac{k_1(k_2 + k_3 - \lambda_2)A_o}{\lambda_2(\lambda_1 - \lambda_2)} \exp(-\lambda_2 t)$$

$$B = \frac{k_1 k_3 A_o}{\lambda_1 \lambda_2} + \frac{k_1(k_3 - \lambda_1)A_o}{\lambda_1(\lambda_1 - \lambda_2)} \exp(-\lambda_1 t) + \frac{k_1(\lambda_2 - k_3)A_o}{\lambda_2(\lambda_1 - \lambda_2)} \exp(-\lambda_2 t)$$

$$C = \frac{k_1 k_2 A_o}{\lambda_1 \lambda_2} + \frac{k_1 k_2 A_o}{\lambda_1(\lambda_1 - \lambda_2)} \exp(-\lambda_1 t) - \frac{k_1 k_2 A_o}{\lambda_2(\lambda_1 - \lambda_2)} \exp(-\lambda_2 t)$$

where

$$\lambda_{1(2)} = \tfrac{1}{2}(k_1 + k_2 + k_3 + k_4) \underset{(-)}{+} \sqrt{(k_1 + k_2 + k_3 + k_4)^2 - 4(k_1 k_2 + k_3 k_4 + k_1 k_3)}$$

varying from 0.01-0.05 M at each $[H^+]$ used. The sample solutions employed mostly 0.1 mM phosphate in 3 M $NaClO_4$ after the 1:1 dilution, but 0.2 mM and 0.5 mM phosphate solutions were used occasionally to verify the first-order dependence of the reaction rate upon phosphate concentration. All these solutions were prepared by dilution of the appropriate stock solutions with distilled, deionized water. The concentrations chosen provided two related advantages. First, since the molybdate concentrations were present in a 100-fold excess over the phosphate concentrations, the total molybdate concentration (and thus the Mo(VI) species concentrations) did not change appreciably as 12-MPA formed. Second, the formation of 12-MPA did not increase the H^+ concentration of the mixed solutions by more than 3%. These two advantages were important because the double exponential kinetics equation requires that some of the phosphate and molybdate be reacted before the maximum 12-MPA formation rate is attained. In addition, since the molybdate was present in such a large excess, a negligible amount of the dimeric 9-MPA was complexed from 12-MPA and 11-MPA.

The stopped-flow experiments were performed on the automated Beckwith system thermostated at 25.0 $\pm$ 0.1°C with water circulating from a constant temperature bath. The solutions, stored in polyethylene bottles to prevent silicate contamination from prolonged contact with the volumetric glassware, were placed in the constant-temperature bath for ten minutes to increase their temperatures to 25° prior to analysis. The monochromator was set at 430 nm (2 nm bandpass). Generally, only the first ten seconds of the 12-MPA reaction were monitored. The maximum rate of 12-MPA formation was taken as the largest slope from

linear regression of the absorbance versus time data over any given 0.5 s interval; there were six data points within such an interval, with 100 analog points averaged for each data point.

The dependence of the maximum 12-MPA formation rate upon free molybdate and acid concentrations were examined with log-log plots of the maximum rate with concentration, with linear regressions on a programmable pocket calculator, and with KINFIT. The logarithmic plots reveal the range of reaction orders in H^+ or any Mo(VI) isopoly species. Use of the inexpensive pocket calculator to do linear regressions on the maximum rate data showed which linear equations fit the data the best and provided values for the rate law constants to be used as initial estimates for the adjustable parameters in the KINFIT program. The description of KINFIT's utility and operation was described earlier in Section B, Chapter III.

3. Results and Discussion

The modeling with a double exponential equation implies that the chemical mechanism for 12-molybdophosphate formation has two rate-determining steps. The initial rate of 12-MPA formation is no longer the maximum rate since $\frac{dC}{dt} = \frac{d[12\text{-MPA}]}{dt}$ would be zero at the start of the reaction (see Table XVI; the intermediate B must form before any 12-MPA forms). Furthermore, if reversible steps are involved in the mechanism, the time at which 12-MPA formation proceeds at its maximum rate ($\frac{d^2C}{dt^2} = 0$) no longer coincides with the time at which the intermediate B reaches steady state, i.e. at its maximum concentration ($\frac{dB}{dt} = 0$). To determine the relationship between $\frac{dC}{dt}$ and the rate law constants for each mechanism, the integrated rate expressions in Table XVI were differentiated

twice with respect to time with the second derivative set equal to zero. The expressions for the maximum $\frac{dC}{dt}$ value are derived for both mechanisms in Table XVII. In both cases, the maximum rate is directly proportional to A_o, the initial phosphate concentration. However, the expressions for the proportionality constants are quite complex, and the rate constants k_1, k_2, k_3, and k_4 may vary with both H^+ and Mo(VI) species concentrations.

Thus, as was the case for analytical methods based upon the equilibrium 12-MPA concentration in solution, the need for reproducible acid and molybdate concentrations between samples and standards reacted with acidified molybdate reagent is emphasized. Different acid and molybdate concentrations can alter the proportionality constant relating the reaction rate with phosphate content and lead to inaccurate analytical results.

Log-log plots of the time rate of change in absorbance versus the acid and molybdate concentrations reveal effective reaction orders ranging from -0.5 to -6 for H^+, 1.0 to 6.0 for $HMoO_3^+$ and $MoO_3(Mo(OH)_6)$, and 0.5 to 3.5 for $HMo_2O_6^+$ and $H_2MoO_6^{2+}$. Most of the graphs in Figures 20 and 21 show some degree of curvature, possibly from the convolution of two or more terms which have different orders in H^+ and Mo(VI). Each curve in Figure 21 represents one particular total molybdate concentration. Though the total Mo(VI) dimer and monomer concentrations are fairly constant with $[H^+]$, the degree of protonation required to form each particular Mo(VI) complex is pH-dependent (see Figure 6).

In the low acid solutions where $[H^+] < 0.30$ M, the measured maximum rates were significantly lower than the rates observed in the 0.3-0.5 M

Table XVII

Theoretical Variation of the Maximum Reaction Rate $(\frac{dC}{dt})$ with reactant concentration (A_o) and rate constants $(k_1, k_2, \text{etc.})$ for the reaction schemes in Table XVI

At $t = 0$, $B_o = C_o = 0$

(1)

$$\frac{dC}{dt} = \frac{k_1 k_2 A_o}{k_2+k_3-k_1} \exp(-k_1 t) - \frac{k_1 k_2 A_o}{k_2+k_3-k_1} \exp(-k_2-k_3)t$$

$$\frac{d^2C}{dt^2} = 0 = -\frac{k_1^2 k_2 A_o}{k_2+k_3-k_1} \exp(-k_1 t) + \frac{k_1 k_2 (k_2+k_3) A_o}{k_1+k_3-k_1} \exp(-k_2-k_3)t$$

$$\Rightarrow \frac{\exp(-k_1 t)}{\exp(-k_2-k_3)t} = \frac{k_2+k_3}{k_1} \Rightarrow t = \frac{1}{k_2+k_3-k_1} \ln \frac{k_2+k_3}{k_1}$$

$$\left(\frac{dC}{dt}\right)_{C''=o} = \frac{k_1 k_2 A_o}{k_2+k_3-k_1} \left[\left(\frac{k_2+k_3}{k_1}\right)^{\frac{-k_1}{k_2+k_3-k_1}} - \left(\frac{k_2+k_3}{k_1}\right)^{\frac{-k_2-k_3}{k_2+k_3-k_1}} \right]$$

(2)

$$\frac{dC}{dt} = \frac{k_1 k_2 A_o}{\lambda_1-\lambda_2} \exp(-\lambda_1 t) + \frac{k_1 k_2 A_o}{\lambda_1-\lambda_2} \exp(-\lambda_2 t)$$

$$\frac{d^2C}{dt^2} = 0 = \frac{\lambda_1 k_1 k_2 A_o}{\lambda_1-\lambda_2} \exp(-\lambda_1 t) - \frac{\lambda_2 k_1 k_2 A_o}{\lambda_1-\lambda_2} \exp(-\lambda_2 t)$$

$$\Rightarrow \frac{\exp(-\lambda_2 t)}{\exp(-\lambda_1 t)} = \frac{\lambda_1}{\lambda_2} \Rightarrow t = \frac{1}{\lambda_1-\lambda_2} \ln \frac{\lambda_1}{\lambda_2}$$

$$\left(\frac{dC}{dt}\right)_{C''=o} = \frac{k_1 k_2 A_o}{\lambda_1-\lambda_2} \left[\left(\frac{\lambda_1}{\lambda_2}\right)^{\frac{-\lambda_2}{\lambda_1-\lambda_2}} - \left(\frac{\lambda_1}{\lambda_2}\right)^{\frac{-\lambda_1}{\lambda_1-\lambda_2}} \right]$$

Figure 20. Kinetics of 12-Molybdophosphate Formation as a Function of Initial Molybdate Concentration

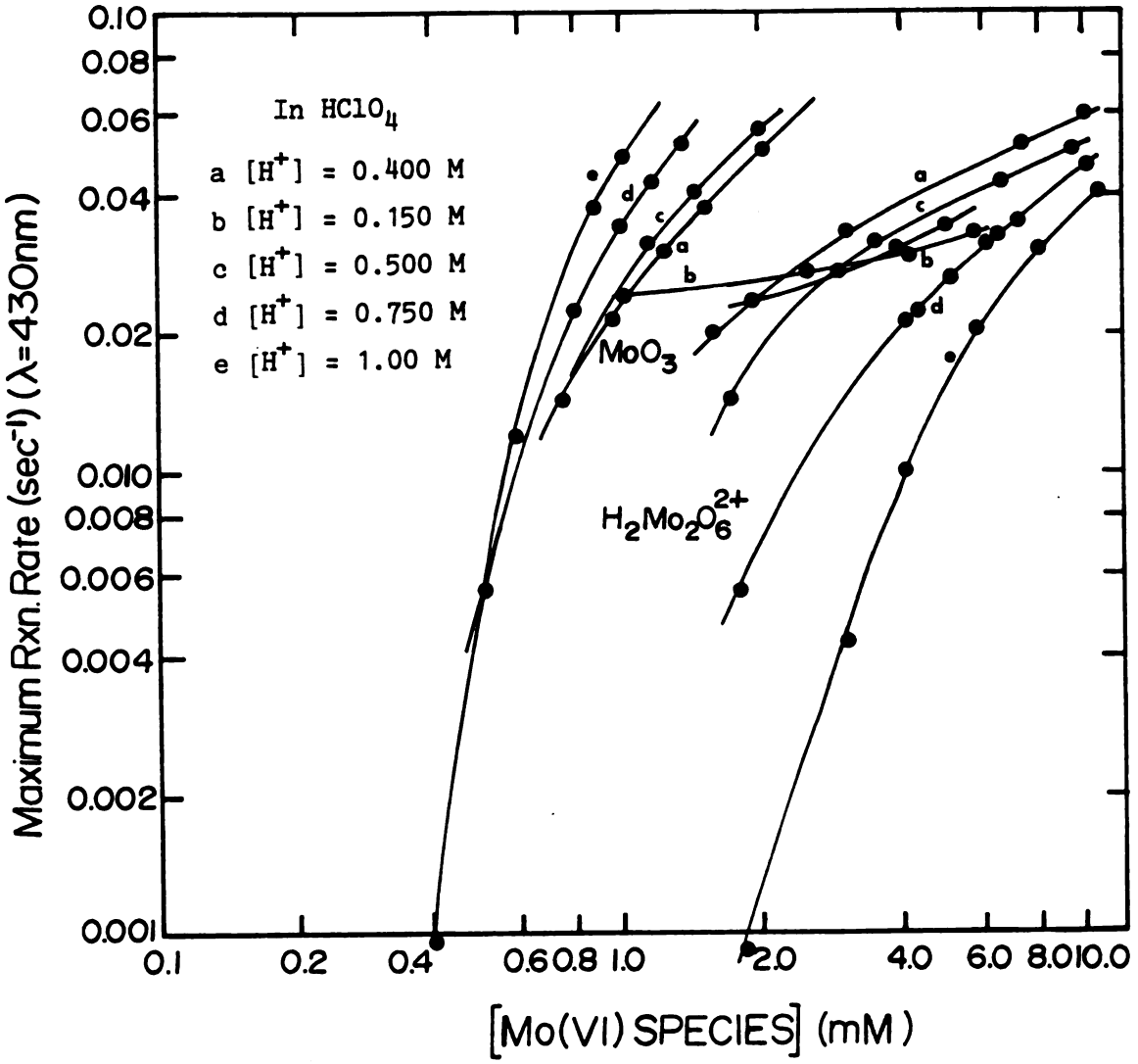

Figure 21. Kinetics of 12-Molybdophosphate Formation as a Function of Hydrogen Ion Concentration

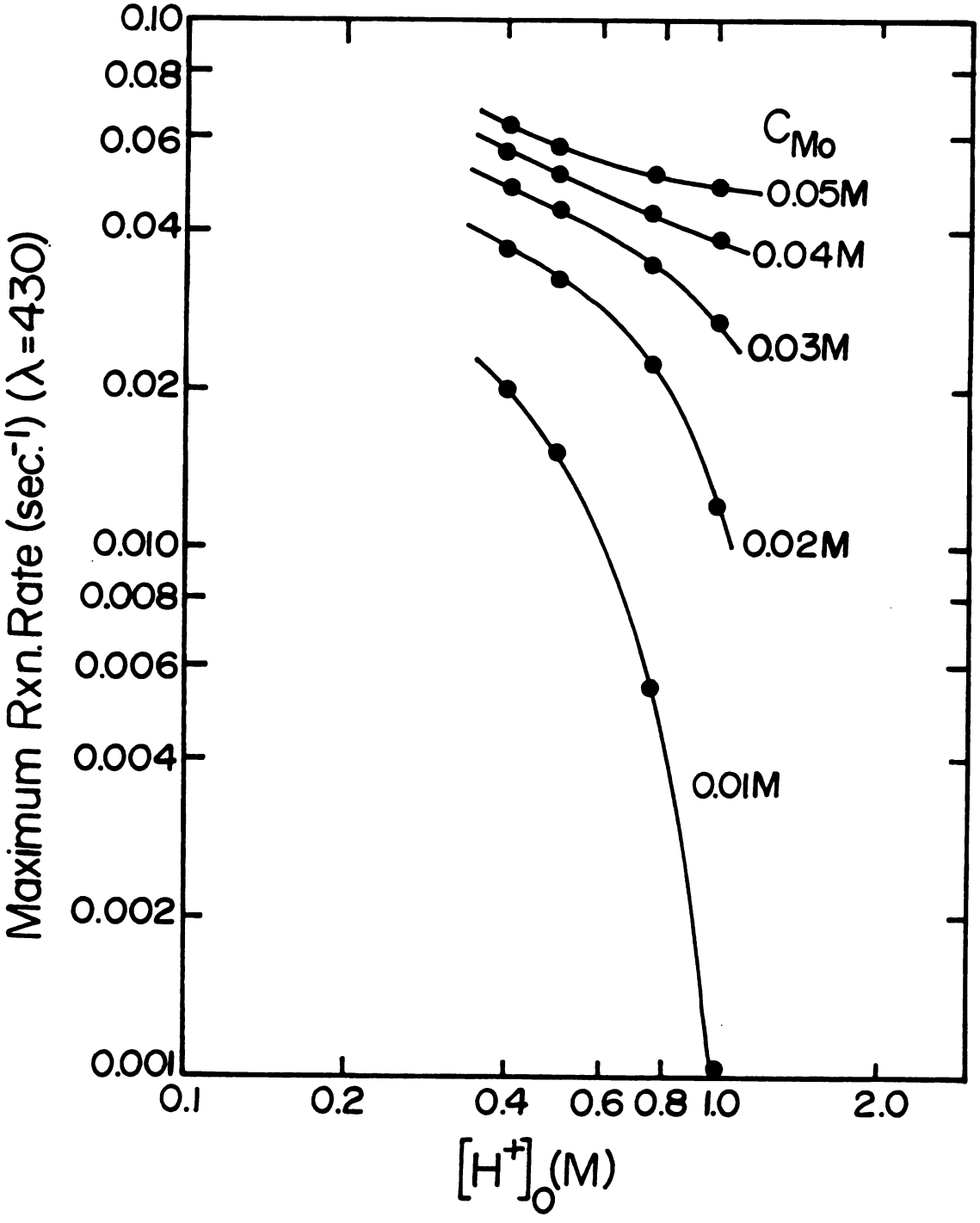

acidity range. Because the pH of these lower acidity solutions is close to the Mo(VI) isoelectric pH of 0.9, the amount of Mo(VI) species available to complex with phosphate was reduced through MoO_3 precipitation. Though no white precipitate was visible, any suspended particles in the solution could scatter the incident 430 nm radiation and cause spectrophotometric background interferences.

With the linear regression program on a HP-25C pocket calculator, various linear equations were found that could fit the variation in the 12-MPA maximum formation rate with molybdate concentration over limited acidity ranges or the variation in the maximum rate with hydrogen ion concentration over certain ranges of molybdate concentration. The equations, slopes, and Y-intercepts that fit the selected experimental conditions in HNO_3 and $HClO_4$ solutions are tabulated in Table XVIII. For the molybdate dependence in the low acid limit between 0.3-0.5 M H^+, the linear equation $\frac{1}{RATE} = \frac{m}{[H_2Mo_2O_6^{2+}]} + b$ gave the best fit of the experimental data. Other equations that were tried included $\frac{[H_2Mo_2O_6^{2+}]}{RATE} = \frac{m}{[H_2Mo_2O_6^{2+}]} + b$, $RATE = m[H_2Mo_2O_6^{2+}] + b$, $RATE = m[HMoO_3^{+}] + b$, $\log(RATE) = m \log[H_2Mo_2O_6^{2+}] + b$, and $\frac{1}{RATE} = \frac{m}{[HMoO_3^{+}]} + b$. Since the equation $\frac{1}{RATE} = \frac{m}{[H_2Mo_2O_6^{2+}]} + b$ held over a fairly wide acidity range, the variation of the constants m and b with $[H^+]$ was tested. The constant b was found to be independent of $[H^+]$ while m varied with the square of $[H^+]$. This equation no longer described the 12-MPA formation data well at $[H^+] = 0.750$ M; instead, the equation $\frac{1}{RATE} = \frac{m}{[H_2Mo_2O_6^{2+}]^2} + b$ gave an excellent fit for the

Table XVIII

Linear Equations Which Best Fit 12-MPA Kinetics Data Over Limited Ranges of Experimental Conditions

	HNO_3	$HClO_4$
$[H^+]_o$ = 0.30-0.50 M $\frac{1}{RATE} = \frac{m[H^+]^2}{[H_2Mo_2O_6^{2+}]}$	b = 10.48 sec m = 0.580 sec/M r_{xy} = 0.9996	b = 9.46 sec m = 0.396 sec/M r_{xy} = 0.9984
$[H^+]_o$ = 0.750 M $\frac{1}{RATE} = \frac{m}{[H_2Mo_2O_6^{2+}]} + b$	b = 16.97 sec m = $1.12\times10^{-3}M^2$sec r_{xy} = 0.9988	b = 17.187 sec m = $5.21\times10^{-4}M^2$sec r_{xy} = 0.9998
$[H^+]_o$ = 1.00 M $\frac{1}{RATE} = \frac{m}{[H_2Mo_2O_6^{2+}]^3} + b$	b = 22.53 sec m = $1.56\times10^{-5}M^3$sec r_{xy} = 0.999+	b = 16.34 sec m = $6.26\times10^{-6}M^3$sec r_{xy} = 0.9999
C_M = 0.01-0.02 M $\frac{1}{RATE} = \frac{m[H^+]^8}{[H_2Mo_2O_6^{2+}]^3} + \frac{b}{[H_2Mo_2O_6^{2+}]}$	b = 0.1515 M sec m = 1.53×10^{-5}sec/M^5 r_{xy} = 0.9997	b = 0.1105 M sec m = 6.00×10^{-6}sec/M^5 r_{xy} = 0.9991
$C_M > 0.04$ M $\frac{1}{RATE} = \frac{m[H^+]}{[H_2Mo_2O_6^{2+}]^2} + b[H_2Mo_2O_6^{2+}]^2$		

This is the best fit linear equation for the experimental data in this C_M concentration range, but is still a relatively poor fit.
($r_{xy} < 0.98$)

data obtained from 0.75 M H^+ solutions. In 1.00 M H^+ solutions the equation $\frac{1}{RATE} = \frac{m}{[H_2Mo_2O_6^{2+}]^3} + b$ fits the data slightly better than the equation $\frac{1}{RATE} = \frac{m}{[H_2Mo_2O_6^{2+}]^4} + b$, but both gave correlation coefficients greater than 0.9990.

To analyze the variation of the maximum rate with acidity, the equation $\frac{1}{RATE} = m[H^+]^8 + b$ provided the best fit of the kinetics data for solutions low in molybdate concentration ($C_M < 0.02$ M). In this equation, b varied inversely with $[H_2Mo_2O_6^{2+}]$, and m varied inversely with $[H_2Mo_2O_6^{2+}]^3$. At higher molybdate concentrations, the equation $\frac{1}{RATE} = \frac{m[H^+]}{[H_2Mo_2O_6^{2+}]^2} + b[H_2Mo_2O_6^{2+}]^2$ provided the best fit, but this fit was poor compared to the other equations described above.

There are at least two possible explanations for the observation of different linear equations to describe the experimental observations. First, the linear equations reflect the predominant terms in the complex rate expressions shown in Table XVII. The relative magnitude and significance of each term in the equation vary with changes in either acid or molybdate concentrations. The second explanation suggests that the same chemical mechanism for 12-molybdophosphate formation does not occur over the entire range of H^+ and Mo(VI) concentrations studied. The mechanisms consistent with the linear equations for the 12-MPA formation are tabulated in Table XIX. The molybdate linear equation in the low acid limit (0.3-0.5 M H^+) suggests that an acidic dissociation occurs prior to combination with $H_2Mo_2O_6^{2+}$ (or $HMo_2O_6^{+}$ or $H_3Mo_2O_6^{3+}$) in the latter rate-determining step. The other mechanisms displayed suggest either a change

Table XIX

Chemical Mechanisms for 12-MPA Formation Corresponding to the Linear Equations in Table XVIII

$$\text{RATE} = \frac{K_1[H_3PO_4][H_2MoO_6^{2+}]}{K_2[H^+]^2 + [H_2Mo_2O_6^{2+}]} \qquad (0.30\ M \leq [H^+] \leq 0.50\ M)$$

$$\underset{A}{\text{INTERMEDIATE}} \rightleftharpoons \underset{B}{\text{INTERMEDIATE}} + 2\ H^+$$

$$B + H_2Mo_2O_6^{2+} \longrightarrow \text{Products}$$

$$\text{RATE} = \frac{K_1[H_3PO_4][H_2Mo_2O_6^{2+}]^3}{K_2[H^+]^z + [H_2Mo_2O_6^{2+}]^3} \qquad ([H^+] = 1.00\ M)$$

$$A \rightleftharpoons B + Z\ H^+$$

$$B + 3\ H_2Mo_2O_6^{2+} \longrightarrow \text{Products}$$

$$\frac{1}{\text{RATE}} = \frac{m[H^+]^8}{[H_2Mo_2O_6^{2+}]^3} + \frac{b}{[H_2Mo_2O_6^{2+}]} \qquad (C_M \leq 0.02\ M)$$

$$A \rightleftharpoons B + 2\ H^+$$

$$B + H_2Mo_2O_6^{2+} \rightleftharpoons C + 2H^+$$

$$C + H_2Mo_2O_6^{2+} \rightleftharpoons D + 2H^+$$

$$D + H_2Mo_2O_6^{2+} \longrightarrow \text{12-MPA} + 2H^+$$

No reasonable mechanism could be postulated for the acid dependence at high molybdate concentrations.

in the number of molybdate species bound to phosphate in the intermediate involved in the rate-determining step or else a switch in rate-determining steps to form different molybdophosphates.

Various attempts to integrate the observed rate equations and fit the experimental data with this integrated equation were performed with KINFIT. The rate equation which gave the best fit had the form

$$\frac{d[12\text{-MPA}]}{dt} = \frac{K_1[H_3PO_4][H_2Mo_2O_6^{2+}]^3}{K_2[H^+]^5 = K_3[H^+]^2[H_2Mo_2O_6^{2+}]^2 + [H_2Mo_2O_6^{2+}]^3}$$

and the values for the rate constants were

	HNO_3	$HClO_4$
K_1 =	0.430 ± 0.028 sec^{-1};	0.406 ± 0.019 sec^{-1}
K_2 =	$(6.7 \pm 1.8) \times 10^{-7}$ M^{-2};	$(2.7 \pm 1.0) \times 10^{-7}$ M^{-2}
K_3 =	0.0394 ± 0.0043 M^{-1};	0.0222 ± 0.0028 M^{-1}

This was the best fit possible with consecutive step modeling. However, the chemical mechanism consistent with the above rate equation suggested that H_3PO_4 dissociates two proton equivalents before being coordinated by molybdate. Because of the negligible formation rate of 12-MPA measured in solutions more alkaline than pH 2,[66] this proposed mechanism cannot be correct. On the other hand, a consecutive step mechanism in which H_3PO_4 initially complexes with a Mo(VI) species (as illustrated in Table VI with related forms of the rate equation in Table V) cannot be valid either. The sum of the squares of the residuals from KINFIT were significantly large, and the standard deviations associated with the final values of the adjustable parameters were ten times larger than the parameter values

themselves. Though the consecutive step mechanism with only one rate-determining step postulated by previous workers[4,5,7,51,52] may have been valid since their solution ionic strengths were 2 M and below, a consecutive reactions mechanism with two rate-determining steps had to be postulated for the 12-MPA formation kinetics as observed in 3.0 M ionic strength solutions.

For a consecutive reactions mechanism the equation relating the maximum reaction rate with $A_o(C_{PO_4})$ and rate constants k_1 and k_2 is

$$\left(\frac{dC}{dt}\right)_{C''=o} = \frac{k_1 k_2 A_o}{k_2-k_1}\left[\left(\frac{k_2}{k_1}\right)^{-\frac{k_1}{k_2-k_1}} - \left(\frac{k_2}{k_1}\right)^{-\frac{k_2}{k_2-k_1}}\right] \qquad (1)$$

The constants k_1 and k_2 each depend on the acid and molybdate concentrations present. Though these dependencies may seem difficult to deduce at first, the 12-MPA formation rate is first-order with respect to the molybdate concentration and follows a simple exponential equation more closely when $0.3\ M \leq [H^+] \leq 0.50\ M$ and $C_M \leq 0.02\ M$. The reaction rate decreases with increased $[H^+]$, and 12-MPA formation releases H^+ into solution. Therefore, k_2 must increase faster than k_1 so that the kinetics are controlled by the first rate-determining step in the low acid limit. Mathematically, as k_2 increases relative to k_1, the above equation becomes $\left(\frac{dC}{dt}\right)_{C''=o} = k_1 A_o\left[\left(\frac{k_2}{k_1}\right)^{\frac{k_1}{k_2}} - \left(\frac{k_2}{k_1}\right)^{-1}\right]$, which approaches $k_1A_o(1.0-0.0) = k_1A_o$ as k_2 approaches $+\infty$.

When $0.3\ M \leq [H^+] \leq 0.50\ M$ and $C_M \leq 0.02\ M$, the maximum reaction rate was proportional to $\frac{[HMoO_3^+]}{[H^+]}$. This relationship was consistent with

previous publication of bimolecular 12-MPA kinetics in the low acid limit[51] if $Mo(OH)_6$ is the species that reacts with H_3PO_4. If one sets k_1 equal to $K_1 \frac{[HMoO_3^+]}{[H^+]}$, K_1 constant, the range of the measured reaction rates from 0.8 A_o to 650 A_o confined k_1 to values ranging from 10 to 650 and set 1.0 as the lower bound for k_2. The k_2 values which, along with the k_1 values, reproduced the measured maximum rates were observed to vary directly with $\frac{[HMoO_3^+]^9}{[H^+]^{10}}$.

With $k_1 = K_1 \frac{[HMoO_3^+]}{[H^+]}$ and $k_2 = K_2 \frac{[HMoO_3^+]^9}{[H^+]^{10}}$, the consecutive reactions rate equation (equation 1) converged during KINFIT execution after only nine iterations. The final values for the adjusted parameters K_1 and K_2 are tabulated in Table XX. The residual errors were reduced by as much as 60% by using this rate equation, and the relative standard deviations associated with the adjusted parameter values were the smallest observed from all the KINFIT executions. The chemical mechanism tabulated in Table XX reproduced the rate equation when equilibrium approximations were applied to MoO_3 (same as $Mo(OH)_6$), $(HPO_4)(MoO_3)^{2-}$, and $(PO_4)(MoO_3)_9^{3-}$.

The proposed mechanism has the following support. First, with equilibrium approximations on the molybdophosphates following the second rate-determining step, the overall 12-MPA reaction stoichiometry

$$H_3PO_4 + 12\ HMoO_3^+ \rightleftharpoons PMo_{12}O_{40}^{3-} + 15\ H^+$$

is reproduced. Secondly, the second rate-determining step (k_2) is the same as the rate-determining step postulated from the 12-MPA acid

Table XX

Rate Law Equation, Constants, and Mechanism for 12-MPA Formation (I = 3.0 M, T = 25.0°C, λ = 430 nm)*

$$\text{MAX. RATE} = \left(\frac{d[\text{12-MPA}]}{dt}\right)_{A_\lambda' = 0} = \frac{k_1 k_2 C_{PO_4}}{k_2 - k_1}\left[\left(\frac{k_2}{k_1}\right)^{\frac{-k_1}{k_2-k_1}} - \left(\frac{k_2}{k_1}\right)^{\frac{-k_2}{k_2-k_1}}\right]$$

where $k_1 = K_1 \frac{[HMoO_3^+]}{[H^+]}$ and $k_2 = K_2 \frac{[HMoO_3^+]^9}{[H^+]^{10}}$

	HNO_3	$HClO_4$
K_1	10.3 ± 0.2 sec^{-1};	12.5 ± 3 sec^{-1}
K_2	$(6.2 \pm 0.7) \times 10^{17}$ M sec^{-1};	$(4.3 \pm 1.4) \times 10^{18}$ M sec^{-1}

$$HMoO_3^+ \rightleftharpoons MoO_3 + H^+ \qquad \text{fast}$$

$$H_3PO_4 + MoO_3 \xrightarrow{k_1} (HPO_4)(MoO_3)^{2-} + 2H^+ \qquad \text{slow}$$

$$(HPO_4)(MoO_3)^{2-} + 8\ MoO_3 \rightleftharpoons (PO_4)(MoO_3)_9^{3-} + H^+ \qquad \text{fast}$$

$$(PO_4)(MoO_3)_9^{3-} + MoO_3 \xrightarrow{k_2} \text{Products} \qquad \text{slow}$$

$$(PO_4)(MoO_3)_{10,11,12}^{3-}$$

*At 430 nm, $\varepsilon_{\text{12-MPA}} = 1061 \pm 78$ l mole^{-1} cm^{-1}

b = 1.87 ± 0.02 cm in the Beckwith stopped-flow observation cell.

decomposition rate equation (see Section C). Thirdly, the k_2 step reflects the competing mechanisms of monomeric 9-MPA coordinating another phosphate to form dimeric 9-MPA or more molybdate to become 12-MPA. Finally, in the higher acid solutions ($[H^+] > 0.5$ M), with equilibrium approximations on all intermediates prior to the k_2 step and consideration of only the first term in the acid decomposition rate equation (see Section C), the 12-MPA equilibrium constant is

$$\text{Keq.} = \frac{k_f}{k_r} = \frac{k_{1f}\,k_{2f}}{k_d\,k_{1r}} = \frac{[\,12\text{-MPA}\,]}{[\,HMoO_3^{+}]^2}\;\frac{[H^+]^{13}}{[HMoO_3^{+}]^{10}\,[H_3PO_4]}.$$

All of the stoichiometric coefficients are reproduced in the equilibrium constant exponents. The H^+ exponent represents the weighted average of the number of H^+ released from each Mo(VI) species during complexation rather than from $HMoO_3^+$ or MoO_3 only (see Table X).

As pointed out by Truesdale, et. al.,[41] knowledge of molybdate and heteropolymolybdate speciation in strong acid solution has revealed more definitive information about the chemistry and kinetics of 12-MPA formation. Analytically, the experimental considerations for reaction-rate phosphate determinations already published[51,52] have amplified significance. Not only does performing the experiment at 0.3 M $\leq [H^+] \leq$ 0.50 M and $C_{Mo} \leq$ 0.02 M give the best sensitivity with faster reaction rates, but the 12-MPA kinetics are simpler and more well-behaved. Under these conditions, the MoO_3 precipitate does not interfere with absorbance measurements. Also, the sensitivity is enhanced in perchloric acid solutions since the rate constants are larger in $HClO_4$ media. The reproducibility of the solution pH, molybdate content, and ionic

strength between reagent solutions mixed with samples and with phosphate standards is again emphasized as each factor affects the 12-MPA reaction rate measured (see also Section D).

An overall chemical scheme that displays the pathways for the molybdophosphate reactions studied in this section (and in Section C) is shown in Table XXI. The intermediate 9-molybdophosphate monomer represents a branching point in the pathways. Depending upon which chemical reagent is present in excess, the 9-molybdophosphate can associate more molybdate to form 10,11, and 12-molybdophosphate products, associate another phosphate and more molybdate to become dimeric 9-MPA, or decompose in the presence of excess H^+ back to phosphoric acid and molybdate constituents.

B. Stopped-Flow Kinetics Studies of β-12-MSA Formation and Decomposition

1. Experimental Conditions and Preliminary Measurements

As mentioned in the previous section, the reproducibility of the β-12-MSA formation rate data was tested with preliminary stopped-flow measurements at 400 nm on solutions with various analytical concentrations of acid, Mo(VI), and silicate. As for the 12-MPA system, the rates measured here agreed with previous data[6] within experimental error, except for solutions with total acid concentrations greater than 0.2 M. Under these experimental conditions, the reaction rates measured here were significantly slower than those rates measured by Gall.[6] The discrepancy was related to the formation of cationic Mo(VI) species rather than the heptameric and octameric polyanions. When $C_H > 0.2$ M, the solution pH was below the Mo(VI) isoelectric pH of 0.9.

Table XXI

Overall Chemical Scheme for Molybdophosphate Reactions

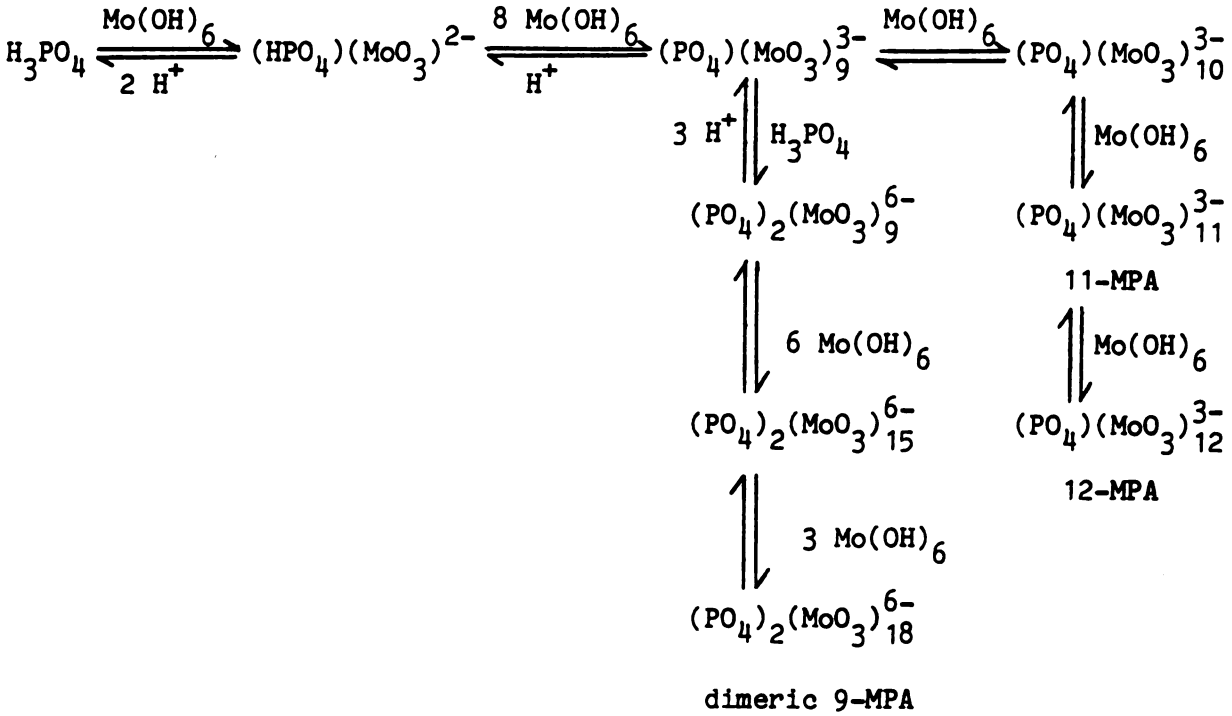

The overall kinetics profile for the formation of β-12-MSA was observed in the pH range 1.2-1.8. A reaction time of 100-200 s was required for equilibrium to be approached. The β-12-MSA absorbance time profile followed a simple exponential equation of the form $A = \Theta_1 + \Theta_2 \exp \Theta_3 t$. A sample $\ln(A_\infty - A_t)$ vs. t plot for β-12-MSA formation is shown in Figure 22 and can be compared with a similar plot for 12-MPA in Figure 19. The monochromator wavelength was 430 nm (2 nm bandpass).

The solutions used for the β-12-MSA kinetics study were prepared in a similar manner as for the 12-MPA study, except that silicate was used instead of phosphate, the solution ionic strengths were 1.0 M, and the C_H and C_M concentrations required to give the correct pH or molybdate content were calculated with the HALTAFALL computer program instead of MOLYB.FT. A typical stopped-flow kinetics run lasted 100 s rather than 10 s as in the phosphate case. The Mo(VI) concentrations varied from 0.01 M to 0.10 M, and the solution pH's employed were 1.2, 1.5, and 1.8. All the solutions were allowed to equilibrate thermally in the 25.0°C temperature bath for ten minutes prior to the stopped-flow run.

2. Rate Equation and Chemical Mechanism in HNO_3 and $HClO_4$ Solutions

Because a simple exponential equation was observed to fit the overall β-12-MSA kinetics profile, the mathematical modeling and the postulation of a chemical mechanism for β-12-MSA formation were easier to perform than for the 12-MPA formation. This absorbance-time behavior indicated that there is only one rate-determining step in the mechanism. The maximum absorbance increase with time corresponded with the initial reaction rate. However, the pH 1.2 solutions exhibited suspiciously low

Figure 22. **Semilogarithmic Plot of β-12-Molybdosilicate Kinetics Data**

I = 1.0M, T = 25.0°C, pH 1.5 in $HClO_4$, C_{Si} = 0.1 mM, C_M = 0.05 M

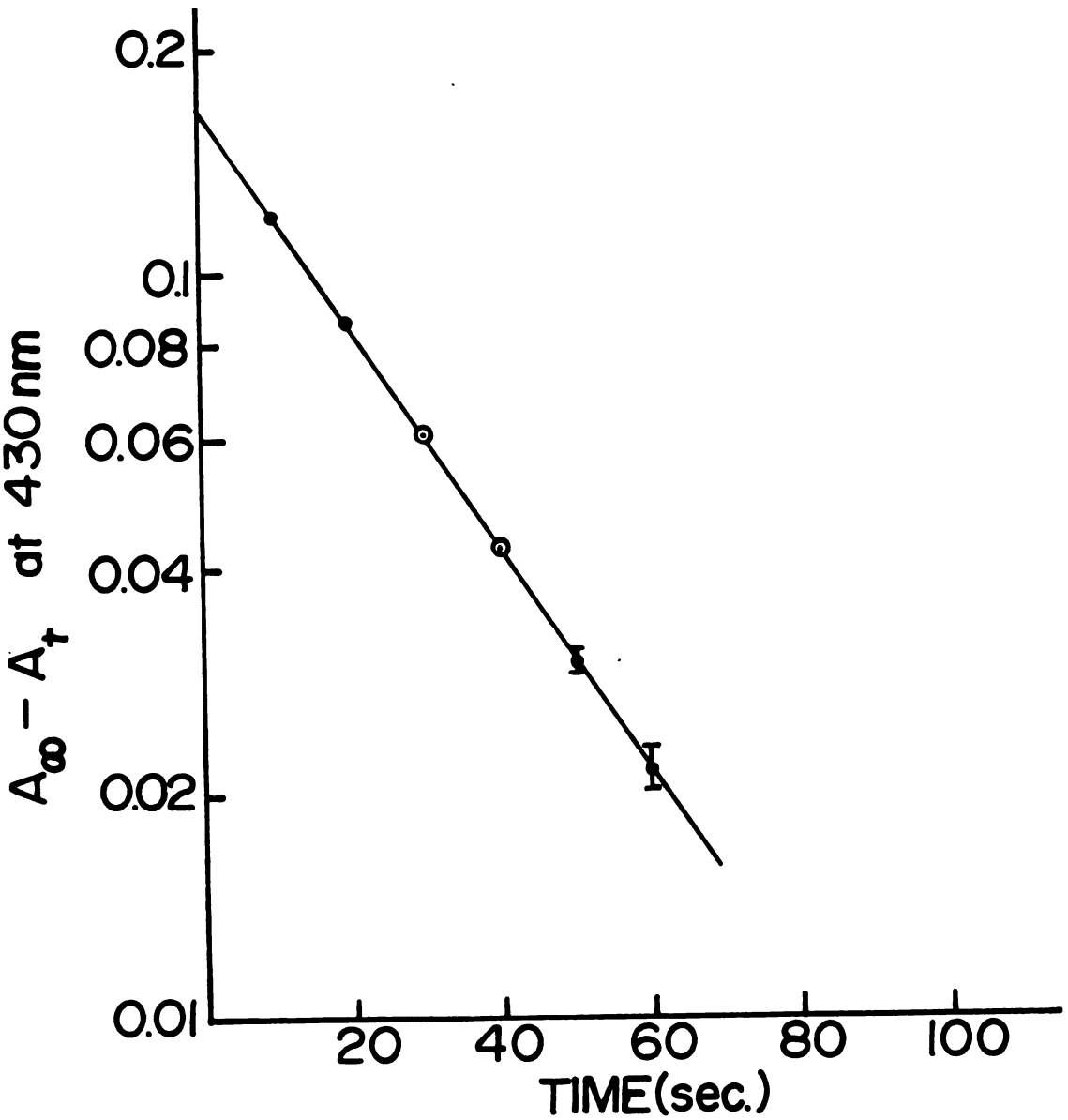

initial rates which were independent of the total molybdate concentration at values exceeding 0.04 M. This behavior suggested precipitation of MoO_3, since pH 1.2 is close to the Mo(VI) isoelectric pH of 0.9. For the solutions at pH 1.5 and 1.8, which did not exhibit any evidence of Mo(VI) precipitation, several linear equations were used in an attempt to fit the experimental data. The equation that best fit the data for molybdate dependence had the form $\frac{[H_2MoO_4]}{RATE} = \frac{m}{[Mo_8O_{26}^{4-}]} + b$. An identical equation has been found to fit similar data in HCl solutions.[41]

The rate constants of Truesdale in HCl solutions at pH 1.2 and the rate constants found here in HNO_3, H_2SO_4, and $HClO_4$ solutions at pH 1.5 and 1.8 are shown in Table XXII. The values differ slightly because of the different pH values and different acidic media used for the experiments. In HCl solutions the Cl^- could have complexed some Mo(VI) species to reduce the free molybdate concentration; under such conditions Truesdale and coworkers would have studied β-12-MSA kinetics without significant MoO_3 precipitation. Truesdale's chemical mechanism consistent with the rate law consists of a rapid equilibration step between silicate and H_2MoO_4 followed by a rate-determining step between the molybdosilicate intermediate and $Mo_8O_{26}^{4-}$.[41] Of course, other Mo(VI) species may be represented in the empirical rate equation, such as $HMoO_4^-$ in place of H_2MoO_4 and $H_2Mo_7O_{24}^{4-}$ in place of $Mo_8O_{26}^{4-}$. However, in the pH range 1.2-1.8, H_2MoO_4 is the predominant molybdate monomer, and $Mo_8O_{26}^{4-}$ is more prevalent than any of the heptameric species.

Table XXII

Rate Constant for β-12-MSA Formation in Various Acidic Media

pH	Acidic Medium	b* (M sec)	m^* (M^2 sec)	r_{xy}	K_1^{**} ($M^{-1}sec^{-1}$)	K_2^{**} (M)
1.2	HCl	----	----	0.987	0.122	0.000791
1.5	HNO_3	0.452	3.25×10^{-4}	0.988	0.332	0.000719
1.5	$HClO_4$	0.508	3.13×10^{-4}	0.999	0.296	0.000616
1.5	H_2SO_4	0.149	3.08×10^{-4}	0.996	1.01	0.00210
1.8	HNO_3	0.219	3.30×10^{-4}	0.986	0.69	0.00150
1.8	$HClO_4$	0.226	3.23×10^{-4}	0.972	0.67	0.00140
1.8	H_2SO_4	0.114	2.79×10^{-4}	0.981	1.31	0.0024

*Constants in $\frac{[H_2MoO_4]}{RATE} = \frac{m}{[Mo_8O_{26}^{4-}]} + b$

**Constants in $\frac{d[\beta\text{-12-MSA}]}{dt} = \frac{K_1[Si(OH)_4][H_2MoO_4][Mo_8O_{26}^{4-}]}{K_2 + [Mo_8O_{26}^{4-}]}$

where $\frac{d[\beta\text{-12-MSA}]}{dt} = \frac{RATE}{\varepsilon b_o}$, $K_1 = \varepsilon b_0 \frac{[Si(OH)_4]}{b}$, and $K_2 = \frac{m}{b}$

$\varepsilon = 803.3\ M^{-1}cm^{-1}$ for β-12-MSA at 430 nm, T = 25.0°C, I = 1.0 M

b_o = 1.87 cm in the Beckwith stopped-flow observation cell.

Because of the propagated errors in calculating the solution pH from HALTAFALL, the experimental errors in measuring the initial reaction rate (5% RSD), and the narrow pH range in which only the β isomer of 12-MSA is formed, the acid dependence for the β-12-MSA reaction was difficult to determine. Inspection of K_1 and K_2 values tabulated in Table XXII suggested inverse relationships between both K_1 and K_2 and the solution $[H^+]$ in HNO_3, H_2SO_4, and $HClO_4$ solutions. To explain these experimental observations, Truesdale's mechanism was modified to include an acidic deprotonation of H_2MoO_4 (or H_2SiO_3) and an acid-catalyzed rate-determining step with $Mo_8O_{26}^{4-}$:

$$H_2MoO_4 \underset{k_{-1}}{\overset{k_1}{\rightleftharpoons}} HMoO_4^- + H^+$$

$$Si(OH)_4 + HMoO_4^- \underset{k_{-2}}{\overset{k_2}{\rightleftharpoons}} A$$

$$A + H^+ + Mo_8O_{26}^{4-} \xrightarrow{k_3} \text{Products} \qquad \text{(slow)}$$

$$\frac{d[\beta\text{-12-MSA}]}{dt} = \frac{K_1[Si(OH)_4][H_2MoO_4][Mo_8O_{26}^{4-}]}{K_2 + K_3[H^+][Mo_8O_{26}^{4-}] + [H_2MoO_4][Mo_8O_{26}^{-}]}$$

where $K_1 = k_1$, $K_2 = \frac{k_{-1}k_{-2}}{k_2k_3}$, $K_3 = \frac{k_{-1}}{k_2}$

This modified mechanism accounted for all the observed dependences in H^+, H_2MoO_4, and $Mo_8O_{26}^{4-}$. The rate law equation converged during KINFIT execution with the experimental data; however, the final values for the adjusted parameters had large standard deviations associated with them. Much of the problem originated from the nonlinearities of the graphs of

$\frac{[H_2MoO_4]}{RATE}$ vs. $\frac{1}{[Mo_8O_{26}^{4-}]}$ shown in Figure 23, though the linearities obtained from other equations were considerably worse.

Because of both acid and molybdate dependence in the β-12-MSA rate equation, reproducible acid concentrations between samples and silicon standards mixed with molybdate reagent are essential to insure the integrity and accuracy of silicate determinations. Not only are both the solution pH and isopolymolybdate concentrations affected, but C_H and C_M also determine which 12-MSA isomer is complexed. Each isomer has a different molar absorptivity at a given wavelength.

Two other comparisons of the constants in Table XXII should be noted. First, the variation of K_1 and K_2 with $[H^+]$ in sulfuric acid solutions was not as large as in the other acidic media. Perhaps the buffering capacity of the HSO_4^--SO_4^{2-} system regulated the hydrogen ion concentration as the molybdosilicate reaction progressed; the second pK_a for H_2SO_4 is 1.51 in 1.0 M ionic strength solutions (see Chapter IV, Section A). Secondly, for any given molybdate concentration, the K_1 rate constant for H_2SO_4 solutions was significantly greater than for any other acid solution over the pH range 1.2-1.8. Thus, because of its inherently faster initial reaction rate, a reagent molybdate solution acidified with H_2SO_4 would provide the best sensitivity in a reaction-rate determination for silicate.

3. β-12-MSA Decomposition in Basic Solution

To complete the characterization of the molybdosilicate chemical system, the decomposition kinetics of β-12-MSA in basic solution were studied. Acidic solutions containing β-12-MSA were mixed with excess hydroxide in the stopped-flow system, and the decrease in

Figure 23. Plots of β-12-Molybdosilicate Formation Rate vs. Molybdenum (VI) Species Concentration in Various Acidic Solutions

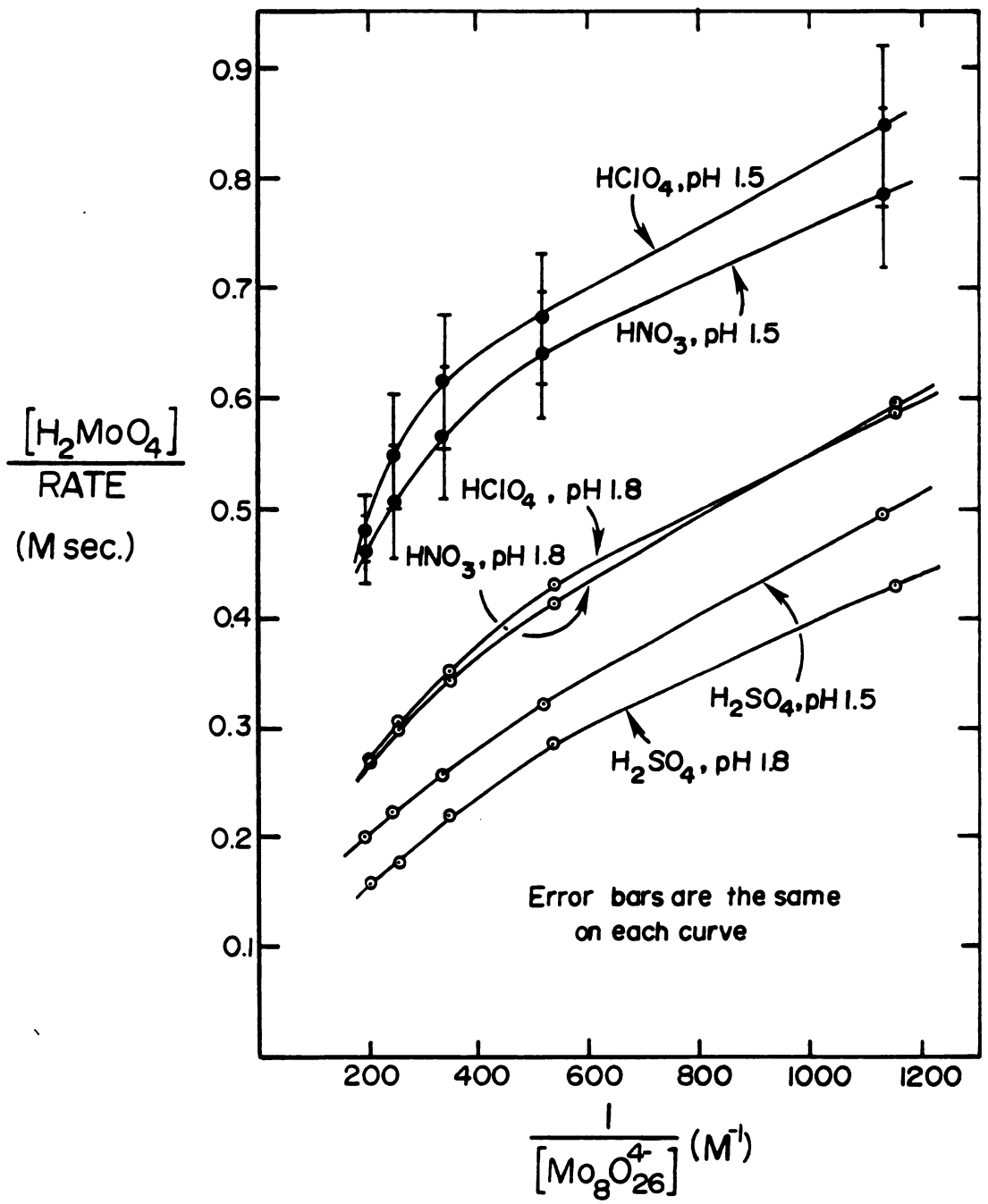

absorbance was measured at 430 nm. These molybdosilicate solutions were prepared by adding silicate to the acidified molybdate solution. Enough silicate was added to produce a substantial yellow color, yet leave the solution pH and free molybdate concentration relatively unchanged. When molybdate was present in a hundred-fold excess, HALTAFALL showed that essentially all silicate was complexed as 12-MSA. The ranges of molybdosilicate, molybdate, and hydroxide concentrations employed were 0.1-0.5 mM, 0.01-0.05 M, and 0.1-0.5 M, respectively. Because the β-12-MSA decomposition occurred rapidly, the fastest data acquisition rates available on the stopped-flow system had to be used. One data point was measured each millisecond, and the reaction time spanned only 100 ms. Refractive index changes caused by temperature changes in the stopped-flow system were negligible, as evidenced by an absorbance change of less than 0.002 when 0.1 M HNO_3 was mixed with 1.0 M NaOH.

The β-12-MSA decomposition kinetics follows the rate law below.

$$\frac{d[\beta\text{-12-MSA}]}{dt} = \frac{K_1[\beta\text{-12-MSA}][OH^-]}{K_2 + [OH]} \qquad (2)$$

with $K_1 = 20.7 \pm 0.5\ sec^{-1}(HNO_3)$ and $20.1 \pm 0.5\ sec^{-1}\ (HClO_4)$

and $K_2 = 0.192 \pm 0.015\ M\ (HNO_3)$ and $0.176 \pm 0.014\ M\ \ (HClO_4)$

Here, $[OH^-]$ represents the excess hydroxide after all acid has been neutralized ($[OH^-] = C_{OH^-} - C_{H^+}$). A possible mechanism for the basic hydrolysis, without hydrogen or oxygen atoms listed, is:

$$\beta\text{-}SiMo_{12} \underset{k_{-1}}{\overset{k_1}{\rightleftharpoons}} I$$

$$I + OH^- \xrightarrow{k_2} \text{Products}$$

If intermediate I is assumed to be a steady-state intermediate, the above rate law is reproduced, with $K_1 = k_1$ and $K_2 = \frac{k_{-1}}{k_2}$. Furthermore, within experimental error, the rate law constants do not vary significantly with different acidic media.

The experimental errors associated with measuring the spectrophotometric transmittances and calculating the rate constants are small because of the large decreases in absorbance observed as β-12-MSA decomposes. However, several model errors arise since the reaction rate is observed to increase slightly for a few milliseconds before decaying exponentially thereafter. This observation could not have resulted from an initial lag period for the decomposition to begin, because the 7 ms delay time between the stopped-flow push and the start of the data-taking sequence should have covered such a lag period. Thus, the reaction speed that can be measured accurately is limited. On the other hand, if the intermediate I also absorbs 430 nm radiation, the apparent increase in the reaction rate results as the steady state in I is established. The error in the measured initial rate is expected to be less than 5% since steady state is attained quickly.

The α isomer of 12-MSA is an attractive possibility for the intermediate since α-12-MSA absorbs 430 nm radiation, though considerably less than the β isomer. Also, the α isomer predominates in solutions slightly more basic (pH 3.8-4.8) than those that favor the β isomer (pH 1.2-1.8). In addition, the equilibration between β and α isomers does not consume any hydroxide equivalents or change the stoichiometry of Mo and Si atoms in the polyanions. As experimental support, the decomposition rate is independent of the free molybdate

concentration and appears to be nonlinearly dependent upon the excess hydroxide concentration. If the β-12-MSA equilibrium had involved a deprotonation, then a linear, first-order hydroxide dependence would have been indicated. The reversibility of the β to α isomeric conversion has not been reported, however, and the constants (equation (2)) give no clue as to what the "equilibrium constant" $\frac{k_1}{k_{-1}}$ might be.

C. 12-MPA Decomposition Kinetics Studies

1. Acidic Decomposition Studies

Since hydrogen ions were released into solution as 12-MPA formed, a kinetics study of 12-MPA decomposition when mixed with a concentrated acid solution provided information about the molybdophosphate reaction in the reverse direction and a comparison with the results in the forward direction. In this study, the ranges of 12-MPA, molybdate, and H^+ concentrations were 0.02-0.20 mM, 0.01-0.05 M, and 0.75-2.00 M, respectively, after stopped-flow mixing. For molybdophosphate solutions in which phosphate was added to acidified molybdate solutions ($[H^+]$ = 0.50 M prior to mixing with the acidic reagent), the general shape of the 12-MPA decomposition profile at 430 nm showed an exponential decay in the absorbance to the final value, as expected. In fact, a semilogarithmic plot of $\ln(A_t-A_\infty)$ versus time was linear over the entire time range (10 s) with no initial curvature as the reaction began. In contrast to the 12-MPA formation reaction, its decomposition followed a simple exponential function. Preliminary reaction rate measurements revealed first order dependence of the decomposition rate upon the initial 12-MPA concentration, also as expected. Surprisingly, no dependence upon the H^+ concentration was observed, which meant that

the rate-determining step involved the dissociation of molybdate from a molybdophosphate and that the molybdate species accepted hydrogen ions in subsequent, rapid equilibrium steps not related to the rate-determining step.

The general shape of the 12-MPA decomposition profile showed anomalous behavior for solutions in which 12-MPA was prepared from the solid reagent. In a typical reaction the 430 nm absorbance increased significantly over a time period that decreased with decreased [12-MPA] and increased $[H^+]$, before the absorbance decreased with time. This initial absorbance increase interfered with decomposition rate measurements as a proportionately higher amount of 12-MPA was formed at the same time that the excess H^+ decomposed the complex. No molybdate or acid was added to these 12-MPA solutions, only enough $NaClO_4$ to bring the ionic strength to 3.0 M. Subsequent experiments showed that the initial absorbance increase is indeed due to additional 12-MPA being complexed in the strong acid solution; in the kinetics run where $[H^+]$ = 1.00 M, the final 430 nm absorbance was greater than the initial absorbance (the pH of the unmixed 12-MPA solutions was about 3). Because the absorbance increased and then decreased instead of decreasing over all time, the formation of 12-MPA occurred at a faster rate than the decomposition under these experimental conditions. In addition, as explained in the next paragraph, the 12-MPA decomposition was inhibited during the course of the reaction as the concentration of unbound molybdate in solution increased.

In solutions where phosphate was added to acidified molybdate to form 12-MPA, the 12-MPA decomposition rate varied inversely with

molybdate concentration. However, none of the linear equations such as $\text{RATE} = \frac{m}{[H_2Mo_2O_6^{2+}]} + b$ or $\text{RATE} = \frac{m}{[HMoO_3^{+}]} + b$ fit the experimental data very well. Several nonlinear equations were tried. One unsuccessful candidate was $\text{RATE} = k_1[\text{12-MPA}] - k_{-1}[HMoO_3^{+}][\text{11-MPA}]$, which was derived with the 12-MPA $\rightleftharpoons$ 11-MPA equilibrium as the rate-determining step and 11-MPA present in significant concentration at the start of the reaction. One nonlinear equation reproduced all the measured decomposition rates to within 5% error; this equation is:

$$-\frac{d[\text{12-MPA}]}{dt} = \left(\frac{K_1}{[H_2Mo_2O_6^{2+}]} + \frac{K_2}{[HMoO_3^{+}]}\right)[\text{12-MPA}]$$

$K_1 = (2.21 \pm 0.06) \times 10^{-4}$M/sec; $K_2 = (9.64 \pm 0.20) \times 10^{-4}$M/sec for HNO_3 solutions

$K_1 = (2.15 \pm 0.08) \times 10^{-4}$M/sec; $K_2 = (4.99 \pm 0.17) \times 10^{-4}$M/sec for $HClO_4$ solutions

Because the decomposition rate equation involves two terms, a branched chemical mechanism is indicated. The mechanism below reproduces the above rate equation with $K_1 = k_1K_{10}K_{11}K_a^2K_d$ and $K_2 = k_2K_{11}K_a$.

$$PO_4(MoO_3)_{12}^{3-} \overset{K_{11}}{\rightleftharpoons} PO_4(MoO_3)_{11}^{3-} + MoO_3$$

$$PO_4(MoO_3)_{11}^{3-} \overset{K_{10}}{\rightleftharpoons} PO_4(MoO_3)_{10}^{3-} + MoO_3$$

$$MoO_3 + H^+ \overset{K_a}{\rightleftharpoons} HMoO_3^+$$

$$2HMoO_3^+ \overset{K_d}{\rightleftharpoons} H_sMo_2O_6^{2+}$$

$$PO_4(MoO_3)_{10}^{3-} \xrightarrow{k_1} \text{Products}$$

$$PO_4(MoO_3)_{11}^{3-} \xrightarrow{k_2} \text{Products}$$

According to this mechanism, the acid decomposition occurs through both 11-MPA and 10-molybdophosphate (10-MPA) intermediates; equilibrium approximations on these intermediates reproduces the observed 12-MPA and molybdate dependences. Since $[MoO_3]$ is a constant linear multiple of $[HMoO_3^+]$, there is still no dependence upon $[H^+]$. One implication from this mechanism is that 10-MPA coexists in equilibrium with 11-MPA and 12-MPA in higher acidity solutions, even when molybdate is in a hundred-fold excess over phosphate. Even so, the molybdophosphate equilibrium constants determined over the lower acidity range 0.2 M $\leq$ $[H^+]$ $\leq$ 0.5 M in Section A, Chapter IV should not be affected significantly since 10-MPA would not predominate in these lower acidity solutions.

2. Decomposition with Excess Phosphate

In this set of kinetics studies, the conversion of 12-MPA to the dimeric 9-MPA when 12-MPA was mixed with a large amount of phosphate was observed. Preliminary measurements revealed a first-order dependence upon the 12-MPA concentration. A second-order dependence would have been observed if the rate-determining step had involved a dimerization such as between two 9-molybdophosphate monomers. Also, plots of $\ln(A_t-A_\infty)$ versus time were linear over the entire time range for most of these kinetics runs, with no curvature indicative of an initial lag period. Thus, as for the acid decomposition kinetics, the 12-MPA to 9-MPA conversion kinetics followed a simple exponential function. The

linear equation that best fit the experimental data for phosphate dependence was $\frac{1}{RATE} = \frac{m}{[H_3PO_4]} + b$, which indicated that the rate-determining step is not the initial dissociation of molybdate from 12-MPA. The molybdate dependence was more complex. The equation $\frac{1}{RATE} = m[HMoO_3^+]^3 + b$ described the rate data in lower acidity solutions (0.40-0.50 M H^+) while $\frac{1}{RATE} = \frac{m}{[HMoO_3^+]^3} + b$ fit the data for 0.75 M H^+ solutions. As was the case in the acid decomposition studies, Mo(VI) dimers could be substituted for $HMoO_3^+$ in the equations with the exponents halved (i.e. $\frac{1}{RATE} = m[H_2Mo_2O_6^{2+}]^{3/2} + b$) and still give the same linearity. The observation of these third-order molybdate dependences and the appearance of trimeric molybdates arranged tetrahedrally about the central phosphate in the 12-MPA structure[61] implies that molybdate dissociation from molybdophosphates could occur with three Mo atoms at a time. Experiments to test the acid dependence of the 12-MPA conversion exhibited zero-order kinetics with respect to $[H^+]$, as was observed in the acid decomposition studies. Either the free molybdate species accept or donate hydrogen ions in rapid equilibrium steps not related to the rate-determining step, or the errors associated with the initial rate measurements are so large that the acid dependence could not have been detected.

From all these experimental observations and linear functions, a consecutive step mechanism was formulated in which there is dissociation of molybdate, combination with the second phosphate, and then molybdate complexation to form the dimeric 9-MPA. With steady state approximations on certain intermediates and equilibrium approximations on the others, various forms of the rate law equation were derived for

use during KINFIT execution, and the constants m and b from the linear equations were used as the initial estimates for the KINFIT adjustable parameters. The best equation is:

$$-\frac{d[12\text{-MPA}]}{dt} = \frac{K_1[12\text{-MPA}][H_3PO_4][HMoO_3^+]^6}{K_2[HMoO_3^+]^3 + K_3[HMoO_3^+]^9 + [H_3PO_4][HMoO_3^+]^6} \qquad (3)$$

and the rate law constants K_1, K_2, and K_3 are tabulated in Table XXIII for HNO_3 and $HClO_4$ solutions. The residuals (differences between the theoretical and experimental initial reaction rates) appear to be randomly distributed over the entire range of initial reaction rates measured. Thus, in spite of the complexities of this molybdophosphate system, the given rate equation converged satisfactorily during KINFIT execution.

The chemical mechanism consistent with the rate equation, with hydrogen and oxygen atoms omitted from the chemical species, is shown below.

$$Mo_1 + Mo_1 \rightleftharpoons Mo_2$$

$$Mo_1 + Mo_2 \rightleftharpoons Mo_3$$

$$PMo_{12} \underset{k_{-1}}{\overset{k_1}{\rightleftharpoons}} PMo_9 + Mo_3$$

$$P + PMo_9 \underset{k_{-2}}{\overset{k_2}{\rightleftharpoons}} P_2Mo_9$$

$$6\ Mo + P_2Mo_9 \xrightarrow{k_3} P_2Mo_{15}$$

Table XXIII

Rate Law Constants for 12-MPA Conversion to Dimeric 9-MPA Obtained From KINFIT Execution

$T = 25^{o}C$, $I = 3.0$ M

$$\frac{-d[12\text{-MPA}]}{dt} = \frac{K_1[12\text{-MPA}][H_3PO_4][HMoO_3^+]^6}{K_2[HMoO_3^+]^3 + K_3[HMoO_3^+]^9 + [H_3PO_4][HMoO_3^+]^6}$$

HNO_3 Solutions	$HClO_4$ Solutions
$K_1 = 0.215 \pm .024$ sec^{-1}	$K_1 = 0.272 \pm .012$ sec^{-1}
$K_2 = (2.8 \pm 2.4) \times 10^{-9}$ M^4	$K_2 = (3. \pm 3.) \times 10^{-10}$ M^4
$K_3 = (1.4 \pm 1.1) \times 10^{4}$ M^{-2}	$K_3 = (4.3 \pm 0.6) \times 10^{4}$ M^{-2}

$$3\ Mo + P_2Mo_{15} \underset{\text{RAPID}}{\rightleftharpoons} P_2Mo_{18}$$

From this mechanism steady state approximations on intermediates PMo_9 and P_2Mo_9 and equilibrium approximations on Mo_2, Mo_3, P_2Mo_{15}, and P_2Mo_{12} are made. The rate equation (equation (3)) is reproduced with $K_1 = k_1$, $K_2 = \frac{k_{-1}k_{-2}}{k_2k_3}$, and $K_3 = \frac{k_{-1}}{k_2}$. This mechanism does not elucidate whether six moles of Mo(VI) monomers, three moles of dimers, or any combination thereof combines with P_2Mo_9 in the k_3 step.

The results from the 12-MPA decomposition studies are incorporated into the overall chemical scheme in Table XXI (Section A). These decompositions proceed via the same pathway up to formation of the monomeric 9-MPA intermediate. The 12-MPA acidic decomposition follows a simple exponential equation because the step preceding 9-MPA formation is rate-determining at 25°C and $[H^+]$ greater than 1.00 M. When 0.50 M < $[H^+]$ < 1.00 M, the association reaction between H_3PO_4 and $Mo(OH)_6$ occurs as slowly as the other rate-determining step so that the 12-MPA formation kinetics is observed to follow a double exponential equation. With higher phosphate concentrations in the 12-MPA to dimeric 9-MPA conversion studies, the steps to associate the second phosphate or additional molybdate species become rate-determining at 25°C, and simple exponential kinetics is observed.

3. 12-MPA Decomposition in Basic Solutions

A kinetics study of 12-MPA decomposition in concentrated hydroxide solutions was attempted. In spite of the fastest stopped-flow data acquisition rates where one data point was measured per millisecond over a 0.100 s reaction time, the 12-MPA decomposition appeared to be complete by the time the solutions were mixed and delivered to the

observation cell. Even though the initial 12-MPA concentrations varied from 0.02 to 0.20 mM, the 430 nm absorbances decreased by nearly the same, unexpectedly small amounts (less than 0.1 absorbance units in all cases). The shape of the decomposition kinetics profile was peculiar; an initial increase in absorbance followed by a decrease with time was observed. A blank kinetics run in which 1 M H^+ solution was mixed with 3 M NaOH (for all solutions I = 3 M, but no 12-MPA was present) showed the same behavior. Thus, what was observed in the experiments resulted from the heat of mixing the strong acid and strong base solutions. This heating effect changed the solution refractive index and caused an apparent absorbance change with time.

D. Heteropolymolybdate Formation at Different Ionic Strengths

The previous experiments of heteropolymolybdate kinetics were conducted at specific solution ionic strengths so that the relationship between measured reaction rates and Mo(VI) species concentrations could be deduced. Because the formation constants for the equilibria among cationic Mo(VI) monomers and dimers were determined in 3.0 M ionic strength, the 12-MPA kinetics studies reported earlier were carried out at I = 3.0 M. Similarly, the β-12-MSA kinetics were studied at I = 1.0 M because the concentration equilibrium constants for the anionic isopolymolybdates were determined in solutions of 1.0 M ionic strength. Although no extrathermodynamic assumptions such as the Debye-Huckel equation are generally applicable to high ionic strength solutions, the variation of the heteropolymolybdate reaction rates with ionic strength was studied for two purposes. The increase or decrease in reaction rate with increased ionic strength was noted, and the data were examined for

changes in the overall kinetics profile as the ionic strength was varied. The measured reaction rates were tabulated with ionic strength in Table XXIV. The initial β-12-MSA formation rate decreased while the maximum 12-MPA formation rate increased with increased ionic strength. With a larger concentration of ions, the increased 12-MPA reaction rate at higher ionic strength indicated that the rate-determining step involves a reaction between oppositely charged ions (Mo(VI) cation and a molybdophosphate anion), and the decreased β-12-MSA formation rate indicates a reaction between ions of the same charge ($Mo_8O_{26}^{4-}$ and a molybdosilicate anion) in the rate-determining step. The plots of $\ln(A_\infty - A_t)$ versus time revealed no changes in the overall kinetics profiles; the β-12-MSA formation followed a simple exponential function while most 12-MPA formation reactions followed a double exponential function, regardless of the solution ionic strength. These complexation reactions do not appear to be as sensitive to ionic strength variations as the conversion from β-12-MSA to α-12-MSA.[64] Nevertheless, the variations are significant enough to emphasize control of ionic strengths among samples and standards for phosphate and silicate determinations that use reaction-rate measurements.

Table XXIV

12-MPA and β-12-MSA Formation Rates at Different Solution Ionic Strengths

C_P or C_{Si} = 0.1 mM, C_{Mo} = 0.02 M, $[H^+]$ = 0.50 M for 12-MPA experiments, pH = 1.5 for β-12-MSA experiments, $HClO_4$ acid medium, T = 25.0°C.

12-MPA		β-12-MSA	
Ionic Strength (M)	Maximum Rate (sec^{-1})(λ=430nm)	Ionic Strength (M)	Initial Rate (sec^{-1})(λ=430nm)
1.50	0.0168	0.50	0.00257
2.00	0.0195	1.00	0.00219
2.50	0.0212	1.50	0.00180
3.00	0.0267	2.00	0.00147

Chapter VI. Simultaneous Reaction-Rate Determination for Phosphate and Silicate

A. Introduction and Literature Background

As previously mentioned in Chapter I, analysis methods based upon measuring chemical reaction rates offer several advantages such as shorter analysis times and elimination of time-invariant interferences. The difficulties associated with reaction-rate methods can be alleviated through good instrumental designs, computer automation of instrumental tasks, judicious choice of the chemical system used in the analysis, and proper preparation of the samples, standards, and reagents. All these considerations help insure that the measured reaction rate will be proportional to the analyte concentration.

The methods used in these determinations differ with the experimental conditions such as the analyte concentrations relative to the concentration of the reacting species.[67] The broad categories of kinetics methods are the proportional equations method, the graphical extrapolation methods, masking methods, and methods involving changes in the kinetics of the system. Masking methods generally involve shifting the equilibria of interfering species or the equilibria among several analytes that react with the same species.[68] Other methods that

alter the kinetics of the system help the chemical analysis either by accelerating or decelerating the reaction rates to a speed that can be measured more precisely or by differentiating one reaction rate relative to another rate so that other selective differential kinetics methods can be applied.[69,70]

In most cases, these two methods cannot differentiate rates of reaction of mixtures. The proportional equations method and the graphical extrapolation methods are used more generally, and each method has its own advantages over the other method.[71] Because the proportional equations method is based upon a constant fraction of the analyte being reacted at any given time, regardless of the initial concentration, this method is less limited with respect to relative initial concentrations of the analytes or to their relative reaction rates than the graphical extrapolation methods. The proportional equations method involves less work and time, which is more suitable for analysis of a large number of samples. The total concentration of all analytes reacting with the same chemical reagent does not need to be determined. In addition, chemical systems with complex kinetics (such as pseudo first-order) may be employed, and mixtures with several components may be analyzed. On the other hand, graphical extrapolation methods offer certain advantages because the rate constants do not need to be known prior to the analysis. Thus, experimental conditions do not need to be controlled so carefully for all the analyses, and samples containing varying amounts of catalysts can be analyzed more easily.

Some mixtures contain components that react at significantly different rates with the same chemical reagent. In such a case, the analysis of the mixture is simple because only one species will be reacting at a significant rate over certain time intervals. In order to perform differential kinetics procedures to determine two analytes in a mixture, we need to be able to measure the slower chemical reaction proceeding at its maximum rate while the faster reaction has already reached equilibrium. If the kinetics is pseudo first-order with respect to both analyte concentrations, the reaction rate measured at the start of the reaction corresponds predominantly to the faster reaction.

Since both phosphate and silicate react with molybdate in acid solution, the presence of silicate would interfere with determinations of phosphate, and visa-versa. Several approaches have been presented to avoid these interferences. The heteropolymolybdates can be extracted selectively with varying compositions of n-butanol, acetate esters, and chloroform in the organic phase,[72-75] but the multiple extraction procedures are cumbersome and introduce considerable error. The use of oxalate or tartrate masks the presence of either 12-molybdophosphate or 12-molybdosilicate, depending upon whether the tartrate is added before or after the heteropolymolybdates are complexed.[76] However, the analysis sensitivity is drastically reduced. Acetone may be used to enhance the 12-MPA molar absorptivity, but the absorptivity does vary with the acetone concentration present.[76] Reduction methods to heteropolymolybdenum blues suffer problems of slower reaction times, deviations in Beer's Law (too much analytical sensitivity), unstable reagents and products, and high blank absorbances. Another procedure measures the

12-MPA formation and then the combined 12-MPA and 12-MSA concentrations in a less acidic solution.[57] As pointed out in the previous chapter, β-12-MSA, 12-MPA, and other heteropolymolybdate concentrations vary with acidity, so this procedure does not produce valid results. Nevertheless, in all these experimental procedures, at least two separate experiments have to be performed to distinguish 12-MPA from 12-MSA formation.

B. Experimental Section

All the kinetics experiments were performed automatically with the Beckwith stopped-flow spectrophotometer (see Chapter I, Section C). The computer programs described in Chapter III, Section A were used to calculate the analytical acid and molybdate concentrations required to give the prescribed H^+ and Mo(VI) species concentrations. Thus, 0.05 M molybdate reagent solutions were prepared with 0.4 M and 0.5 M H^+ present from HNO_3 and $HClO_4$ stock solutions and with pH 1.5 and 1.8 from $HClO_4$ and H_2SO_4 media. In the preliminary kinetics studies, the molybdate concentration was varied from 0.01 M to 0.05 M. The sample solutions for phosphate and silicate determinations were prepared with both species present. In a Latin square experimental design, the phosphate concentrations varied from 0.01-1.00 mM with the silicate concentration held constant. The silicate concentration was varied successively from 0.01-1.00 mM for each series of phosphate solutions.

C. Kinetics of β-12-MSA Formation in Strong Acid Solution

The kinetics rate law equation, constants, and chemical mechanism for 12-MPA formation in strong acid solutions (pH < 0.9) is reported in Chapter V. In the low acid limit where 0.3 M < $[H^+]$ < 0.5 M, second-

order kinetics is observed.

$$\frac{d[12\text{-MPA}]}{dt} = k_1[H_3PO_4][Mo(OH)_6]$$

In order to determine silicate and phosphate simultaneously, information on the kinetics of 12-MSA formation in strong acid solutions is desirable. Since the β isomer of 12-MSA predominates in solutions with pH values between 1.0 and 1.8,[43] it is assumed that only β-12-MSA is complexed from silicate and molybdate under more acidic conditions. The absorbance-time profiles can be described mathematically with a simple exponential equation; however, the initial rates are significantly slower (over 100-fold) than the corresponding 12-MPA formation rates. When $[H^+]$= 0.5 M, the initial rates are not measurable except at higher molybdate concentrations. Nevertheless, the rate law equation for β-12-MSA formation appears similar to the form reported by Gall:[6]

$$\frac{d[\beta\text{-}12\text{-MSA}]}{dt} = \frac{K_1[H_2Mo_2O_6^{2+}][Si(OH)_4]}{\frac{K_2[H^+]^8}{[H_2Mo_2O_6^{2+}]^4} + \frac{K_3[H^+]^3}{[H_2Mo_2O_6^{2+}]^2} + 1}$$

Some concern could be expressed since second-order kinetics are not observed for β-12-MSA formation as for 12-MPA formation. Provided that the same molybdate reagent is used for all analyses with samples and standards and that the samples do not contain significant amounts of Mo(VI), the accuracy of the silicate determinations should not be affected.

D. Kinetics of 12-MPA Formation in Dilute Acid Solution

The kinetics of β-12-MSA formation has also been reported in the last chapter. Between pH 1.2 and pH 1.8 the rate law equation is:

$$\frac{d[\beta\text{-12-MSA}]}{dt} = \frac{K_1[Si(OH)_4][H_2MoO_4][Mo_8O_{26}^{4-}]}{K_2 + [Mo_8O_{26}^{4-}][H^+]}$$

As in the previous section information on the kinetics of 12-MPA formation under the same experimental conditions would be useful for simultaneous phosphate and silicate determinations. Within experimental error, the 12-MPA rate law equation is:

$$\frac{d[12\text{-MPA}]}{dt} = \frac{K_1[H_3PO_4][H_2MoO_4]}{[H^+]},$$

which is identical to the above equation for β-12-MSA formation with a significantly smaller K_2 rate constant.

E. Theoretical Considerations

In order to determine both phosphate and silicate in one kinetics run, we need to be able to measure the slower chemical reaction proceeding at its maximum rate while the faster reaction has already reached equilibrium. Under these conditions, the subtraction of the slower rate from the total reaction rate at the start of the reaction is possible. In order to predict how much slower the second reaction has to be relative to the first reaction, experimental conditions are assumed where pseudo first-order kinetics with respect to the analyte concentrations is followed. This is the general practice for reaction-rate phosphate and silicate determinations[26,77] and is followed in this

work. The half-life for the pseudo first-order reaction is $T = \frac{0.693}{k}$, where the rate constant k varies with the acid and molybdate concentrations. The half-life is independent of the analyte concentrations.

The ratios of reaction half-lives that impart model errors to the differential kinetics measurements are tabulated in Table XXV. When $[H^+]$ = 0.40 M, the 12-MPA reaction proceeds about 130 times faster than the β-12-MSA reaction, thus imparting an inherent 3-4% error to the differential kinetics measurements. A kinetics plot for 12-MPA and β-12-MSA formation under these conditions is given in Figure 24. It is relatively easy to locate and measure the second reaction rate and to subtract this rate from the total reaction rate. On the other hand, at pH 1.8 the β-12-MSA reaction is only 1.3 times faster than the 12-MPA reaction. Thus, there is an inherently large error in the differential kinetics measurements as illustrated in the kinetics plot of Figure 25. Locating the second reaction rate within this curve is much more difficult.

F. Simultaneous Phosphate and Silicate Determinations

The reaction rates measured for the simultaneous determinations of phosphate and silicate are tabulated in Tables XXVI-XXIX. The data for pH 1.8 solutions (Table XXVI) is displayed to show that the initial reaction rate varies linearly with phosphate or silicate concentration (C_P or C_{Si}) within a given column or row, respectively. The Y-intercepts are proportional to C_{Si} or C_P, respectively, and the slopes are identical for all the columns or all the rows (within experimental error), except when C_P = 1.00 mM or C_{Si} = 1.00 mM.

Table XXV

Ratios of Reaction Half-Lives Which Impart Certain Errors To Differential Kinetics Measurements

$$(A \xrightarrow{k_1} P_1,\ B \xrightarrow{k_2} P_2;\ C_A = C_B)$$

0.1% error

Time for first reaction to be 99.9% completed: $t = \frac{\ln 0.001}{-k_1} = 9.97\ T_1$

Time for second reaction to proceed at 99.9% of its maximum rate:

$$t = \frac{\ln 0.999}{-k_2} = 0.00144\ T_2$$

$$\frac{T_2}{T_1} = 6922$$

1.0% error

Time for first reaction to be 99% completed: $t = \frac{\ln 0.01}{-k_1} = 6.65\ T_1$

Time for second reaction to proceed at 99.9% of its maximum rate:

$$t = \frac{\ln 0.99}{-k_2} = 0.0145\ T_2$$

$$\frac{T_2}{T_1} = 458$$

10% error

Time for first reaction to be 90% completed: $t = \frac{\ln 0.1}{-k_1} = 3.32\ T_1$

Time for second reaction to proceed at 90% of its maximum rate;

$$t = \frac{\ln 0.90}{-k_2} = 0.152\ T_2$$

$$\frac{T_2}{T_1} = 21.9$$

Figure 24. Kinetics Plot of Heteropolymolybdate Formation ($[H^+]$ = 0.4 M)

C_P = 0.05 mM; C_{Si} = 1.00 mM, C_M = 0.05 M, T = 21°C

Slopes 1 and 2 are tabulated in Tables XXVII and XXVIII

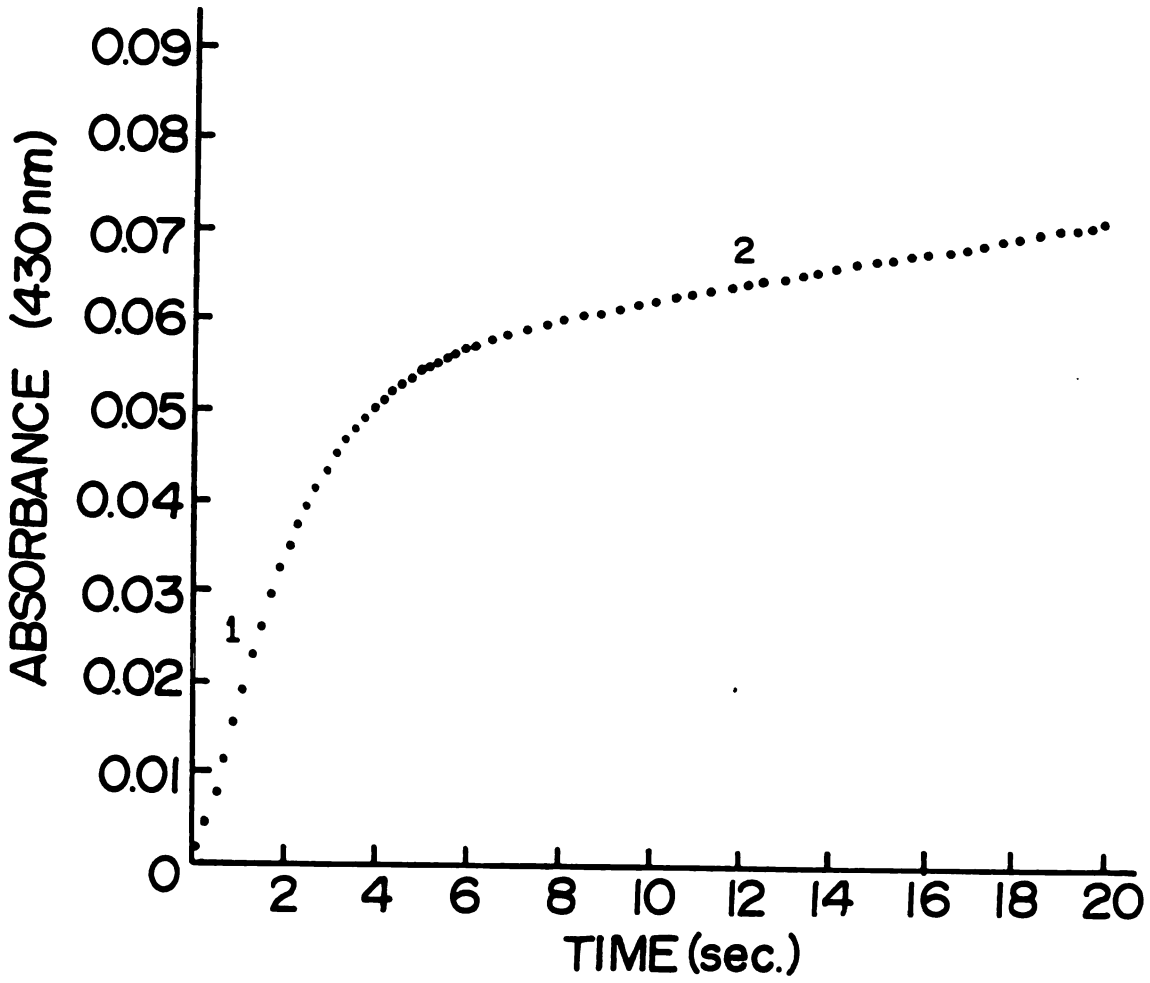

Figure 25. Kinetics Plot of Heteropolymolybdate Formation (pH 1.8)

C_P = 0.10 mM; C_{Si} = 0.20 mM; C_M = 0.05 M; T = 21°C

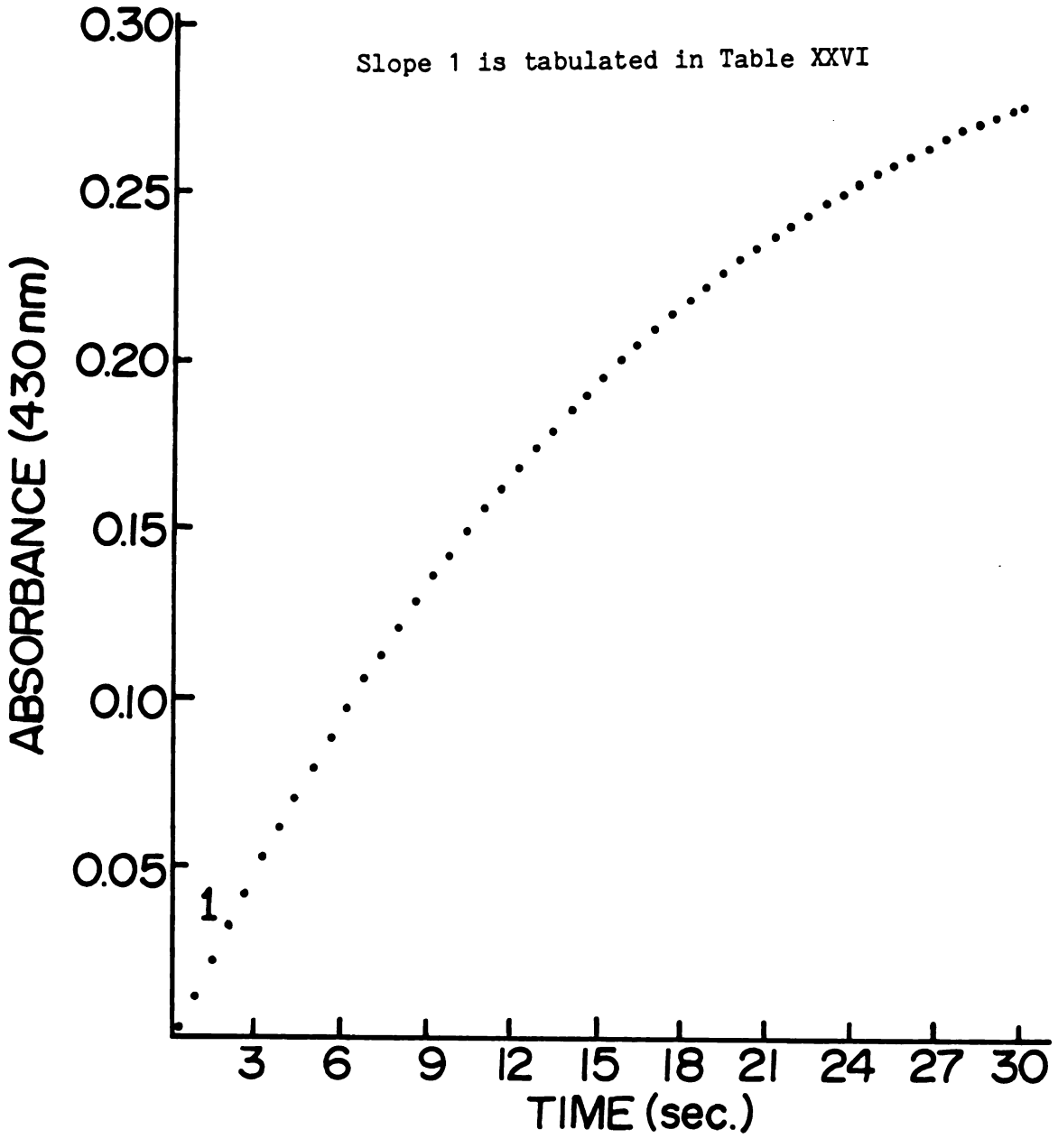

Table XXVI

Reaction Rates for Heteropolymolybdate Formation as a Function of C_P and C_{Si}

Reagent solution: C_M = 0.05 M, C_H = 0.0312 M $HClO_4$ or 0.0188 M H_2SO_4 (pH 1.8)

a = $HClO_4$ medium, b = H_2SO_4 medium, 1 = slope as shown in Figure 25

Ionic strength not controlled; room temperature (~21°C); λ = 430 nm

Reaction rates are in sec^{-1}.

C_P(mM) \ C_{Si}(mM)	0.01	0.05	0.20	1.00
0.01	a 1 0.00127 b 1 0.00149	a 1 0.00316 b 1 0.00371	a 1 0.01012 b 1 0.01172	a 1 0.04764 b 1 0.05714
0.05	a 1 0.00273 b 1 0.00328	a 1 0.00436 b 1 0.00491	a 1 0.01091 b 1 0.01280	a 1 0.04781 b 1 0.05847
0.10	a 1 0.00487 b 1 0.00597	a 1 0.00624 b 1 0.00742	a 1 0.01200 b 1 0.01537	a 1 0.04780 b 1 0.06352
0.20	a 1 0.00947 b 1 0.01030	a 1 0.01046 b 1 0.01169	a 1 0.01586 b 1 0.01965	a 1 00.4760 b 1 0.06517
1.00	a 1 0.04190 b 1 ------	a 1 0.04201 b 1 -------	a 1 0.04392 b 1 -------	a 1 0.05385 b 1 -------

Table XXVII

Reaction Rates for Heteropolymolybdate Formation
As a Function of Both C_P and C_{Si}

Ionic strength not controlled; room temperature (~21°C); λ = 430 nm

Reagent solution: C_M = 0.05 M, C_H = 0.5427 M ($[H^+]$ = 0.400 M)

a = HNO_3 medium; b = $HClO_4$ medium; 1,2 = slope as shown in Figure 24

Reaction rates are in sec^{-1}

C_P(mM) \ C_{Si}(mM)	0.01	0.05	0.20	1.00
0.01	a 1 0.00278 a 2 0.00006 b 1 0.00401 b 2 0.00002	a 1 0.00285 a 2 0.00005 b 1 0.00382 b 2 0.00004	a 1 0.00309 a 2 0.00011 b 1 0.00418 b 2 0.00018	a 1 0.00349 a 2 0.00051 b 1 0.00463 b 2 0.00086
0.05	a 1 0.01251 a 2 0.00006 b 1 0.01719 b 2 0.00005	a 1 0.01350 a 2 0.00007 b 1 0.01762 b 2 0.00006	a 1 0.01368 a 2 0.00013 b 1 0.01794 b 2 0.00018	a 1 0.01393 a 2 0.00050 b 1 0.01847 b 2 0.00092
0.10	a 1 0.02587 a 2 0.00008 b 1 0.03405 b 2 0.00003	a 1 0.02581 a 2 0.00007 b 1 0.03459 b 2 0.00013	a 1 0.02674 a 2 0.00013 b 1 0.03500 b 2 0.00018	a 1 0.02705 a 2 0.00053 b 1 0.03562 b 2 0.00087
0.20	a 1 0.05364 a 2 0.00006 b 1 0.06950 b 2 0.00021	a 1 0.05419 a 2 0.00007 b 1 0.07071 b 2 0.00025	a 1 0.05403 a 2 0.00013 b 1 0.07070 b 2 0.00021	a 1 0.05473 a 2 0.00051 b 1 0.07105 b 2 0.00082
1.00	a 1 0.22230 a 2 0.00023 b 1 0.29790 b 2 0.00020	a 1 0.22771 a 2 0.00024 b 1 0.29891 b 2 0.00021	a 1 0.23035 a 2 0.00025 b 1 0.29943 b 2 0.00026	a 1 0.23042 a 2 0.00037 b 1 0.29986 b 2 0.00037

Table XXVIII

Reaction Rates for Heteropolymolybdate Formation
As a Function of Both C_P and C_{Si}

Ionic strength = 3.0 M, T = 25.0 ± 0.1°C, λ = 430 nm

Reagent solution: C_M = 0.05 M, C_H = 0.5427 M ($[H^+]$ = 0.400 M)

a = HNO_3 medium; b = $HClO_4$ medium; 1,2 = slope as shown in Figure 24

Reaction rates are in sec^{-1}

C_P(mM)	C_{Si}(mM)	0.05	0.10	0.20	1.00
0.01	a 1	0.00873	0.00909	0.00921	0.01198
	a 2	0.00022	0.00045	0.00087	0.00404
	b 1	0.00936	0.01011	0.01070	0.01423
	b 2	0.00028	0.00052	0.00111	0.00491
0.05	a 1	0.02942	0.02920	0.03047	0.03328
	a 2	0.00023	0.00046	0.00086	0.00395
	b 1	0.03467	0.03486	0.03554	0.03828
	b 2	0.00027	0.00053	0.00101	0.00469
0.10	a 1	0.05520	0.05590	0.05579	0.05865
	a 2	0.00021	0.00042	0.00083	0.00385
	b 1	0.06431	0.06522	0.06538	0.06833
	b 2	0.00027	0.00050	0.00099	0.00460
0.20	a 1	0.10568	0.10821	0.10902	0.11122
	a 2	0.00017	0.00036	0.00074	0.00352
	b 1	0.12424	0.12577	0.12630	0.12939
	b 2	0.00025	0.00048	0.00093	0.00420
1.00	a 1	0.47179	0.47388	0.47628	0.47362
	a 2	0.00009	0.00022	0.00026	0.00107
	b 1	0.55089	0.54512	0.54899	0.54704
	b 2	0.00015	0.00025	0.00039	0.00135

Table XXIX

Reaction Rates for Heteropolymolybdate Formation as a Function of Both C_P and C_{Si}

Ionic strength = 3.0 M, T = 25.0° ± 0.1°C, λ = 430 nm

Reagent Solution: C_M = 0.05 M, $[H^+]$ = 0.500 M in $HClO_4$

Reaction rates in sec^{-1}

C_P(mM)	C_{Si}(mM)	0.05		0.10		0.20		1.00
0.01	1	0.00872	1	0.00889	1	0.00897	1	0.00918
	2	0.00005	2	0.00012	2	0.00023	2	0.00098
0.05	1	0.03125	1	0.03132	1	0.03151	1	0.03262
	2	0.00007	2	0.00011	2	0.00023	2	0.00103
0.10	1	0.05801	1	0.05925	1	0.05922	1	0.05968
	2	0.00007	2	0.00010	2	0.00021	2	0.00093
0.20	1	0.11370	1	0.11582	1	0.11547	1	0.11670
	2	0.00004	2	0.00010	2	0.00020	2	0.00090
1.00	1	0.50152	1	0.50135	1	0.50041	1	0.49972
	2	0.00009	2	0.00012	2	0.00015	2	0.00028

The same observations are seen for the data in 0.4 M and 0.5 M H^+ solutions, only with no exception for the column where C_{Si} is 1.00 mM. The reaction rates for the slower reaction are linearly proportional to C_{Si}, and the differences between these values and the total initial reaction rates are linearly proportional to C_P. The limit of detection for the increase in absorbance with time seems to be about 0.00005 sec^{-1} at 430 nm. Though the linear range for phosphate determinations spans 0.01-1.00 mM, the range could be extended at least another order of magnitude lower before the limit of detection is reached. At C_P = 1.00 mM the absorption of 430 nm radiation by 12-MPA begins to deviate from Beer's Law as the reaction proceeds. Perchloric acid is the acidic medium of choice because the measured reaction rates are about 1.4 times larger than in HNO_3 solutions. Consequently, $HClO_4$ extends the linear range for silicate determinations from 0.10-1.00 mM down to 0.05-1.00 mM. This linear range could possibly be extended beyond the 1.00 mM upper limit if a higher molybdate concentration is present in the reagent.

G. Sources of Error

The reaction rates observed in strong acid solution are reproducible to within 2% RSD. This deviation is smaller than the error inherently produced from the differential rate measurements, as discussed earlier. When the reagent ionic strength is not adjusted (Table XXVII), the major source of error arises from a synergistic effect where a faster β-12-MSA formation rate causes an apparent increase in the 12-MPA formation rate (though C_P is constant), and vice-versa. This synergistic effect imparts less than 10% positive error in all cases.

The error is less than 5% in many cases, even though the concentration of the interfering analyte spans two orders of magnitude.

When all solution ionic strengths are 3.0 M, the synergistic effects on the 12-MPA reaction rate disappear. However, the rapid 12-MPA formation rate at high phosphate concentrations causes an apparent decrease in the β-12-MSA formation rate. Thus, as shown here (Table XXX) and elsewhere,[77] there is significant negative error in measuring the silicate concentration in solutions with high phosphate concentrations. This error is larger than the errors that would have been propagated from measurements of small spectrophotometric transmittances. Instead, the error arises from changes in the acid and molybdate concentrations as 12-MPA and other molybdophosphates are produced. Some of this error could be reduced with a higher molybdate concentration in the reagent solution, but the change in the acid concentration will always limit the accuracy of the silicate determination. Typically, a 1 mM phosphate solution mixed with an acidic molybdate solution at 0.400 M H^+ would increase the acid concentration from 0.400 M to 0.412 M, enough to slow down the β-12-MSA reaction by at least 10%.

In addition, the faster reaction being 99.9% completed does not necessarily imply that the measurement of the slower reaction rate will have a low associated error. In the 0.2 mM and 1.0 mM phosphate solutions (see the bottom row of Table XXVII), the slope 2 value reported is only 0.1% of the value for slope 1, but is much larger than expected for β-12-MSA formation at the lower silicate concentrations.

Table XXX

Simultaneous Determination of Phosphate and Silicate

	Concentration of mixtures taken (mM)		Concentrations of mixtures found			
	C_{Si}	C_P	$C_{Si,\ mM}$	Rel. Error %	$C_{P,mM}$	Rel. Error %
#1	0.15	0.50	0.10	-33%	0.49	-3%
#2	0.40	0.025	0.41	+2%	0.023	-8%
#3	0.080	0.080	0.081	+1%	0.082	+2%
#4	0.080	0.080*	0.151	+89%	0.086	+8%

C_M = 0.05 M, $[H^+]$ = 0.40 M ($HClO_4$), I = 3 M, T = 25°C, λ = 430 nm

0.1 mM C_P = 9.5 ppm PO_4^{3-}

0.1 mM C_{Si} = 7.6 ppm SiO_3^{2-}

*means solution also contains 0.1 M $NaC_2H_3O_2$.

For unknowns where C_P is large and C_{Si} is small, the reaction time after stopped-flow mixing must be lengthened so that the second reaction rate measured is due to β-12-MSA formation rather than 12-MPA formation before equilibrium is approached.

Finally, as can be seen from comparing Tables XXVII and XXVIII, the ionic strength of the molybdate reagent and temperature of the stopped-flow instrument do not affect the analytical results significantly unless the same molybdate reagent is not used for all the determinations or the heat of mixing the sample and reagent solutions is large. Each experimental condition in Tables XXVII and XXVIII would give suitable analytical working curves. However, acidity, ionic strength, and buffer capacity (see Table XXX, unknown #4) will affect the results significantly if these concentrations are significantly different in the unknowns than in the phosphate and silicate standards. Each concentration will affect the final pH of the solutions mixed in the stopped-flow and thus alter the calibration between the reaction rates and the phosphate and silicate concentrations. Of course, if the samples also contain chemical species that reduce the free molybdate concentration through complexation, the analysis is impaired.

REFERENCES

REFERENCES

1. B. Chance, J. Franklin Inst. 229 (1940), p. 455.

2. B. Chance, J. Franklin Inst. 229 (1940), p. 613.

3. B. Chance, J. Franklin Inst. 229 (1940), p. 737.

4. P.K. Notz, Ph.D. Dissertation, Michigan State University, 1977.

5. P.M. Beckwith, Ph.D. Dissertation, Michigan State University, 1972.

6. R.S. Gall, Ph.D. Dissertation, Michigan State University, 1978.

7. R. Balciunas, Ph.D. Dissertation, Michigan State University, 1981.

8. K.J. Caserta, Ph.D. Dissertation, Michigan State University, 1974.

9. M. Sasaki, F. Amita, and J. Osugi, Rev. Sci. Inst. 50 (1979), p. 1104.

10. S. Stieg and T.A. Nieman, Anal. Chem. 52 (1980), p. 796.

11. F.J. Holler and W.C. Mateyka, Anal. Chem. 52 (1980), p. 354.

12. F.C. Knowles, Anal. Biochem. 93 (1979), p. 407.

13. B.F. Peterman, Anal. Biochem. 93 (1979), p. 442.

14. F.J. Holler, C.G. Enke, and S.R. Crouch, Anal. Chim. Acta 117 (1980), p. 99.

15. C. Paul, K. Kirschner, and G. Haenisch, Anal. Biochem. 101 (1980), p. 442.

16. G.E. Mieling and H.L. Pardue, Anal. Chem. 50 (1978), p. 1333.

17. R.I. Martinez and J.T. Herron, Chem. Phys. Let. 72 (1980), p. 74.

18. T. Okubo, H. Kitano, T. Ishiwatari, and N. Ise, Proc. R. Soc. London, Ser. A, 336, #1724 (1979), p. 81.

19. M. Malyj, P.D. Smith, B. Balko, and R.L. Berger, Rev. Sci. Inst. 51 (1980), p. 896.

20. R.O. Kuehne, T. Schaffhauser, A. Wokaun, and R.R. Ernst, J. Magnet. Reson. 35 (1979), p. 39.

21. N. Klimes, G. Lassmann, and B. Ebert, J. Magnet. Reson. 37 (1980), p. 53.

22. I. Tabushi, K. Yamamura, and T. Nishiya, JACS 101 (1979), p. 2785.

23. D.F. Boltz and M.G. Mellon, Anal. Chem. 20 (1948), p. 749.

24. A. Halasz and E. Pungor, Talanta 18 (1971), p. 557.

25. W. Rieman and J. Beukenkamp, "Treatise on Analytical Chemistry," I.M. Kolthoff and P.J. Elving, Eds., Part II, Vol. 5, Wiley, New York (1961), p. 317.

26. A.C. Javier, S.R. Crouch, and H.V. Malmstadt, Anal. Chem. 41 (1969), p. 239.

27. S.R. Crouch and H.V. Malmstadt, Anal. Chem. 39 (1967), p. 1090.

28. V.W. Truesdale and C.J. Smith, Analyst 101 (1976), p. 19.

29. J.D.H. Strickland, JACS 74 (1952),pp. 862, 868, 872.

30. A. Halasz and E. Pungor, Talanta 18 (1971), p. 569.

31. S.R. Crouch and H.V. Malmstadt, Anal. Chem. 39 (1967), p. 1084.

32. H.Wu, J. Biol. Chem.43 (1920), p. 189.

33. G.A. Tsigdinos, Climax Molyb. Co., New York, Bulletin Cdb-12a (1969).

34. H.K. El-Shamy and M.F. Iskander, J. Inorg. Nucl. Chem. 35 (1973), p. 1227.

35. H. Hahn and G. Schmidt, Naturwissenschaften 49 (1962), p. 513.

36. E. Bamann, K. Schriever, A. Freytag, and R. Toussant, Ann. Chem. Liebigs 605 (1957), p. 65.

37. E.E. Kriss, V.K. Rudenko, and K.B. Yatsimirskii, Zh. Anal. Khim. 26 (1971), p. 1953.

38. J.P. Launay, R. Massart, and P. Souchay, "Chemistry and Uses of Molybdenum," P.C.H. Mitchell, Ed., Climax Mo Company (1973), p.71.

39. Haupt and Schroeder, Wasser 6 (1932), p. 217.

40. G.P. Haight and D.R. Boston, "Chemistry and Uses of Molybdenum," P.C.H. Mitchell, Ed., Climax Mo Company (1973), p. 48.

41. V.W. Truesdale, P.J. Smith, and C.J. Smith, Analyst 104 (1979), p. 897.

42. J.J. Cruywagen, J.B.B. Heyns, and E.F.C.H. Rohwer, J. Inorg. Nucl. Chem. 40 (1978), p. 53.

43. V.W. Truesdale and C.J. Smith, Analyst 100 (1975), p. 203.

44. P. Souchay, Pure Appl. Chem. 6 (1963), p. 61.

45. D.S. Honig and K. Kustin, J. Phys. Chem. 76 (1972), p. 1575.

46. D.V.S. Dain, Indian J. Chem. 8 (1970), p. 945.

47. D.S. Honig and K. Kustin, Inorg. Chem. 11 (1972), p. 65.

48. J.P. Collin, P. Lagrange, and J.P. Schwing, "Chemistry and Uses of Molybdenum," P.C.H. Mitchell, Ed., Climax Mo Company (1973), p. 59.

49. J.F. Ojo, R.S. Taylor, and A.G. Sykes, J.C.S. Dalton (1975), p. 500.

50. R. Mellstrom and N. Ingri, Acta Chem. Scand. A 28 (1974), p. 703.

51. A.C. Javier, S.R. Crouch, and H.V. Malmstadt, Anal. Chem. 40 (1968), p. 1922.

52. P.M. Beckwith, A. Scheeline, and S.R. Crouch, Anal. Chem. 47 (1975), p. 1930.

53. J. Aveston, E.W. Anacker, and J.S. Johnson, Inorg. Chem. 3 (1964), p. 735.

54. N. Ingri, W. Kakolowicz, L.G. Sillen, and B. Warnquist, Talanta 14 (1967), p. 1261.

55. J.L. Dye and V.A. Nicely, J. Chem. Ed. 48 (1971), p. 443.

56. K. Murata and T. Kiba, J. Inorg. Nucl. Chem. 32 (1970), p. 1667.

57. A. Halasz, E. Pungor, and K. Polyak, Talanta 18 (1971), p. 577.

58. P. Souchay and J. Faucherre, Bull. Soc. Chim. Fr. (1951), p. 355.

59. J.D. Ingle, Jr., Ph.D. Dissertation, Michigan State University, 1971.

60. CRC Handbook of Chemistry and Physics, 48th Ed. (1968), p. D-80.

61. J.F. Keggin, Nature 131 (1933), p. 908; Proc. Roy. Soc. (London) A144 (1934), p. 75.

62. P. Job, Ann. Chim. 9 (1928), p. 113.

63. D. Perrin, Organic Complexing Reagents, Interscience, New York (1964), p. 293.

64. G.C. Dehne and M.G. Mellon, Anal. Chem. 35 (1965), p. 1382.

65. V.W. Truesdale, P.J. Smith, and C.J. Smith, Analyst 102 (1977), p. 73.

66. C.C. Kircher, preliminary measurements of 12-MPA formation kinetics.

67. H.B. Mark and G.A. Rechnitz, "Kinetics in Analytical Chemistry," Interscience Publishers, New York, N.Y., 1968.

68. F.J. Welcher, "The Analytical Uses of Ethylenediamine Tetraacetic Acid," Van Nostrand, New York, 1958, Chap. IV.

69. R.G. Garmon, Ph.D. Dissertation, Univ. of North Carolina, Chapel Hill, 1961.

70. D.W. Rogers, D.A. Aikens, and C.N. Reilley, J. Phys. Chem. 66 (1962), p. 1582.

71. H.B. Mark, Jr., L.J. Papa, and C.N. Reilley, "Advances in Analytical Chemistry and Instrumentation," Vol. 2, Wiley, New York, N.Y. (1963), pp. 255-385.

72. R.I. Alekseyev, Zavodsk. Lab. 11 (1945), p. 123.

73. J. Paul, Mikrochim. Acta, (1965), p. 830.

74. J. Paul, Mikrochim. Acta, (1965), p. 836.

75. J. Paul, Anal. Chim. Acta 35 (1966), p. 200.

76. R.A. Chalmers and A.G. Sinclair, Anal. Chim. Acta 34 (1966), p. 412.

77. J.D. Ingle, Jr. and S. R. Crouch, Anal. Chem. 41 (1969), p. 239.

APPENDIX

Selected Program Listings

MOLYB.FT

```
C    THIS PROGRAM SUCCESSIVELY APPROXIMATES THE [HMOO3] AND [H] IN
C            SOLUTIONS USED FOR THE KINETIC STUDY OF HETERO POLYMOLYBDATES
         COMMON C1,C2,C3,CD,CH,CM,HC,FC,SALT,CR
         CR=0.0
11       READ(1,12) CH,CM
12       FORMAT('ENTER TOTAL [H] AND [MO] IN 10 COLUMN F FORMAT',/2F10.0)
         IF(CM) 45,45,13
45       CALL EXIT
13       C=CH-3.0*CM
         C1=11.36
         C2=4.7
         C3=0.24
         CD=97.0
15       FC=(-1.0-1.0/(C1*C)+SQRT((1.0+1.0/(C1*C))**2+8.0*CM*CD
         1*(1.0/(C2*
         1C)+1.0+C3*C)))/(4.0*CD*(1.0/(C2*C)+1.0+C3*C))
         HC=(CH-3.0*FC-6.0*CD*FC**2+SQRT((3.0*FC+6.0*CD*FC**2-CH)
         1**2-4.0*(1.0+7.0*CD*C3*FC**2)*(2.0*FC/C1+5.0*CD*FC**2/C2)))/
         1(2.0*(1.0+7.0*CD*C3*FC**2))
         EH=ABS(HC-C)/C-0.001
         IF(EH) 20,20,8
8        C=HC
         GO TO 15
20       SALT=(6.0-HC-CH-2.0*CM-FC-CD*FC**2*(1.0/(C2*HC)+4.0+9.0*
         1C3*HC))/2.0
         CALL CHAIN ('MOOUT')
         END
```

MOS04.FT

```
C   THIS PROGRAM SUCCESSIVELY APPROXIMATES THE [HMO03] AND [H] IN
C          SOLUTIONS USED FOR THE KINETIC STUDY OF HETERO POLYMOLYBDATES
      COMMON C1,C2,C3,CD,CH,CM,HC,FC,SALT,CA
11    READ(1,12) CH,CA,CM
12    FORMAT('ENTER TOTAL [H], ITS 2ND KA, AND [MO] IN 10 COLUMN F FOR
     1MAT',/3F10.0)
      IF(CM) 45,45,13
45    CALL EXIT
13    C=CH-3.0*CM
      C1=11.36
      C2=4.7
      C3=0.24
      CD=97.0
15    FC=(-1.0-1.0/(C1*C)+SQRT((1.0+1.0/(C1*C))**2+8.0*CM*CD*(1.0/(C2*
     1C)+1.0+C3*C)))/(4.0*CD*(1.0/(C2*C)+1.0+C3*C))
      A=1.0+7.0*CD*FC**2
      P=(CA-CH+3.0*FC+CD*FC**2*(6.0+7.0*C3*CA))/A
      Q=(2.0*FC/C1-2.0*CH*CA+3.0*CA*FC+CD*FC**2*(5.0/C2+6.0*CA))/A
      R=(2.0*CA*FC/C1+5.0*CD*FC**2*CA/C2)/A
      PHI=ATAN(SQRT(-4.0*(3.0*Q-P**2)**3/(2.0*P**3-9.0*P*Q+27.0*R)
     1**2-1.0))
      HC=-P/3.0+2.0*SQRT((P**2-3.0*Q)/9.0)*COS(PHI/3.0)
      EH=ABS(HC-C)/C-0.001
      IF(EH) 20,20,8
8     C=HC
      GO TO 15
20    SALT=(6.0-HC-CH*((HC+4.0*CA)/(CA+HC))-2.0*CM-FC-CD*FC**2*(1.0/
     1(C2*HC)+4.0+9.0*C3*HC))/2.0
      CALL CHAIN ('MOOUT')
      END
```

MOOUT.FT

```
C   THIS PROGRAM WRITES OUT THE EQUILIBRIUM CONCENTRATIONS OF ALL
C       MO SPECIES AND H+ IN STRONG ACID SOLUTION.
        COMMON C1,C2,C3,CD,CH,CM,HC,FC,SALT,CA
        WRITE(1,17) CH
17      FORMAT('TOTAL [ACID] = ',E15.4,' M')
        WRITE(1,18) CM
18      FORMAT('TOTAL [MOLYBDENUM] = ',E15.4,' M')
        WRITE(1,30) FC
30      FORMAT('[HMOO3+] = ',E15.4,' M')
        WRITE(1,35) HC
35      FORMAT('[H+] = ',E15.4,' M')
        FC22=CD*FC**2
        WRITE(1,36) FC22
36      FORMAT('[H2MO2O6] = ',E15.4,' M')
        FC12=CD*FC**2*1.0/(C2*HC)
        WRITE(1,37) FC12
37      FORMAT('[HMO2O6+] = ',E15.4,' M')
        FC32=CD*FC**2*C3*HC
        WRITE(1,38) FC32
38      FORMAT('[H3MO2O6] = ',E15.4,' M')
        FC01=FC/(C1*HC)
        WRITE(1,39) FC01
39      FORMAT('[MO(OH)6] = ',E15.4,' M')
        WRITE(1,40) SALT
40      FORMAT('[NACLO4] REQUIRED FOR 3.0 IONIC STRENGTH = ',E15.4,' M')
        IF (CA) 41,41,42
41      CALL CHAIN ('MOLYB')
42      CALL CHAIN ('MOSO4')
        END
```

EXPO.FT

```
C THIS PROGRAM FITS OVERALL CHEM. KINETICS DATA TO A SIMPLE EXPONENTIAL
C     CURVE  Y= A + B EXP(CT)  OR A SUM-OF-THE-EXPONENTIALS CURVE
C     Y= A + B EXP(CT) + D EXP(ET).  IN THE LATTER CASE THE USER MUST SPECIFY
C     A TIME INTERVAL IN WHICH A SIMPLE EXPONENTIAL MODEL IS FOLLOWED AS WELL
C     AS AN INTERVAL WHEN ALL TERMS ARE SIGNIFICANT.  THE Y VALUE AT INFINITE
C     TIME MUST ALSO BE SPECIFIED.
      DIMENSION TIME(100),AB(100),SDEV(100)
5     READ(1,10) FNAME
10    FORMAT('WHICH FILE WOULD YOU LIKE TO WORK WITH?'A6)
      READ(1,15) ICHECK
15    FORMAT('ARE YOU SURE? 1=YES, 0=NO   ?'I2)
      IF (ICHECK-1) 5,16,5
16    READ(1,25) MODEL
25    FORMAT('WHICH TYPE OF MODEL WOULD YOU LIKE TO FIT?'/'0 = SIMPLE
      1 EXPONENTIAL'/'1 = SUM-OF-THE-EXPONENTIALS'/'2 = STOP'/'?'I2)
      IF (MODEL-1) 27,27,31
27    CALL IOPEN ('FLP2',FNAME)
      READ(4,20) IRATE,NPAVG,ITIBD,NDP,IDLY,NSFPR,NDPF
20    FORMAT(7I4)
      READ(4,21) (TIME(I),AB(I),SDEV(I),I=1,NDP)
21    FORMAT(3E13.6)
29    READ(1,26) AMAX
26    FORMAT('MAX.(MIN.) Y-VALUE FOR THIS RUN?'F10.0)
      IF (MODEL-1) 30,30,31
30    READ(1,35) TMIN
35    FORMAT('ENTER THE TIME INTERVAL WITH ONLY ONE SIGNIFICANT EXPONENTIAL
      1 TERM'/'BEGINNING TIME (SEC.) ?'F10.0)
      READ(1,36) TMAX
36    FORMAT('ENDING TIME (SEC.) ?'F10.0)
      READ(1,37) ICHECK
37    FORMAT('ARE YOU SURE? 1=YES, 0=NO   ?'I2)
      IF (ICHECK-1)30,39,30
5     PAGE
```

```
39      N=0
        SUMX=0.0
        SUMX2=0.0
        SUMY=0.0
        SUMY2=0.0
        SUMXY=0.0
        DO 40 I=1,NDP
        IF (TIME(I)-TMIN) 40,41,41
41      IF (TIME(I)-TMAX) 42,42,40
42      SUMX=SUMX+TIME(I)
        SUMX2=SUMX2+TIME(I)**2
        SUMY=SUMY+ALOG(ABS(AMAX-AB(I)))
        SUMY2=SUMY2+ALOG(ABS(AMAX-AB(I)))**2
        SUMXY=SUMXY+TIME(I)*ALOG(ABS(AMAX-AB(I)))
        N=N+1
40      CONTINUE
        T3=(SUMXY-SUMX*SUMY/FLOAT(N))/(SUMX2-SUMX**2/FLOAT(N))
        THETA2=-EXP(SUMY/FLOAT(N)-T3*SUMX/FLOAT(N))
        WRITE(1,45) THETA2
45      FORMAT('PARAMETER 2 = ',E12.5)
        RXY=(SUMXY-SUMX*SUMY/FLOAT(N))**2/((SUMX2-SUMX**2/FLOAT(N))*
        1(SUMY2-SUMY**2/FLOAT(N)))
        WRITE(1,46) T3
46      FORMAT('PARAMETER 3 = ',E12.5)
        WRITE(1,47) RXY
47      FORMAT('THE CORRELATION COEFFICIENT = ',E12.5)
        IF (MODEL-1) 50,60,31
60      READ(1,65) TMIN
65      FORMAT('ENTER TIME INTERVAL WHERE BOTH EXPONENTIALS APPLY'/
        1 'BEGINNING TIME (SEC.) ? 'F10.0)
        READ(1,66) TMAX
66      FORMAT('ENDING TIME (SEC.) ? 'F10.0)
        READ(1,67) ICHECK
67      FORMAT('ARE YOU SURE? 1=YES, 0=NO   ?'I2)
        IF (ICHECK-1) 60,69,60
5       PAGE
```

```
69      N=0
        SUMX=0.0
        SUMX2=0.0
        SUMY=0.0
        SUMY2=0.0
        SUMXY=0.0
        DO 70 I=1,NDP
        IF (TIME(I)-TMIN) 70,71,71
71      IF (TIME(I)-TMAX) 72,72,70
72      SUMX=SUMX+TIME(I)
        SUMX2=SUMX2+TIME(I)**2
        SUMY=SUMY+ALOG(ABS(AMAX+THETA2*EXP(T3*TIME(I))-AB(I)))
        SUMY2=SUMY2+ALOG(ABS(AMAX+THETA2*EXP(T3*TIME(I))-AB(I)))**2
        SUMXY=SUMXY+TIME(I)*ALOG(ABS(AMAX+THETA2*EXP(T3*TIME(I))-AB(I)
        1))
        N=N+1
70      CONTINUE
        T5=(SUMXY-SUMX*SUMY/FLOAT(N))/(SUMX2-SUMX**2/FLOAT(N))
        THETA4=EXP(SUMY/FLOAT(N)-T5*SUMX/FLOAT(N))
        WRITE(1,75) THETA4
75      FORMAT('PARAMETER 4 = ',E12.5)
        RXY=(SUMXY-SUMX*SUMY/FLOAT(N))**2/((SUMX2-SUMX**2/FLOAT(N))*
        1(SUMY2-SUMY**2/FLOAT(N)))
5       PAGE
        WRITE(1,76) T5
76      FORMAT('PARAMETER 5 = ',E12.5)
        WRITE(1,77) RXY
77      FORMAT('THE CORRELATION COEFFICIENT = ',E12.5)
50      READ(1,80) NEXT
80      FORMAT('WHAT NOW?'/'0 = CHOOSE ANOTHER TIME INTERVAL'/'1 = LOOK AT
        1 ANOTHER FILE'/'2 = STOP'/'?'I2)
        IF (NEXT-1) 29,5,31
31      CALL EXIT
        STOP
        END
```